INFORMATION TO USERS

This manuscript has been reproduced from the microfilm master. UMI films the text directly from the original or copy submitted. Thus, some thesis and dissertation copies are in typewriter face, while others may be from any type of computer printer.

The quality of this reproduction is dependent upon the quality of the copy submitted. Broken or indistinct print, colored or poor quality illustrations and photographs, print bleedthrough, substandard margins, and improper alignment can adversely affect reproduction.

In the unlikely event that the author did not send UMI a complete manuscript and there are missing pages, these will be noted. Also, if unauthorized copyright material had to be removed, a note will indicate the deletion.

Oversize materials (e.g., maps, drawings, charts) are reproduced by sectioning the original, beginning at the upper left-hand corner and continuing from left to right in equal sections with small overlaps.

Photographs included in the original manuscript have been reproduced xerographically in this copy. Higher quality 6" x 9" black and white photographic prints are available for any photographs or illustrations appearing in this copy for an additional charge. Contact UMI directly to order.

ProQuest Information and Learning
300 North Zeeb Road, Ann Arbor, MI 48106-1346 USA
800-521-0600

SDMA/TDMA DYNAMIC SLOT ASSIGNMENT USING A SMART ANTENNA BASESTATION

BY
FAISAL SHAD, B.ENG. (COMPUTER SYSTEMS ENGINEERING)
DECEMBER 1999

A THESIS
SUBMITTED TO THE DEPARTMENT OF ELECTRICAL AND COMPUTER ENGINEERING
AND THE COMMITTEE ON GRADUATE STUDIES
OF MCMASTER UNIVERSITY
IN PARTIAL FULFILLMENT OF THE REQUIREMENTS
FOR THE DEGREE OF
DOCTOR OF PHILOSOPHY

SDMA/TDMA DYNAMIC SLOT ASSIGNMENT USING A SMART ANTENNA BASESTATION

Doctor of Philosophy (2000)
(Electrical and Computer Engineering)

McMaster University
Hamilton, Ontario

TITLE:	SDMA/TDMA Dynamic Slot Assignment Using a Smart Antenna Basestation
AUTHOR:	Faisal Shad, B.Eng. (Computer Systems Engineering) (Carleton University, Ottawa, ON, Canada)
SUPERVISOR:	Dr. Terence D. Todd, Professor of Electrical and Computer Engineering, B.A.Sc., M.A.Sc., Ph.D. (University of Waterloo)
NUMBER OF PAGES:	1,182

Abstract

There is an increasing demand today for the deployment of wireless services such as cellular telephony, paging, wireless local area networks, digital broadcast television, and wireless Internet. The demand for bandwidth from these services continues to increase as more people adopt the technology and the applications become more sophisticated. In the recent years, researchers have demonstrated that smart antennas are capable of improving wireless link quality and increasing coverage area. In addition to this, it has also been demonstrated that smart antennas can permit the reuse of the frequency spectrum in the same wireless coverage area using space division multiple access (SDMA). SDMA has the potential to provide a tremendous increase in system capacity over conventional wireless systems.

In this thesis we consider the application of smart antennas for packet switched SDMA networks. The system considered is an infrastructure network employing a smart antenna basestation which communicates with portable stations that have omnidirectional antennas. A time division multiple access (TDMA) packet switched system that incorporates SDMA is considered. Several heuristic dynamic slot assignment (DSA) strategies are proposed. DSA is the name given to the process of allocating packets to the time slots in real-time on a frame by frame basis. The primary objective of DSA is to maximize the frame capacity. Both a theoretical Rayleigh fading channel model and experimental data collected using an 8 element circular antenna array built at the Communications Research Laboratory at McMaster University is used to measure the frame capacity of the heuristics. Analytic, simulated, and experimental results demonstrate that the SDMA/TMDA frame capacity is several times higher than the single omnidirectional basestation antenna case. The results also

provide insight into how the protocol performance is affected by parameters such as wireless channel model, slot assignment complexity, power control, pedestrian motion in the channel, and signal to noise ratio (SNR).

The well known slotted ALOHA protocol which is best suited for bursty data communication between a large population of portable stations is adapted for operation with a smart antenna basestation. Versions of this protocol are considered where contention takes place in the data slot directly and when a reservation channel feeds a contention free data channel. The DSA heuristics developed earlier are applied to the contention free data channel to improve system capacity. An SDMA version of the slotted ALOHA protocol is modified for operation in a multicell situation.

Simulation and analytic results show that the single cell slotted ALOHA system can achieve a many-fold increase in system capacity, especially when intelligent slot scheduling is done at the basestation. The sensitivity of the protocol capacity to factors such as the hardware complexity, packet size, SNR, and protocol complexity is examined. An analysis of the multicell slotted ALOHA protocol reveals that it is possible to reuse the frequency in every cell and still achieve a per cell capacity similar to ordinary single-cell slotted ALOHA with only a modest degree of smart antenna beamforming hardware at the basestations.

The DSA heuristics are then extended to multicell situations. Several DSA techniques requiring various degrees of coordination between the basestations are examined. DSA enhancements are also proposed for systems with variable length packets.

Acknowledgments

I would like to thank the following people for helping me out during my four year stay at McMaster University. I am very grateful to my supervisor, Dr. Terry Todd for encouraging me to pursue a Ph.D. and guiding me through it. Dr. Todd provided many hours of valuable supervision for this thesis, course work, paper publications, and even job hunting. I would also like to thank my Ph.D. committee members Dr. Jim Reilly and Dr. John Litva for offering useful hints at my committee meetings. Vytas Kezys was also of a great help with the collection of the measurements and for showing me how to process to the experimental data offline. Brian Currie, Jean Larorque, and Shiping He were involved in the collection of the experimental data and I thank them for their assistance. The other members of Dr. Todd's wireless networking group, Rupam Sinha, Charbel Sakr, Ahmed Almhdie, Jack Xu, and Osama Abu Amara also provided me with helpul insights. Graduate students Nima Ahmadvand and Kaywan Afkhmie were very helpful with some parts of my thesis and courses. Among others, Gaurav Patel, Tim Davidson and Pramod Gupta provided valuable insights for my comprehensive exam. Finally, I would like to thank my parents, brother, and sister for their support for the time I have spent in school.

Contents

List of Tables

List of Figures

List of Acronyms

R	Data rate
σ_l	Standard deviation of lognormal fading
l_{crc}	Length of CRC field
l_{data}	Size of data slot
l_{pn}	Length of the PN sequence
l_{sid}	Length of mobile station identifier field
n	Exponential power path loss exponent
n_{bfm}	Number of beamforming modules located in each smart antenna basestation
t_a	Basestation acquisition period
AMPS	Advanced mobile phone system
ATM	Asynchronous transfer mode
AUC	Authentication register
BPSK	Binary phase shift keying
CCITT/SS7	CCITT signalling system number 7
CDMA	Code division multiple access
CRC	Cyclic redundancy check
CRL	Communications Research Laboratory
CSMA	Carrier sense multiple access
CSMA/CA	Carrier sense multiple access with collision avoidance
CSMA/CD	Carrier sense multiple access with collision detection

CTS	Clear to send
CW	Continuous wave
DMI	Direct matrix inversion
DSA	Dynamic slot assignment
DSP	Digital signal processor
DSSS	Direct-sequence spread spectrum
EIR	Equipment identity register
EOF	End-of-frame
FCFS	First-come-first-served
FDD	Frequency division duplexed
FDMA	Frequency division multiple access
FHSS	Frequency hopping spread spectrum
FIFO	First-in first-out
FLOPS	Floating point operations
GPS	Global positioning system
GSM	Global system for mobile communications
HIPER-LAN	High performance European radio LAN
HLR	Home location register
ISI	Intersymbol interference

ISM	Industry, scientific, and medical
JDC	Japanese digital cellular
LAN	Local area network
LMS	Least-mean squares
LOS	Line-of-sight
MAC	Medium access control
MCS-L1	Mobile cellular service L1
MPSK	M-ary phase shift keying
MRC	Maximum ratio combining
MTTF	Mean time to failure
M	Number of mobiles per cell
NMT	Nordic mobile telephone
NOS	Network operation system
NU-LOS	No unobstructed line-of-sight
N	Number of antennas at the basestation
PAM	Pulse amplitude modulation
PCS	Personal communication systems
PHS	Personal handyphone system
PN	Pseudo-noise
PSA	Pre-sampled signature acquisition

PSTN	Public switched telephone network
QAM	Quadrature amplitude modulation
RLS	Recursive least squares
RTS	Request to send
S-ALOHA	Slotted ALOHA
SA-MOB	S-ALOHA with SDMA
SA-MRC	S-ALOHA with MRC
SARMS	SDMA S-ALOHA with a mini-slotted reservation channel
SDMA	Space division multiple access
SINR	Mean signal power to mean interference plus noise power ratio
SNR	Mean signal power to mean noise power ratio
TDD	Time-division duplexing
TDMA	Time division multiple access
U-LOS	Unobstructed line-of-sight
VLR	Visitor location register
WEP	Wired equivalent privacy
WLAN	Wireless local area network
WLANA	Wireless LAN alliance
WLL	Wireless local loop
XDATA	Transmit data slot
XPERM	Transmit permission slot

Chapter 1

Introduction

The past several years have witnessed a tremendous growth in the area of wireless communications [Pah94]. For fixed access, wireless communication eliminates the need for costly land line subscriber loops. It facilitates communication in environments which are not accessible by wire, such as a moving vehicle. As the public has become more aware of the benefits of wireless communication, demand has increased for a more advanced form of wireless service known as personal communication systems (PCS) [LQ95]. The goal of PCS is to make possible the exchange any kind of information, be it voice, video, or data, with anyone, anywhere, and anytime. The number of wireless subscribers in the United States was 27 million in 1995, and around 60 million by 1998.

As PCS gains popularity, it has become necessary to carry a large volume of traffic in a limited frequency spectrum. In order to do this, the geographic region over which communication takes place is divided into cells [Rap96]. Each cell has a basestation that communicates with the mobile stations located within its coverage area. The same frequency can be reused by another cell located far enough away so as not to interfere. One way to increase the traffic carrying capacity is by using smaller sized cells so that the frequency can be reused more often. The problem with this solution is that increasing the number of cells, and hence basestations, is expensive.

One strategy for increasing system capacity without adding basestations is to use

a smart antenna at the basestation. A smart antenna is an antenna which dynamically modifies its radiation pattern to enhance the gain to and from the desired user. The type of smart antenna which will be used in this thesis is known as an adaptive antenna array [App76]. Using spatial diversity, the adaptive antenna array can improve link performance by providing array gain, resilience to fading, and nulling of interfering signals. Adaptive antenna arrays have traditionally been used for military applications such as long-range surveillance radar and active jammer rejection. More recently, they have been considered for PCS applications. Swales has looked at the use of an adaptive antenna array to increase the capacity of a cellular network [SBEM90]. Ward has examined the performance gain due to an adaptive antenna array in a packet radio system [WC92, WC93]. Okamoto [OX96] and Sughihara [SES95] have investigated the application of adaptive antenna arrays for improving the throughput of the popular carrier sense multiple access (CSMA) protocol which is used for wireless local area networks (WLANs). These studies indicate that an adaptive antenna array greatly enhances the capacity of the wireless channel.

1.1 Motivation

The motivation behind this thesis is the need for the development of medium access control (MAC) protocols that improve the capacity and quality of a wireless channel which is both bandwidth and power limited. Protocols need to be developed which work with very low signal to noise ratios. The low signal to noise ratios are needed to conserve battery life at portable stations and also to minimize interference to other systems that are sharing the same frequency spectrum.

Although the total usable bandwidth of the earth's atmosphere is several 10's of Gigahertz, most of the higher quality regions are reserved for special purposes such as aviation and police radio, television, cellular phones, and so on. A small amount of the bandwidth is unlicensed and available for use with lower power applications (maximum 1 Watt radiated power) such as WLANs in the industry, scientific, and medical (ISM) bands located at 902-928 Mhz, 2.4000-2.4835 Ghz, and 5.725-5.850 Ghz. Typical wireless LANs today operate at data rates of around 2 Mbps, so it

can be seen that this limited spectrum gets used up very quickly. Therefore a prime motivation of this thesis is to maximize the use of the channel bandwidth for indoor packet switched networks such as WLANs.

Another feature of the wireless channel that makes it difficult to work with is that it changes very rapidly. Even if the transmitter is fixed with respect to the receiver, variations in the channel due to pedestrian traffic, the opening and closing of doors, and moving objects decorrelate the received signal envelope quickly. The protocol designer needs to take this into consideration when selecting the size of the transmit frame. The computational complexity of the protocol should be such that it is feasible to implement using current technology. In 1965 Gordon Moore observed that the microchip capacity doubled every 18 months. This often quoted formula, referred to as Moore's Law, has proven to be remarkably precise. The performance of the fastest digital signal processor (DSP) available today, the Texas Instruments TMS320C62xx, is about 1600 MIPS. The protocols developed in this thesis are all designed to be able to work with this much processing power.

At the physical level, primarily two non-exclusive adaptive signal processing techniques have been developed to increase the channel capacity. The first technique is called adaptive equalization. Here the signal is passed through an adaptive finite impulse response filter to remove the intersymbol interference. The second technique, which requires the use of the smart antenna, is spatial filtering or adaptive beamforming. With adaptive beamforming the outputs of the smart antenna are electrically combined to increase the desired signal power to interference plus noise power ratio. When adaptive equalization is combined with spatial filtering, it is referred to as space-time processing [PP97]. The protocols developed in this thesis will rely on using a smart antenna for adaptive beamforming.

1.2 Scope

This thesis evaluates several time division multiple access (TDMA) protocols for packet switched data communications which employ a smart antenna basestation. These protocols rely on a technique called space division multiple access (SDMA)

to improve the channel capacity. SDMA exploits the spatial diversity of the wireless channel to permit multiple stations to transmit at the same time and frequency within the same wireless coverage area. In this thesis a narrowband wireless channel is assumed, which means that the intersymbol interference is negligible. For indoor narrowband systems, data rates in the low Mbps are possible. For outdoor narrowband systems, the data rates have to be significantly lower due to the greater multipath delay.

The primary innovation in this thesis is dynamic slot assignment (DSA). DSA relies on pre-sampled signature acquisition (PSA) to form the SDMA/TDMA frame. The term signature refers to the narrowband vector channel response measured at the smart antenna basestation. It is the estimate of the phase shift and attenuation of the desired signal impinging upon the smart antenna in the presence of white noise and possibly other interferers. With PSA, the signatures sampled on the reverse link are used to construct the SDMA/TDMA frame which is transmitted at the same frequency. The object of the frame construction process is to minimize the size of the frame in order to maximize system capacity. The capacity performance of DSA with both theoretical and experimental signature models is calculated.

The capacity advantage realizable with DSA is clearly quantified in the first chapter on DSA. In the next chapter a well known random access based transmission protocol known as slotted ALOHA is adapted for operation with a smart antenna, and the various tradeoffs between capacity and hardware complexity are evaluated. Extensive capacity and delay results give insight into the protocol's performance for various packet sizes and SNR levels. As the cellular frequency reuse concept has become an increasingly popular method for enhancing system capacity, a basic smart antenna based slotted ALOHA system is adapted for operation in a network employing multiple basestations with overlapping coverage area. Finally, one of the more sophisticated DSA techniques is modified for the multicell scenario to increase the capacity. Capacity gains are achieved through various degrees of real-time synchronization between the basestations.

1.3 Organization

In Chapter 2 two types of wireless networks known as local area networks and cellular networks are discussed. The chapter also discusses the two main techniques by which the nodes and the internal transmission links in a network are shared: packet switching and circuit switching. Then the different ways to subdivide the time, frequency, and space dimensions for multiple access are discussed. Finally, the indoor wireless channel is characterized in detail.

Chapter 3 discusses the smart antenna or adaptive antenna array which is used for the protocols implemented in this thesis. A literature review of smart antennas as they pertain to wireless communication networks is given. Then the optimal (in the least mean square error sense) steady state reverse link (portable station to basestation) weight vector for the adaptive antenna array is derived. Several reference signal based adaptive beamforming techniques which converge to the optimal solution are examined. After this different smart antenna geometries are given and some basic outage probability curves are considered. Various methods of power control are also discussed.

Chapter 4 is devoted to examining the DSA frame capacity. The smart antenna basestation which is used to implement a number of DSA protocols is described. Following this are some preliminary experimental results taken at the Communications Research Laboratory at McMaster University which demonstrate the feasibility of employing a smart antenna basestation to increase system capacity. After this several heuristic DSA protocols are given. Their performance is evaluated with a theoretical Rayleigh fading channel and also with experimental results. A DSA based protocol is proposed which exploits the doppler fading present when the portable stations are moving in order to increase system capacity.

Chapter 5 considers slotted ALOHA protocols as examples of random access protocols which can benefit from the DSA techniques proposed in the previous chapter. The slotted ALOHA protocols developed in this chapter have been adapted for operation with a smart antenna basestation. Protocols are considered where contention takes place in the data slots directly, and where a contention based reservation channel

is used to feed a higher capacity contention free data channel. Particular attention is given to the hardware complexity needed to implement the slotted ALOHA protocols. Throughput and delay results for the protocols are compared for different packet sizes and SNR levels using analytic and simulation models. The slotted ALOHA protocol is adapted for operation in a multicell situation where the frequency is reused in every cell. For the multicell situation, protocol innovations are made for the acquisition of the nearest basestation.

Chapter 6 examines various DSA frame generation innovations for the multicell case. In this chapter DSA protocols requiring various levels of synchronization between the basestations are considered. The performance of DSA with a smart antenna which exploits the macroscopic diversity of the cell sites is evaluated. DSA is also adapted for operation with packets which vary in size.

Finally, Chapter 7 highlights some of the conclusions which were drawn from this thesis. Additionally, some areas for future work in smart antenna research are outlined.

Chapter 2

Background

2.1 Overview

This chapter provides some fundamental background information about communication networks and the wireless propagation medium. Wireless local area networks are used as an example of a consumer product that has benefited from the recent advances in wireless technology. The concept of cellular wireless networks for the purpose of increasing wireless channel capacity through frequency reuse is introduced. Then the concept of switching in computer networks is explained. The different ways in which multiple stations can share the wireless channel are covered. Specific attention is given to methods used by computer networks to share the channel. Finally, the characteristics peculiar to indoor wireless propagation are given.

2.2 Wireless Local Area Networks

The rapid progress of radio technology has vastly increased the number of subscribers for wireless products. The wireless service revenues are currently increasing at 40 per cent per year. Although much of the interest in wireless is for voice carrying digital phones, recently there has also been a modest but significant demand for wireless local area networks (WLANs). The current annual WLAN revenues of 210 million in 1997 are expected to increase rapidly to 2 billion by the year 2000 according to the

BRG Research group. In Europe, a new technical committee, ETSI RES10, has been established to specify the High Performance European Radio LAN (HIPER-LAN). In North America, the IEEE 802.11 standard has been developed for WLANs. A non-profit consortium of WLAN vendors called the Wireless LAN Alliance (WLANA) has been created for the purpose of providing ongoing education about specific applications, current technologies, and future directions of WLANs.

WLANs have gained significant popularity over the last eight years in the health care, retail, manufacturing, warehousing, and educational markets. As the price of WLANs drops, they are expected to be recognized as a general purpose connectivity alternative by a broad range of business customers. Some of the benefits of WLANs over conventional wired LANs are increased mobility, faster installation speed, and reduced cost of ownership when frequent moves, adds, and changes are needed.

In a typical WLAN, a transceiver called an access point is connected to the wired network through a fixed location. At the very least, the access point receives, buffers, and transmits data between the wired network and the portable computers. A single access point can accommodate several mobile computers in its coverage area of several hundred feet. The access point's antenna is located high to maximize the coverage. The mobile computers access the airwaves through WLAN adapter cards in laptops, or fully integrated devices with hand held computers. The WLAN adapters provide a transparent interface between the client computer's network operation system (NOS) and the airwaves.

The simplest way for computers on a WLAN to communicate is through an independent peer-to-peer infrastructure, as shown in Figure 2.1(a). This type of ad hoc network can be set up very quickly and no wireline network is required. By using an access point as a repeater as shown in Figure 2.1(b), the maximum distance between a pair of mobile computers is doubled. A more sophisticated infrastructure configuration shown in Figure 2.2 connects the mobile computers to an existing wired network via access points. In the figure, there are two access points for which the coverage area, called a microcell, is indicated by the shaded circles. Some WLAN NOSs permit roaming, meaning when a portable station moves from one microcell into another, the connection is automatically handed off to the other access point.

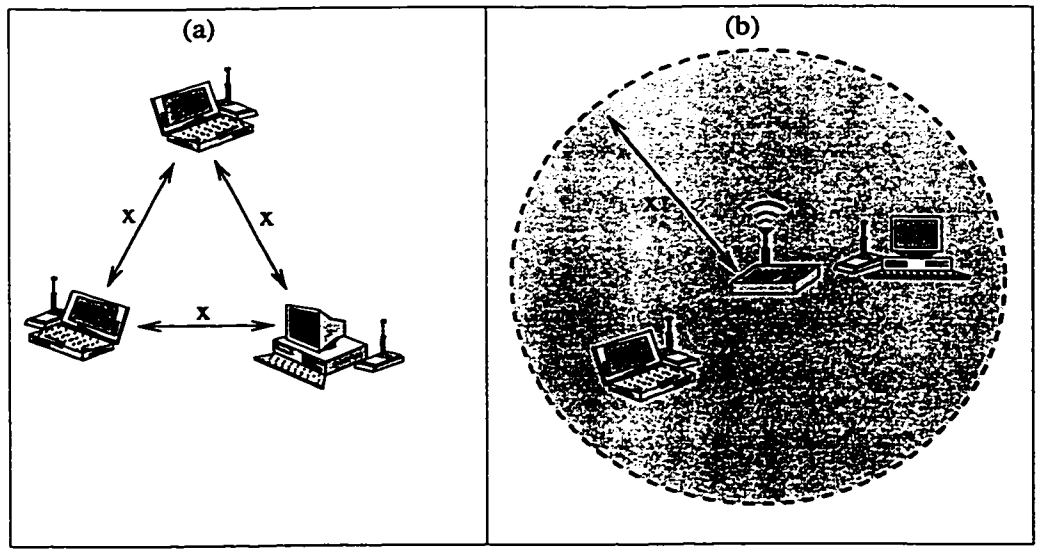

Figure 2.1: Independent WLAN (a) without and (b) with an access point functioning as a repeater.

In the indoor propagation environment in which WLANs are used, a particularly nasty problem is multipath which tends to degrade the quality of the received signal (more will be said about the propagation environment in Section 2.7). WLAN designers have successfully appealed to spread-spectrum transmission to solve this problem. With spread-spectrum, which is called this because the signal is broadened in the frequency domain, the signal is either multiplied by a known pseudo-noise chip sequence or the carrier frequency is changed in a known pattern. The former is called direct-sequence spread spectrum (DSSS) and the latter is called frequency hopping spread spectrum (FHSS). The spread-spectrum signal occupies a broad enough bandwidth that the channel characteristics are likely to be good in some regions.

One concern about WLANs is that of security because an unwanted user tuned into the correct frequency can listen in on the traffic. The use of spread-spectrum provides a limited amount security against this as the receiver needs to be aware of the chip sequence for DSSS or the frequency hopping pattern for FHSS. Many WLAN products include the same encryption features which are found in wired LANs. For example, the IEEE 802.11 standard includes a security technique known as wired equivalent privacy (WEP), which is based on the use of 64 bit keys and the RC4 encryption algorithm.

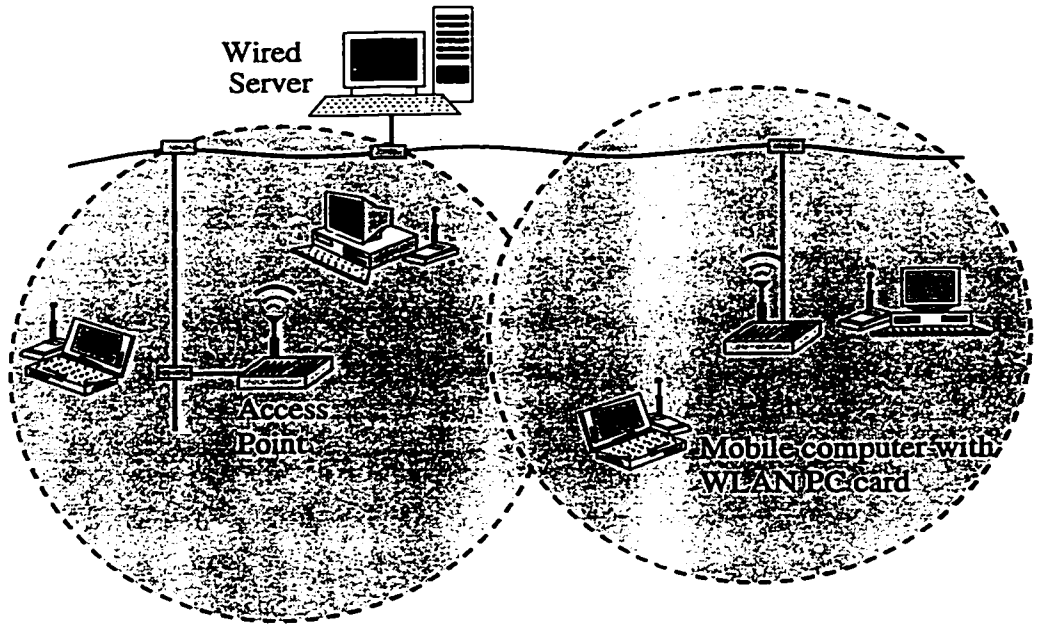

Figure 2.2: Infrastructure WLAN with 2 microcells.

Users without the key cannot decode the packets. Most WLAN products can also lock out individual portable stations as an authentication management function.

Portable stations hoping to recover the transmitted packets also require knowledge of radio domains, channels, sub-channels, security identifiers, and passwords. Thus the NOS can make it very difficult for malicious users to capture and decode the packets. Infrared-based WLANs are an attractive choice for high security applications. Because infrared signals cannot penetrate walls like radio frequency signals, an independent infrared-based WLAN can allow a team to have a WLAN which is completely isolated from the outside world.

2.3 Cellular Networks

Radio telephones have been available for decades, but until the late 1970's they were not widely available because of limited capacity. The breakthrough in radio telephony came with the development of the cellular network concept. In a cellular network, the geographic area is divided up into cells, and the frequency is reused some distance

away. The cell denotes the wireless coverage area of the basestation which is located at the center. The cells can be of any polygon shape for which there are no gaps or overlap when the cells are placed side by side, such as equilateral triangle, square, or hexagon. However, for the same center-to-vertex distance, the hexagon has the greatest area so it is the basic polygon unit that is employed for basestation placement in most cellular systems. Because adjacent cells use a different frequency, when a mobile user moves from one coverage area to another, a hand-off or hand-over is performed to transfer control to the new basestation.

The first generation of wireless systems are based on analog transmission technology that was pioneered in the late 1970's and 1980's. The cellular concept is used, and several capacity improvement techniques such as cell sectorization, cell splitting, dynamic frequency assignment, and frequency reassignment have been employed. Examples of first generation systems which use this analog technology are Nordic mobile telephone (NMT) by Ericsson, advanced mobile phone system (AMPS) by AT&T, and mobile cellular service L1 (MCS-L1) by NTT.

The second generation systems which are available today use digital transmission technology. With digital transmission, the system capacity is several times higher than analog systems. As well, second generation systems have greater services, increased security, higher quality, and lower cost. Examples of second generation systems include Global system for mobile communications (GSM) in Europe, Digital AMPS in North America, and Japanese digital cellular (JDC) in Japan [Kuc91].

Third generation wireless networks are expected to provide PCS level services. That is, they should permit the transfer of voice, video, and data traffic over the same network. As well, the telephone number should be associated with a particular person or service instead of a handset. Third generation networks are expected to gradually evolve from existing second generation networks, and thus they will use much of the existing technology. Figure 2.3, taken from [LQ95], is a picture of the logical architecture of a GSM/DCS1800 derived PCS network architecture. The network entities shown in the figure communicate with one another using the existing CCITT signalling system number 7 (CCITT/SS7) over conventional wireline. The basestations are connected to a basestation controller. The basestation controller

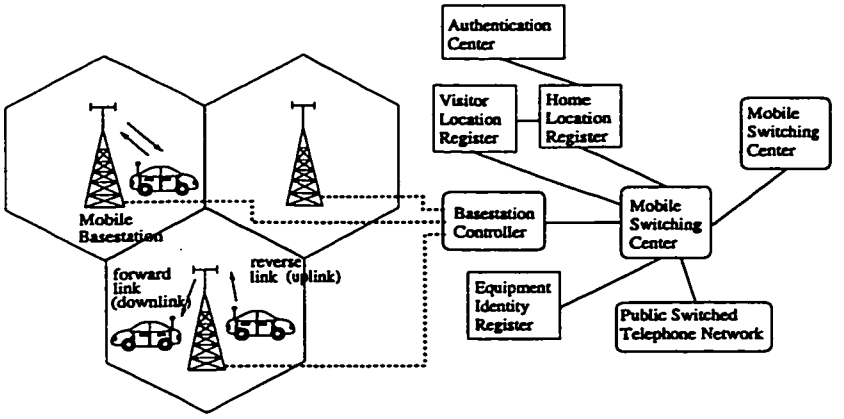

Figure 2.3: GSM/DCS1800 based third generation PCS network architecture.

helps to distribute the increased network load by reducing the amount of work for the mobile switching center. The mobile switching center is the primary interface between the basestation controllers and the wired public switched telephone network (PSTN). The key functions which permit global roaming in a PCS network are called the mobility management functions. This includes location registration, location update, paging, and handoff. Several network entities are shown in Figure 2.3 that facilitate mobility management. The home location register (HLR) stores the permanent information of each user in its subscription area. The visitor location register (VLR) stores the information on users currently visiting its area. The equipment identity register (EIR) and authentication register (AUC) are used in conjunction to verify the authentication and authorization of the user and network entities in order minimize the chance of illegal access to the network.

2.4 Switching

Switching is the method used to dynamically share the internal network transmission links and nodes. The easiest way to permit communication among the nodes in a network is to have a physical connection between each node and every other node. In a large network of many nodes, this is not practical since it would require $N(N-1)/2$ connections, where N is the number of nodes. However, if the network is equipped

with one or more switches which can electronically connect the appropriate input-output ports, then it is possible for distance nodes to communicate with a modest amount of physical connections. There are two main methods with which a signal is switched from the source node to the destination node, namely, circuit switching and packet switching. In circuit switching, a dedicated physical path is set up between the source and destination before any data is sent. This can take several seconds. Once the path is setup, data can be transmitted without interruption. Such a system is ideal for voice communication because of the low delay associated with the dedicated path.

The weakness of circuit switching with bursty data traffic is that the path remains idle for long periods of time. This is particularly problematic for wireless communication since the spectrum is very limited. The solution to this problem is packet switching. In packet switching, the message is broken up into packets which are transmitted individually. The key advantage of packet switching is that bandwidth is allocated on demand. This means that during the long idle periods between bursts of data, the spectrum can be used by other stations. In datagram mode, each packet comes complete with a source and destination address so it can be routed independently. Virtual circuit mode is a special type of packet switching which emulates circuit switching for the end user. In virtual circuit mode, an implicit path is created between the source node and destination node. With virtual circuits the switching is faster and packets arrive in the same order in which they were sent. Asynchronous transfer mode (ATM) is a recent packet switched protocol that uses virtual circuits [Pry93].

2.5 Multiple Access In Wireless Communications

Since the wireless spectrum is broadcast by nature, a mechanism is necessary to arbitrate its use. The spectrum can be sliced up into four basic non-exclusive categories.

Time division multiple access (TDMA) is when the spectrum is split up into non-overlapping time slots. Stations take turns transmitting during their dedicated time slots. The advantage of TDMA is that the transmitted signal occupies a lot of

bandwidth, so it is resilient to multipath fading and jamming. The disadvantage is that the signal must be digitally buffered and synchronized to transmit in a short burst in the allocated time slot. Also, adaptive equalization may be necessary to combat intersymbol interference (ISI).

In frequency division multiple access (FDMA), the spectrum is divided into different frequency bands. Stations transmit simultaneously in non-overlapping frequency bands. An advantage of FDMA is that it is relatively easy to implement with analog technology. An example of a system which uses FDMA is AM radio which is allocated spectrum between 500 and 1500 Khz.

In code division multiple access (CDMA), stations transmit concurrently with mathematically near orthogonal codes. CDMA is very secure because only stations with knowledge of the code are able to recover the signal. However, since the signals overlap in time and frequency, the stations have to control their transmit power very carefully.

Space division multiple access (SDMA) means that stations are physically far enough apart not to interfere with each other even though they transmit at the same time and frequency. A simple example of SDMA is a group of people engaged in multiple conversations in the same room. Using smart antennas, stations located very close to each other can be permitted to transmit simultaneously by electronically enhancing the gain from desired stations and suppressing the gain from undesired stations.

2.6 Medium Access Control Protocols

The protocol used to arbitrate the access of multiple stations to a shared medium is referred to as a medium access control (MAC) protocol. What follows is a brief description of some popular TDMA based MAC protocols.

The wireless channel can be reserved for an arbitrary length of time by the stations. Short term reservation can be done by polling the individual stations through a centralized basestation. Once the basestation knows who has data to transmit, it notifies the stations of the transmission sequence. The reservation can also be done

for a longer term by setting up a circuit for the duration of the call as discussed in Section 2.4.

The wireless channel may also be accessed "on the fly", and this is referred to as random access. One of the earliest random access MAC protocols is known as pure ALOHA. It was developed by Norman Abramson and his colleagues at the University of Hawaii [Abr70]. In pure ALOHA, stations transmit whenever they have a packet to send. A packet transmission is successful if it does not overlap with other packets. If two or more packets overlap, there is a collision and the packets must be retransmitted. Assuming an infinite population and Poisson arrivals, the probability that k packets are generated in a frame whose duration is the length of the packet is

$$P[K = k] = \frac{G^k e^{-G}}{k!}, \tag{2.1}$$

where G is the average number of packets generated in one frame. The throughput S, which is the mean number of successful packets in a frame, is G times the probability that no other packets are generated in a vulnerability period of two packet durations. Therefore $S = Ge^{-2G}$. The maximum throughput occurs at $G = 0.5$ and it is equal to $S_{max} = \frac{1}{2e} = 0.18$.

In 1975 Roberts developed slotted ALOHA [Rob75], which has double the capacity of pure ALOHA. In slotted ALOHA, the time axis is divided up into time slots equal to the length of the packet, and stations synchronize their transmission to the start of the time slot. The vulnerability period is now just one time slot, so $S = Ge^{-G}$ and $S_{max} = \frac{1}{e} = 0.36$ at $G = 1.0$.

The weakness of the ALOHA protocols is that data is sent even if the channel is busy. Protocols which listen to the channel for activity before transmission are referred to as carrier sense protocols. In the carrier sense multiple access (CSMA) protocol, the station first listens to the channel for activity before transmission. If the channel is idle, the packet is sent. Otherwise, the station waits until the channel becomes idle. In 1-persistent CSMA, the station transmits immediately once the channel becomes idle. If a collision occurs it waits a random amount of time before starting again.

Under high load, with 1-persistent CSMA the throughput can be compromised in

that multiple stations may transmit simultaneously once the channel becomes idle. In nonpersistent CSMA, stations do not transmit immediately after the channel becomes idle. If a channel is busy, they sense it periodically and transmit when it is sensed as idle. Nonpersistent CSMA has a higher capacity than 1-persistent CSMA at the cost of higher delay. S_{max} for the CSMA protocols is well above 0.50 [Tan96].

Although CSMA is more efficient than ALOHA or slotted ALOHA, it has one major inefficiency. Because of the non-zero propagation delay, it is possible for two stations to transmit frames which overlap in which case there is a collision. When two frames collide, the channel remains unusable for the duration of the transmission of both corrupted frames. If the frames are long, the amount of wasted bandwidth is considerable. In the carrier sense multiple access with collision detection (CSMA/CD) protocol, the station continues to listen to the channel while it is transmitting. If a collision is detected during the transmission, transmission is ceased immediately and a brief jamming signal is sent to ensure that all stations become aware of the collision. After waiting a random amount of time, transmission begins again using the standard CSMA protocol. The original baseband implementation of the CSMA/CD protocol was developed and patented by the Xerox company [MB76].

In the wireless channel collision detection is unfortunately not possible because the received signal's strength is much weaker than that of the transmitted signal. The carrier sense multiple access with collision avoidance (CSMA/CA) protocol used in the IEEE 802.11 WLAN standard [Dep96] reduces the chances of a collision by reserving the bandwidth required for the data packet before sending it. When the source station has a packet which is ready to send, it transmits a request to send (RTS) packet using the standard CSMA protocol. The destination replies to this with a clear to send (CTS) packet. Upon hearing the CTS, the source station transmits its data packet. This way, if a hidden station does not detect the RTS packet from the source station, it will hear the CTS and suspend its transmission until the source station's data packet is sent.

2.7 Indoor Wireless Channel

In an indoor environment, the signal travels through a number of different paths to get from the transmitter to the receiver. The direct path from the transmitter to the receiver is called the line-of-sight (LOS) path. The received signal is much weaker than the transmitted signal from path loss, shadowing effects, and cancellation of the signal due to destructive interference at the receiver. Shadowing effects, which change the mean received signal strength averaged over many wavelengths, occur from obstructions such as furniture, walls, and doors, and give rise to slow fading. The abrupt signal variation seen over the span of a wavelength, known as fast fading, is created by constructive and destructive interference arising from multipath. Because of the different path lengths, the received signal is spread in the time dimension. The time varying multipath lengths due to movement of the transmitter or receiver spreads the signal in the frequency dimension. In the next few sub-sections each of these wireless channel characteristics will be considered.

2.7.1 Path Loss

In ideal free space propagation, the received signal power is proportional to d^{-2}, where d is the distance between the transmitter and receiver. The indoor propagation environment is very complicated and a similar universally acceptable path loss model is not yet available [Has93]. Several empirical path loss models have been proposed in literature, and validated with measurements. The following four are some of the models proposed in literature:

Model 1 The received signal power follows an inverse exponent law, so

$$P(d) = P_0 d^{-n}. \tag{2.2}$$

The reported values for n are as little as 1.5-1.8 for factory channels [RM89, Rap89] with an unobstructed line-of-sight (U-LOS) path between the transmitter and receiver, to as high as 6 for university campus buildings [TT92]. Values for n that are less than 2 can arise if the different multipaths with small phase

differences combine constructively in a long narrow pathway. Path losses lower than free space can be accounted for by the waveguide effect of narrow hallways, where the received signals interfere constructively due to small phase differences. Large path losses occur when the multipaths have to penetrate through objects such as walls, floors, and doors.

Model 2 The received signal power follows an inverse exponent law similar to Model 1, except here the exponent is distance dependent [Ake88]. The suggested value for n is 2 for $1 < d < 10$ m, 3 for $10 < d < 20$ m, 6 for $20 < d < 40$ m, and 12 for $d > 40$ m. The exponent increases with d because the signal has to penetrate a greater number of obstructions.

Model 3 This model associates a logarithmic attenuation for each type of structure that the signal penetrates. For example, the attenuation through a concrete block wall was measured as 13 dB [Rap91]. The total path loss in dB can be calculated by adding the individual dB path losses.

Model 4 This model assumes a free space attenuation plus a dB per unit of distance path loss. That is, $P_{dB}(d) = 10\log_{10}P_0 - 10n\log_{10}d - kd$, where k is the dB per unit distance path loss. In [SP86], k was found to be 0.42 dB/ft for $d < 70$ ft, and 0.27 dB/ft for $d > 70$ ft from measurements taken at 850 Mhz.

2.7.2 Slow Fading

Slow fading is the fluctuation in mean signal strength, averaged over many wavelengths, that takes place due to shadowing caused by objects such as doors, furniture, and walls. It has been explained well by the lognormal distribution [Vit95, GP91], and is referred to as lognormal shadowing in literature. This distribution arises because the received power is the product of the attenuation through several obstructions. If the distribution of the attenuation through each obstruction is independent and identically distributed, then the log of the net attenuation is a sum of the log of each attenuation. By the central limit theorem [Hay78], if there are many obstructions, then the log of the net attenuation approaches a normal distribution. Typical

values for the lognormal distribution's standard deviation are 8 dB for residential complexes, and 10 dB for office buildings [PL95].

2.7.3 Fast Fading

The small scale amplitude fluctuation in a multipath environment takes place due to the vector addition of the multipaths. It is referred to as fast fading since the amplitude can become completely decorrelated in one wavelength. A well accepted model for the fast fading of the envelope when there is no unobstructed line-of-sight (NU-LOS) path between the transmitter and receiver is the Rayleigh distribution [TM88].

When a U-LOS path exists between the transmitter and receiver, the envelope of the received signal exhibits a Rician distribution [Bul86]. The Rician distribution models a strong U-LOS path plus many weaker multipaths. A typical value of the LOS-factor l, which is the proportion of power in the deterministic U-LOS path, is $l = 0.8$ [Bul87].

Experimental Fast Fading Envelope Distribution Results

Channel sounding was done in the CRL building at McMaster University to validate a model for the fast fading distribution. Figure 2.4 is a map of the ground floor of the CRL building where the data was collected at 1.86 Ghz. The details of the equipment used to sample the channel can found in Appendix A and Section 4.3. Samples were collected by walking with the transmitter in the various rooms. The receiving antenna array receiver was located just outside room 102, as indicated by Â on Figure 2.4. Approximately 800 samples spaced about 10 cm apart were collected for each room. For each sample, the complex envelope at each antenna array was recorded. The complex envelope is the estimate of the phase shift and attenuation of the signal at the antenna output. The data from the first antenna array was processed off-line to remove the shadowing and the power was averaged to 1 Watt.

The Weibull distribution, which has no theoretically motivated explanation, has been used to characterize the fast fading in an indoor environment [HP91, She77,

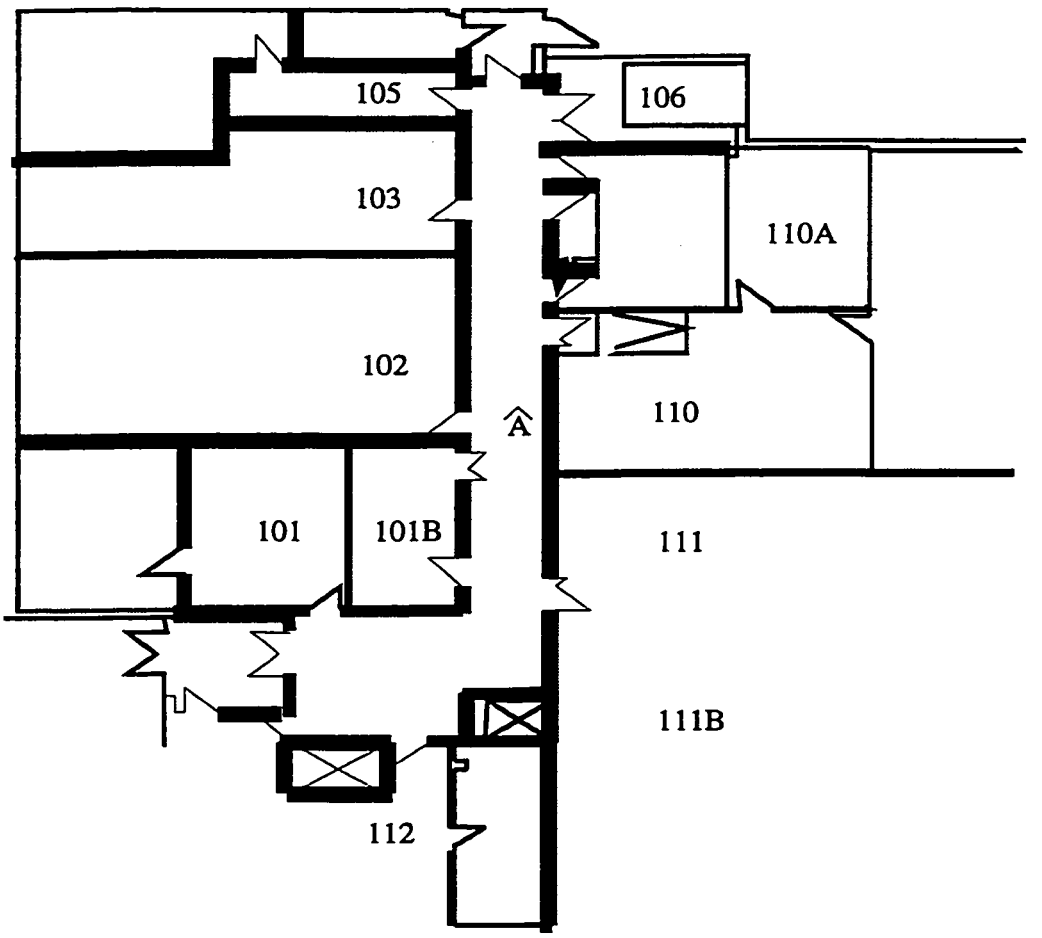

Figure 2.4: Floor map of ground floor of CRL.

PL95]. The Weibull distribution has the probability density function [Dou90],

$$p_R(r) = \alpha\beta r^{\beta-1} e^{-\alpha r^\beta}, \quad r \geq 0, \tag{2.3}$$

where the mean μ is

$$\mu = \alpha^{\frac{-1}{\beta}} \Gamma(1 + \frac{1}{\beta}),$$

and the variance κ is

$$\kappa = \alpha^{\frac{-2}{\beta}} \left[\Gamma(1 + \frac{2}{\beta}) - \Gamma^2(1 + \frac{1}{\beta}) \right],$$

where $\Gamma(\cdot)$ is the Gamma function. For the special case of $\beta = 2$, the Weibull distribution is the same as the Rayleigh distribution.

Transmitter Location	β	D-Statistic
Room 103	2.03 ± 0.22	0.52 ± 0.07
Room 106	2.13 ± 0.31	0.56 ± 0.12
Room 110	2.19 ± 0.27	0.58 ± 0.13
Room 110a	2.07 ± 0.25	0.51 ± 0.09
Room 105	2.22 ± 0.17	0.55 ± 0.08
Room 101	2.17 ± 0.18	0.55 ± 0.09
Room 112	2.53 ± 0.29	0.85 ± 0.30
Room 111	1.95 ± 0.13	0.56 ± 0.10
Room 111b	2.06 ± 0.17	0.54 ± 0.06

Table 2.1: The hypothesis is that the fading has a Weibull distribution. The value of β and the corresponding D-statistic is given, along with the 95 per cent confidence interval.

To validate a model for the distribution of the magnitude of the complex envelope, the K-S D-statistic continuous distribution hypothesis test [SM82] was used. The hypothesis was that in a NU-LOS situation, the distribution of the magnitude of the complex envelope was Weibull with all parameters known. The shaping parameter β was manually adjusted in increments of 0.01 to obtain the value which gave the closest fit. Table 2.1 indicates which value of β gave the closest fit for each room, and the corresponding value of the D-statistic.[1] The hypothesis that the indoor fast fading follows a Weibull distribution can be accepted for all rooms considered in Table 2.1 at a significance level of 0.15. In Figure 2.5, the cumulative density function of the experimental fading envelope and the corresponding Weibull distribution model is given for two of the situations in Table 2.1. This figure shows that the cumulative distribution function of the Weibull distribution closely matches that of the experimental fading envelope.

[1]The cutoff levels at the significance levels of 0.01, 0.025, 0.05, 0.10, and 0.15 are 1.626, 1.480, 1.358, 1.224, and 1.138, respectively. If the D-statistic is larger than the cutoff value at the specified significance level, then there is sufficient evidence to reject the hypothesis. For example, at a significance level of 0.01, if the D-statistic is larger than 1.626, we reject the hypothesis that the fast fading is Weibull. It should be noted that if the hypothesis is accepted, it does not imply that there is no other distribution which yields a better fit.

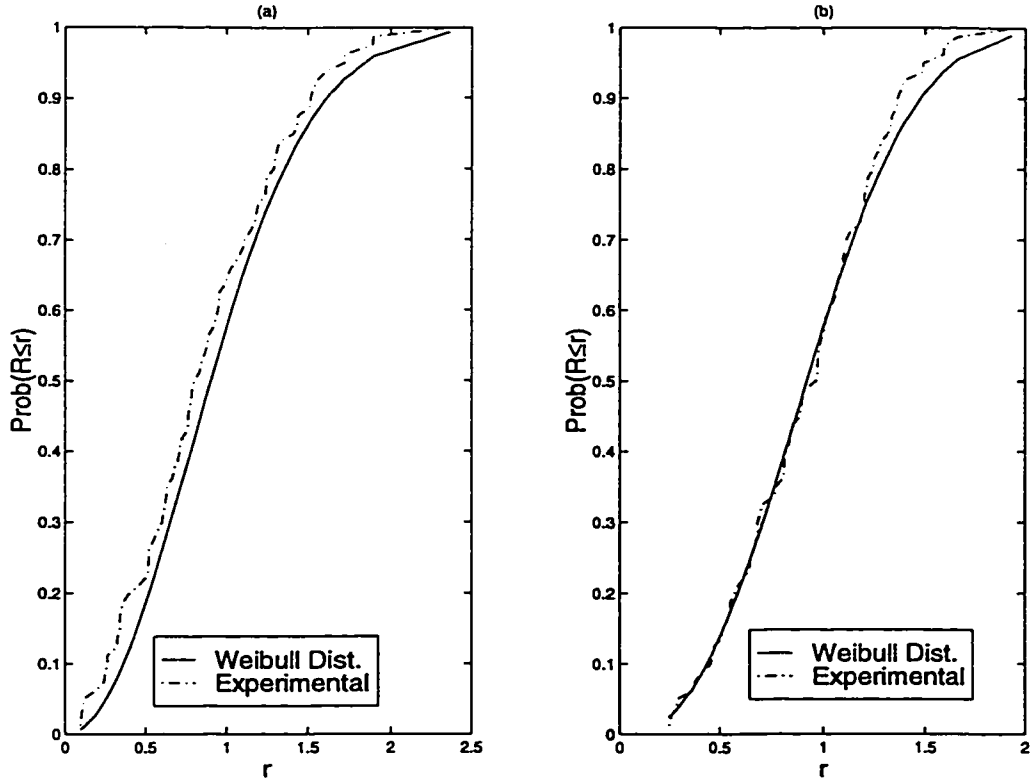

Figure 2.5: Cumulative density function for experimental fading envelope, and cumulative density function for the closest fit of the Weibull distribution to the experimental data. (a) Room 110a (b) Room 112.

2.7.4 Time Spreading

Because the signal propagates at a finite speed of $c = 3\times10^8$ m/s, the multipaths arrive at different times, which gives rise to delay spread. One measure of delay spread is the root mean square delay spread, defined as

$$\tau_{rms} = \sqrt{\frac{\sum_k (t_k - \tau_m - t_1)^2 a_k^2}{\sum_k a_k^2}}, \tag{2.4}$$

where a_k and t_k are the amplitude and arrival time, respectively, of the k^{th} arriving path, and τ_m is the mean excess delay, defined as

$$\tau_m = \frac{\sum_k (t_k - t_1) a_k^2}{\sum_k a_k^2}. \tag{2.5}$$

τ_m and τ_{rms} are the mean and standard deviation of the power delay profile with respect to the first path. Numerical values for τ_m and τ_{rms} are as little as between 20 and 50 ns for small and medium sized office buildings [SV87], and up to 200 ns in large office buildings [Dev87]. If τ_{rms} is significantly below the duration of a transmitted symbol T_{symbol}, say less than $0.2T_{symbol}$ [Rap96], then the intersymbol interference is negligible.[2] This situation is known as flat fading because in the frequency domain the channel is flat in the bandwidth occupied by the transmitted signal.

The coherence bandwidth, which is proportional to $\frac{1}{\tau_{rms}}$, is the largest bandwidth possible for the transmitted signal such that the intersymbol interference remains minimal. If τ_{rms} is large compared to T_{symbol}, which in the frequency domain means that the transmitted signal's bandwidth exceeds the coherence bandwidth, then the channel is said to have frequency selective fading. Frequency selective fading is not considered in this thesis.

2.7.5 Frequency Spreading

If the transmitter is moving with respect to the receiver, the signal level at the receiver fluctuates due to the time varying lengths of the multipaths. The LOS path fades at a Doppler frequency equal to $f_d = \frac{v}{\lambda}$, where v is the relative velocity and λ is the wavelength. If the $\frac{1}{f_d}$ is significantly larger than T_{symbol}, then the distortion of the received signal is minimal. This is typically the case in an indoor environment where v is at most 2 m/s.

2.8 Conclusions

The goal of this chapter was to introduce some basic wireless communication network principles. WLANs were discussed as an example of a product that has benefited from the tremendous improvements in wireless technologies which have taken place in the

[2] With an adaptive array receiver, the array can use its degrees of freedom to treat delayed versions of the symbol as separate signals. Specifically, an adaptive array with N antennas can eliminate delay spread of $T_{symbol}(N-1)/2$ symbols, or cancel $N-1$ delayed signals over any delay [Win98]. The problem with using the degrees of freedom in this way is that fewer than $N-1$ interfering stations can be nulled.

recent past. The underlying network infrastructures which support cellular telephony were briefly examined, and the idea of frequency reuse was introduced. The concept of circuit switching and packet switching was described next. A key advantage of packet switching is that it only dedicates as much bandwidth as needed, which is very advantageous for bursty data communication networks such as the Internet. Four non-exclusive ways in which the limited wireless spectrum can be shared among the users were briefly described. Then some specific MAC protocols used for data networks were examined. Finally, the features which characterize an indoor wireless channel were described. Measurements which were taken at the Communications Research Lab at McMaster University were used to show that the Weibull fading distribution can be used to accurately model the fast fading characteristics of the signal envelope.

Chapter 3

Smart Antennas

3.1 Overview

The gain of an antenna is an important factor in determining the performance of the radio system. Highly directional mechanically steered antennas have been used for fixed-link applications such as microwave towers and geostationary satellite. However, in applications such as cellular telephony and wireless LANs, the system has to be able to provide 360 degree coverage and adapt rapidly to changes in the environment. Electronically steered adaptive antennas based on phased-array antenna techniques have been used for applications in military and space industries. In the past such systems have been very expensive. The rapid advancement of electronic integration techniques have now made adaptive antennas viable for commercial communication applications. For example the ArrayComm company has verified adaptive array technology in the personal handyphone system (PHS), fixed wireless local loop (WLL), PCS-1900 and DCS-1800 (GSM), and advanced mobile phone system (AMPS). Adaptive antenna arrays are often referred to as smart antennas in literature. A smart antenna is an adaptive antenna array which dynamically modifies its radiation pattern to enhance the quality of the desired signal. The first person to use the word "smart" antennas to refer to adaptive antenna arrays appears to be Gabriel [Gab76]. In this thesis the term adaptive antenna array and smart antenna will be used interchangeably.

In Section 3.2 a literature review of the development of smart antennas for communication networks is given. In Section 3.3 two simple ways to control the smart antenna known as selection diversity and switched diversity are discussed. In Section 3.4 the optimal reverse link beamforming solution for the adaptive antenna array is derived. The outage probability performance of the adaptive antenna array is then evaluated under various propagation environments for both the linear and circular array. The value of performing power control is examined, and the impact of mutual coupling between the antenna outputs is evaluated.

3.2 Smart Antennas in Communication Systems

The history of smart antennas or adaptive antenna arrays goes back nearly 40 years. One of the first developments was the intermediate frequency sidelobe canceler by Howells [How65]. By mid-1957 Howells had developed a sidelobe canceler which can automatically null the effect of one jammer. The sidelobe canceler used a primary high gain antenna and a reference omni-directional low gain antenna to form a two-element smart antenna with one degree of freedom. He demonstrated that it is possible to steer a deep null anywhere in the sidelobe region of the combined antenna pattern to reduce the signal strength from the jammer. Then in 1966 Applebaum developed a control law for operating an antenna array [App66]. A control loop for each antenna element would maximize the signal to interference plus noise ratio (SINR) by setting the complex weights of a linear combiner. Another major early contribution to smart antennas was the least-mean square (LMS) algorithm proposed by Widrow [WMGG67]. The LMS algorithm adaptively changes the weights to minimize the mean square error. Another important advancement was by Capcon [CGK67] who proposed a smart antenna system which would minimize the output variance subject to a desired signal protection constraint. In 1974 Reed developed an important formula which relates the number of data samples required to implement Applebaum's control law to the number of antenna elements [RMB74]. In 1981 Compton was able to show that the array output SINR becomes more sensitive to errors in the steering vector as the number of antennas increases [Com82]. In 1989 Ganz studied a

technique for implementing a LMS array which does not require an explicit reference signal [GC89]. His technique was based on a channel encoding procedure in which the bit stream to be sent over the communication link was given a statistical dependence between the bits. Some of the books on adaptive antenna array theory include Monzingo and Miller [MM80], Hudson [Hud81], Compton [Com88], Johnson [JD93], and Litva [LL96].

Most of the work on smart antennas has been concentrated on physical layer signal processing techniques for improving the antenna gain. Relatively little work has been done on the application of smart antennas to civil land and mobile radio communication networks for the purpose of improving system capacity. However, in the last 15 years several researchers have made important contributions which demonstrate the feasibility of using smart antenna technology for increasing the system capacity.

Winters has authored a number of papers on the fundamental advantages of optimal combining, i.e., maximizing the SINR after beamforming. In [Win84], he shows that the bit error rate (BER) performance in an independent flat-Rayleigh fading environment with optimum combining is much better than through maximum ratio combining (MRC), especially as the number of antennas increases. MRC refers to when the adaptive beamforming is done to only maximize the gain against random noise. The paper also describes how optimum combining can be implemented in a digital radio with LMS adaptive arrays. In [Win87b], Winters considers the capacity performance with optimum combining in a independent flat-Rayleigh fading channel. He shows that in a high SNR situation, a system with M antennas at the basestation and a single antenna at the remote can achieve either an M-fold increase in capacity or tolerate $M-1$ interferers. In [WSG94], Winters shows that for independent flat-Rayleigh fading wireless systems with N mutually interfering users, with $K+N$ antennas, $N-1$ interferers can be nulled out and $K+1$ path diversity improvement can be achieved for each of the N users. This statement can be interpreted as follows. Each antenna provides a degree of freedom which is used to remove the interference from an interfering user. Once all interferers are nulled, the remaining degrees of freedom make the system behave as if there were no interferers and the system was maximizing the gain against random noise. Simulation results in the

paper also demonstrate that this results holds with frequency-selective fading. The paper shows that for the IS-54 digital cell phone standard, with 2 or 3 antennas the capacity is more than doubled at fading rates up to 100 Hz (75 mi/hr) in the 900 Mhz band.

Smart antennas have also been studied as a potential technology for improving the performance of the cellular CDMA multiple access scheme. In [NPK94], it is shown that by using an antenna array at the basestation it is possible to dramatically increase the capacity. For example, with 30 degree beamwidths, the uplink capacity of IS-95 CDMA increases from 31 users per cell to 320 users per cell. In [NP96], the performance of wireless CDMA with M-ary orthogonal modulation is considered. In this paper the array serves as a front end beamsteering processor feeding a conventional noncoherent RAKE combiner. The maximum number of users for a given BER performance is seen to increase almost by the number of antennas.

Smart antennas have recently been proposed as a technique for improving the capacity of packet radio networks. In [WC92], smart antennas are used to improve the performance of a slotted ALOHA packet radio network. Ward proposes a technique which uses a known pseudo noise (PN) code and a randomized packet arrival time to dynamically acquire packet transmissions. The analysis of this singlebeam system reveals that the capacity performance of slotted ALOHA is similar to CSMA. In [WC93], the analysis is extended to a multibeam case. Each beam captures a different packet by automatically pointing its maximum at one packet in the slot and adaptively nulling other packets in that slot. In [XL94], a smart antenna is used to improve the performance of reservation ALOHA. In reservation ALOHA, a small random access reservation channel is used feed a larger contention free data channel.

In [Aca96], a time division duplexed (TDD) singlebeam smart antenna based wireless ATM protocol is proposed. In this protocol, omnidirectional polling is first done to determine which portable stations have packets to transmit in the uplink direction. Then in the uplink part of the frame, before a packet is sent, a pilot tone is sent to train the smart antenna. Once the smart antenna is trained, the uplink packet is received with the array gain. Similarly, in the downlink portion of the frame the basestation sends a stimulus to each portable station that is going to receive a

packet. The portable station immediately acknowledges this with a pilot tone which trains the smart antenna, and the downlink packet is sent under the protection of the array.

Smart antennas have also been considered as a technology for improving the performance of wireless local area networks (WLANs). In [SES95] smart antennas are used to mitigate the hidden terminal problem with the slotted nonpersistent CSMA protocol. The hidden terminal problem is when terminals A and B are both transmitting a packet to C, but they cannot hear each other. Without a smart antenna, this causes a collision at C so both packets are lost. With the smart antenna, it is possible to place a null on the second packet so the first one is successfully received. In [ST97], a multibeam CSMA protocol is proposed. In this protocol once a station senses the carrier it defines an "uncertainty interval" over which it can randomize a transmission of a packet. The intent here is to accumulate a set of packets for the basestation smart antenna to resolve. IEEE 802.11 WLAN [Dep96] style RTS/CTS packet exchanges are used to resolve the hidden station problem.

3.3 Selection and Switched Diversity

Smart antennas are currently being used in mobile radio systems to provide resilience to fast fading by means of antenna diversity. Two or more antennas are located at the receiver and/or transmitter. The antennas are spaced far enough apart such that the fast fading at each element is significantly decorrelated. If the probability of a signal being too weak, i.e. in outage, at one antenna is p_o, then with N uncorrelated antennas this reduces to p_o^N.

One technique used for diversity is switched diversity, as shown in Figure 3.1(a). In this scheme, only the output from one antenna is monitored at any given time. If an outage occurs at the current antenna, the system quickly scans the remaining antennas for one which has sufficient signal strength. The data transmitted during the time it takes to find a new antenna is lost. A slightly more powerful technique known as selection diversity [RCM96] is given in Figure 3.1(b). With selection diversity all antennas are monitored simultaneously, and when the signal level falls below the

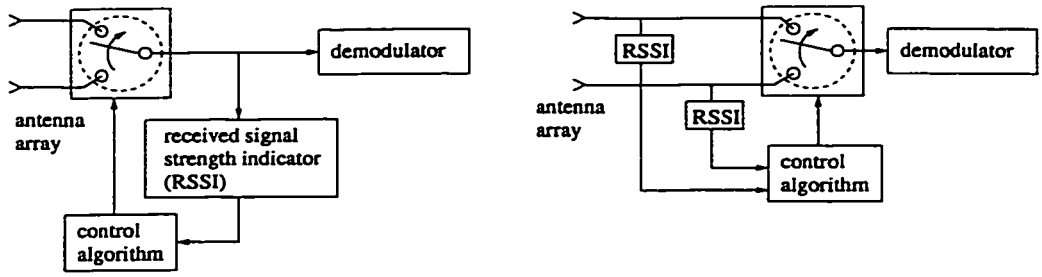

Figure 3.1: (a) Switched Diversity. (b) Selection Diversity.

threshold the control algorithm switches to the antenna with the highest gain. It should be noted that with selection and switched diversity, the outputs from multiple antennas are not combined, so the antenna radiation pattern is omnidirectional. The optimum beamforming technique which will be explained next is much more powerful since it dynamically changes the radiation pattern to optimize SINR performance.

3.4 Optimal Reverse Link Beamforming Solution for Adaptive Antenna Array

In this section the optimal reverse link solution to the adaptive array beamformer is derived. This is the type of smart antenna which will be used in this thesis, and the term smart antenna will be synonymous with adaptive antenna array from here on. The optimum solution derived here minimizes the mean square error between the output of the beamformer and a reference signal. The derivation given here closely resembles that given in [Hay96]. An alternate derivation in which the mean signal to mean interference plus noise ratio is maximized is given in [App76].

Figure 3.2 is a diagram of the reverse link smart antenna beamformer. The received baseband signal at time k at antenna i is $u_i(k)$. The output of the beamformer, $y(k)$, is equal to

$$y(k) = \sum_{i=1}^{N} w_i^* u_i(k), \tag{3.1}$$

where N is the number of antennas, and * denotes the complex conjugate. The complex weights w_i are conjugated to conform to the definition of a complex inner

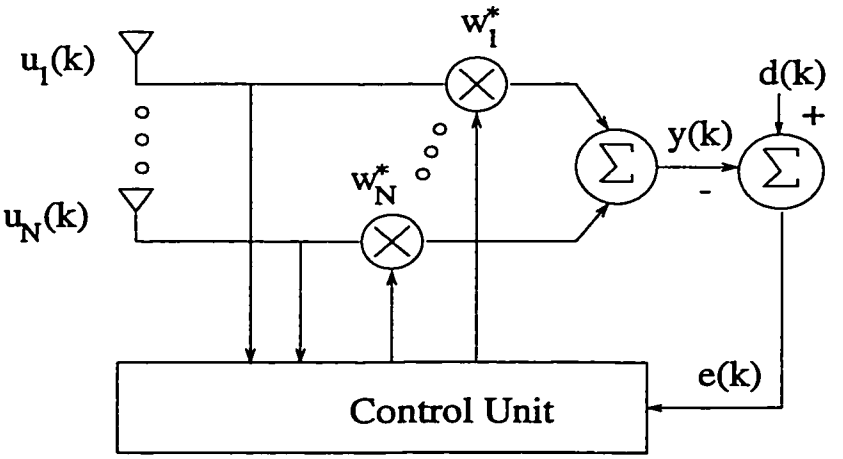

Figure 3.2: Smart antenna beamformer.

product.

The error between the output and the training sequence $d(k)$ is

$$\begin{aligned} e(k) &= d(k) - y(k) \\ &= d(k) - \sum_{i=1}^{N} w_i^* u_i(k). \end{aligned} \tag{3.2}$$

The mean square error J is therefore equal to

$$\begin{aligned} J &= E[|e(k)|^2] \\ &= E[e(k)e^*(k)] \\ &= E[|d(k)|^2] - \sum_{i=1}^{N} w_i^* E[u_i(k)d^*(k)] - \sum_{i=1}^{N} w_i E[u_i^*(k)d(k)] + \ldots \\ &\quad \sum_{i=1}^{N}\sum_{j=1}^{N} w_i^* w_j E[u_i(k)u_j^*(k)]. \end{aligned} \tag{3.3}$$

The first term is the power of the training sequence. Therefore,

$$E[|d(k)|^2] = \sigma_d^2. \tag{3.4}$$

The cross-correlation between $u_i(k)$ and $d(k)$ is defined as

$$p(i) = E[u_i(k)d^*(k)]. \tag{3.5}$$

The autocorrelation between $u_i(k)$ and $u_j(k)$ is defined as

$$r(i-j) = E[u_i(k)u_j^*(k)]. \tag{3.6}$$

Substituting (3.4),(3.5), and (3.6) into (3.3) yields

$$J = \sigma_d^2 - \sum_{i=1}^{N} w_i^* p(i) - \sum_{i=1}^{N} w_i p^*(i) + \sum_{i=1}^{N}\sum_{j=1}^{N} w_i^* w_j r(i-j). \tag{3.7}$$

The mean square error given above is a second order function of the weights, and it looks like an N-dimensional bowl shaped surface with a unique global minimum.

At the minimum value of J, $\frac{\partial J}{\partial w_i^*} = 0$ for all $i = 1, \ldots, N$. By using the rules $\frac{\partial w_i}{\partial w_i^*} = 0$ and $\frac{\partial w_i^*}{\partial w_i^*} = 1$, and the chain rule of calculus,

$$\frac{\partial J}{\partial w_i^*} = -p(i) + \sum_{j=1}^{N} w_j r(i-j). \tag{3.8}$$

Setting the above to 0 for all $i = 1, \ldots, N$, we get the following set of N linear equations.

$$\sum_{j=1}^{N} w_j r(i-j) = p(i), \qquad \text{for all } i = 1, \ldots, N. \tag{3.9}$$

In matrix form, the above can be written in the form

$$\mathbf{R}\mathbf{w}_o = \mathbf{p}, \tag{3.10}$$

where

$$\mathbf{R} = E[\mathbf{u}(k)\mathbf{u}^H(k)], \tag{3.11}$$

$\mathbf{w}_o$ is the $N \times 1$ optimal weight vector,

$$\mathbf{p} = E[\mathbf{u}(k)d^*(k)], \tag{3.12}$$

and

$$\mathbf{u}(k) = [u_1(k)\, u_2(k)\, \cdots\, u_N(k)]^T. \tag{3.13}$$

The transpose ^{T} means rows and columns are interchanged. The hermitian transpose ^{H} means the transpose is conjugated.

The autocorrelation matrix $\mathbf{R}$ and the cross-correlation vector $\mathbf{p}$ can now be specified for the special case of M narrowband signals and white noise impinging upon the smart antenna.

The received baseband signal $u_i(k)$ can be decomposed as

$$u_i(k) = \sum_{m=1}^{M} s_m(k) v_{m,i} + n_i(k), \tag{3.14}$$

where $s_m(k)$ is the symbol transmitted by mobile m, $v_{m,i}$ is the complex envelope of the carrier from mobile m at antenna i, and $n_i(k)$ is the independent noise process at antenna i. The probability density function of the magnitude of the envelope arising under different propagation conditions was discussed in Section 2.7. $s_m(k)$ is real valued for digital modulation schemes where phase information is not required (i.e. BPSK, PAM), and complex valued where it is (i.e. MPSK, QAM) [Skl88].

If the symbols from the different mobiles are orthogonal and of unit power, then

$$E[s_i(k)s_j^*(k)] = \begin{cases} 1, & i = j \\ 0, & i \neq j. \end{cases} \tag{3.15}$$

Similarly, if the noise process at each antenna output is white and of zero mean, then

$$E[n_i(k)n_j^*(k)] = \begin{cases} \sigma_n^2, & i = j \\ 0, & i \neq j. \end{cases} \tag{3.16}$$

Using (3.14),(3.15), and (3.16), (3.11) simplifies to

$$\mathbf{R} = \sum_{m=1}^{M} \mathbf{v}_m \mathbf{v}_m^H + \sigma_n^2 \mathbf{I}, \tag{3.17}$$

where $\mathbf{v}_m$ is the complex envelope vector pertaining to mobile m, which will be referred to as the station signature vector from here on.

Since the goal of the adaptive array beamformer is to receive a particular signal, say the signal from mobile d, $d(k)$ in (3.12) is set equal to $s_d(k)$. By using (3.14) and (3.15), (3.12) simplifies to

$$\mathbf{p} = \mathbf{v}_d. \tag{3.18}$$

From Equation (3.10), the optimal weight vector is equal to

$$\mathbf{w}_o = \mathbf{R}^{-1}\mathbf{v}_d. \tag{3.19}$$

The post-combining reverse link mean signal power to mean interference power plus noise ratio is equal to

$$\text{SINR}_r = \frac{|\mathbf{w}_o^H \mathbf{v}_d|^2}{\sum_{\substack{i=1 \\ i \neq d}}^{M} |\mathbf{w}_o^H \mathbf{v}_i|^2 + \sigma_n^2 \|\mathbf{w}_o\|_2^2}, \tag{3.20}$$

where $\| \cdot \|_2$ denotes the 2-norm of a vector. Substituting Equation (3.19) into Equation (3.20), and normalizing each weight vector to unity norm, we get

$$\text{SINR}_r = \frac{\frac{|\mathbf{v}_d^H \mathbf{R}^{-H} \mathbf{v}_d|^2}{\|\mathbf{R}^{-1}\mathbf{v}_d\|_2^2}}{\sum_{\substack{i=1 \\ i \neq d}}^{M} \frac{|\mathbf{v}_d^H \mathbf{R}^{-H} \mathbf{v}_i|^2}{\|\mathbf{R}^{-1}\mathbf{v}_d\|_2^2} + \sigma_n^2}. \tag{3.21}$$

If the same weights are applied on the forward link, we get

$$\begin{aligned} \text{SINR}_f &= \frac{|\mathbf{w}_o^H \mathbf{v}_d|^2}{\sum_{\substack{i=1 \\ i \neq d}}^{M} |\mathbf{w}_i^H \mathbf{v}_d|^2 + \sigma_n^2} \\ &= \frac{\frac{|\mathbf{v}_d^H \mathbf{R}^{-H} \mathbf{v}_d|^2}{\|\mathbf{R}^{-1}\mathbf{v}_d\|_2^2}}{\sum_{\substack{i=1 \\ i \neq d}}^{M} \frac{|\mathbf{v}_i^H \mathbf{R}^{-H} \mathbf{v}_d|^2}{\|\mathbf{R}^{-1}\mathbf{v}_i\|_2^2} + \sigma_n^2}. \end{aligned} \tag{3.22}$$

The expected value of Equations (3.21) and (3.22) are in fact identical so reverse and forward link SINRs are on average the same when the weights are scaled to have unity norm. The SNR for the reverse link is defined to be the mean signal power to mean noise power ratio at each antenna output, so it is equal to

$$\text{SNR} = \frac{E[|v_{m,i}|^2]}{\sigma_n^2}, \tag{3.23}$$

where $v_{m,i}$ is the signature of user m at antenna i. For the forward link, the SNR is the total mean signal power to mean noise power at the portable station antenna output which is equal to

$$\text{SNR} = \frac{NE[|w_{om,i} v_{m,i}|^2]}{\sigma_n^2} = \frac{E[|v_{m,i}|^2]}{\sigma_n^2}, \tag{3.24}$$

where $E[|w_{om,i}|^2] = 1/N$ is the i^{th} element of the weight vector for transmitting to mobile m.

3.4.1 Adaptive Algorithms

The optimal weight vector $\mathbf{w}_o$ in Equation (3.19) requires the autocorrelation matrix $\mathbf{R}$ and the cross-correlation vector $\mathbf{p}$ to be known in advance. In practice this is not possible since the channel is not known a priori, and in general it is time variant so $\mathbf{w}_o$ needs to be a function of time k. A number of algorithms have been developed which give a close to optimal solution of the weight vector. These algorithms vary in terms of converge time and implementation complexity. A few of these algorithms, summarized from [LL96] are described below.

The least-mean squares (LMS) algorithm [Smi80] is based on the steepest-descent method. The LMS algorithm uses the intuitively satisfying rule that the weight vector corrections should be made in the negative of the direction of the gradient. Therefore, the updated weight vector at time $k+1$ is computed as

$$\mathbf{w}(k+1) = \mathbf{w}(k) + \frac{1}{2}\mu[-\nabla(E[|e(k)|^2])], \tag{3.25}$$

where $\nabla(E[|e(k)|^2])$ is the multidimensional complex gradient vector. From Equation (3.8), it can be seen that the above can be written as

$$\mathbf{w}(k+1) = \mathbf{w}(k) + \mu[\mathbf{p} - \mathbf{R}\mathbf{w}(k)]. \tag{3.26}$$

In the LMS algorithm, the time averages $\mathbf{R}$ and $\mathbf{p}$ are replaced with instantaneous values so

$$\begin{aligned} \hat{\mathbf{w}}(k+1) &= \hat{\mathbf{w}}(k) + \mu\mathbf{u}(k)[d^*(k) - \mathbf{u}^H(k)\hat{\mathbf{w}}(k)] \\ &= \hat{\mathbf{w}}(k) + \mu[\mathbf{u}(k)e^*(k)], \end{aligned} \tag{3.27}$$

where μ is the gain constant which controls the learning rate of the algorithm. The LMS algorithm runs very fast, and it works well when the statistics related to the signal environment are stationary. When the eigenvalues of the $\hat{\mathbf{R}} = \mathbf{u}(k)\mathbf{u}^H(k)$ matrix are widely spread, the convergence is slow.

The Direct Matrix Inversion (DMI) technique has a faster convergence rate. Estimates of $\mathbf{R}$ and $\mathbf{p}$ are used directly in Equation (3.19). The estimates are evaluated over the observation interval from time s to f as

$$\hat{\mathbf{R}} = \sum_{k=s}^{f} \mathbf{u}(k)\mathbf{u}^H(k), \tag{3.28}$$

and

$$\hat{\mathbf{p}} = \sum_{k=s}^{f} d^*(k)\mathbf{u}(k), \tag{3.29}$$

respectively. The estimate of the weight vector is then equal to

$$\hat{\mathbf{w}} = \hat{\mathbf{R}}^{-1}\hat{\mathbf{p}}. \tag{3.30}$$

A larger window size $f - s$ is better in a slowly changing environment since a greater number of samples improve the processing gain against noise. In fact, in [RMB74] it was shown that with a window size equal to twice the number of antennas, the SINR obtained using $\hat{\mathbf{w}}$ is within 3 dB of the optimum SINR. In a time-varying environment DMI can be used by recomputing the weight vector at regular intervals. The primary difficulty of this technique is the increased computational complexity of matrix inversion, and the numerical instability resulting from the use of finite-precision arithmetic.

The recursive least squares (RLS) algorithm can be used to achieve a faster convergence rate. In the RLS algorithm all of the samples from time 1 to the current time k are used to compute the weight vector. Also, the weighing factor $0 \leq \lambda \leq 1$ is used to place greater emphasis on more recent samples. The estimates of $\mathbf{R}$ and $\mathbf{p}$ are written as

$$\mathbf{R}(k) = \sum_{i=1}^{k} \lambda^{k-i}\mathbf{u}(i)\mathbf{u}^H(i) \tag{3.31}$$

and

$$\mathbf{p}(k) = \sum_{i=1}^{k} \lambda^{k-i}\mathbf{u}(i)d^*(i). \tag{3.32}$$

If the terms corresponding to $i = k$ are factored out in both Equations (3.31) and (3.32),

$$\mathbf{R}(k) = \lambda\mathbf{R}(k-1) + \mathbf{u}(k)\mathbf{u}^H(k) \tag{3.33}$$

and

$$\mathbf{p}(k) = \lambda\mathbf{p}(k-1) + d^*(k)\mathbf{u}(k). \tag{3.34}$$

Using the Matrix Inversion Lemma, the following recursive equation is obtained from Equation (3.33).

$$\mathbf{R}^{-1}(k) = \lambda^{-1}\mathbf{R}^{-1}(k-1) - \lambda^{-1}\mathbf{q}(k)\mathbf{u}^H(k)\mathbf{R}^{-1}(k-1), \tag{3.35}$$

where

$$\mathbf{q}(k) = \frac{\lambda^{-1}\mathbf{R}^{-1}(k-1)\mathbf{u}(k)}{1+\lambda^{-1}\mathbf{u}^H(k)\mathbf{R}^{-1}(k-1)\mathbf{u}(k)}. \tag{3.36}$$

The least squares estimate $\hat{\mathbf{w}}(k)$ can then be written as

$$\begin{aligned}\hat{\mathbf{w}}(k) &= \mathbf{R}^{-1}(k)\mathbf{p}(k) \\ &= \hat{\mathbf{w}}(k-1) + \mathbf{q}(k)[d^*(k) - \mathbf{u}^H(k)\hat{\mathbf{w}}(k-1)]\end{aligned} \tag{3.37}$$

The important feature of the RLS algorithm is that the inversion of the $\mathbf{R}$ matrix is propagated using Equation (3.35), which is much faster than taking a matrix inverse directly. Under high SNR, the RLS algorithm typically converges at a rate one order of magnitude higher than the LMS algorithm.

All of the above algorithms require a training sequence $d(k)$ which is known by both the transmitter and receiver. If useful information is to be sent over the channel, obviously this training sequence cannot be sent continuously. If the channel is varying relatively slowly, then the training sequence can be periodically retransmitted to re-initialize the beamformer. Another effective approach which can be employed is the use of decision directed equalization [LSEJW68]. Since under normal operating conditions the bit error rate is low, the output of the decision device of the receiver can be used as the desired response. This permits the beamformer to track the changes in the channel without the need for a training sequence to be periodically sent by the transmitter. Note, however, that it is necessary to initialize the system with a known training sequence so that the bit error rate is sufficiently low before decision directed equalization can be used.

3.4.2 Outage Probability with Optimum Beamforming

In this section the outage probability with optimum beamforming is examined. The outage probability is the probability that the optimum post-combining SINR given by Equation (3.21) is below the specified threshold SINR_{min}. SINR_{min} depends on things such as the modulation scheme, channel encoding, and the maximum bit error probability [Skl88]. We choose outage probability since it can be used to determine the region in which most of the users have sufficient SINR. Other measures of

Parameter	Value
Mobiles (M)	4
Antennas (N)	8
Array geometry	Circular
Antenna separation	1.2λ
$SINR_{min}$ (Minimum post-combining SINR)	10 dB
pre-combining SNR at antenna outputs	10 dB
Slow fading	None
Fast fading model	Rayleigh
Path loss	none

Table 3.1: Default parameters for outage probability curves.

the smart antenna performance are the mean post-combining SINR [STKL97b] and the maximum error-free data rate normalized to the single antenna Shannon capacity [SXLK98]. The following default parameters are used unless otherwise specified.

Antenna Geometry

In Section 2.7.3, it was explained that in an U-LOS situation, there is a strong deterministic component impinging upon the array. In this section the component of station signature vector due to the deterministic component for a circular and linear array is developed.

Figure 3.3 shows a uniformly spaced linear array with N antenna outputs. The antenna outputs are indicated by a $\bullet$ in the figure. The spacing between the elements is d. Careful attention needs to be given in selecting the value for d. If d is too small, then the antenna outputs become too correlated. If d is too large, then grating lobes appear [LL96], which means that the same signature vector arises from different directions. If the source of the signal is far away from the array, then the impinging signal can be approximated as a plane wave. If the arrival angle of the plane wave with respect to the array normal is θ, then the path distance between two adjacent antenna outputs is $d\sin\phi$. The phase difference in radians is therefore equal to $\frac{2\pi}{\lambda}d\sin\phi$. Hence,

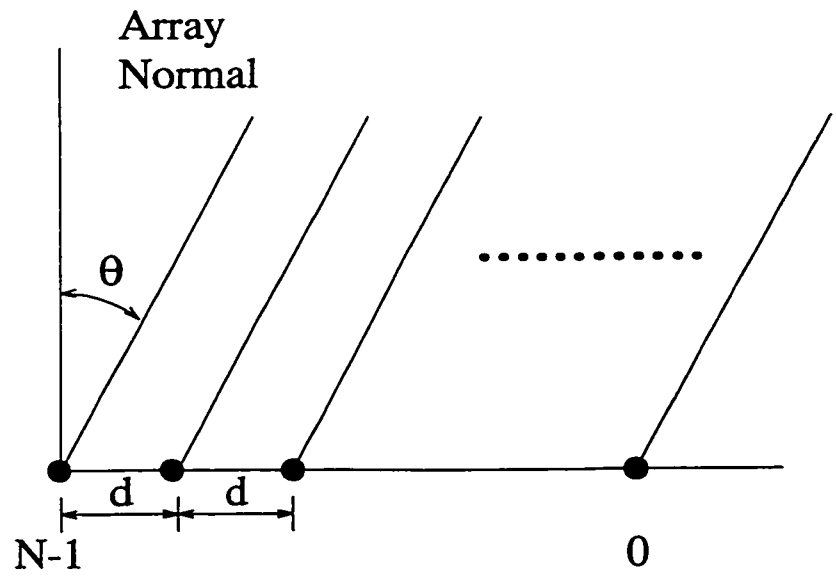

Figure 3.3: Linear array with N elements.

the signature vector is equal to

$$\mathbf{v} = \sigma_d \begin{bmatrix} 1 \\ e^{-j\frac{2\pi}{\lambda}d\sin\phi} \\ e^{-j2\frac{2\pi}{\lambda}d\sin\phi} \\ \vdots \\ e^{-j(N-1)\frac{2\pi}{\lambda}d\sin\phi} \end{bmatrix}, \tag{3.38}$$

where σ_d is the voltage at the antenna output.

Figure 3.4 shows a circular array with N evenly spaced elements. The radius of the circle is R. If the arrival angle of plane wave is θ, then the relative phase of the k^{th} element with respect to the center of the array is $\frac{2\pi}{\lambda}R\cos(\theta - \theta_k)$, where θ_k is the angle of the k^{th} element. Hence, the signature vector is equal to

$$\mathbf{v} = \sigma_d \begin{bmatrix} 1 \\ e^{-j\frac{2\pi}{\lambda}R\cos(\theta-\frac{2\pi}{N})} \\ e^{-j\frac{2\pi}{\lambda}R\cos(\theta-\frac{4\pi}{N})} \\ \vdots \\ e^{-j\frac{2\pi}{\lambda}R\cos(\theta-\frac{2(N-1)\pi}{N})} \end{bmatrix}. \tag{3.39}$$

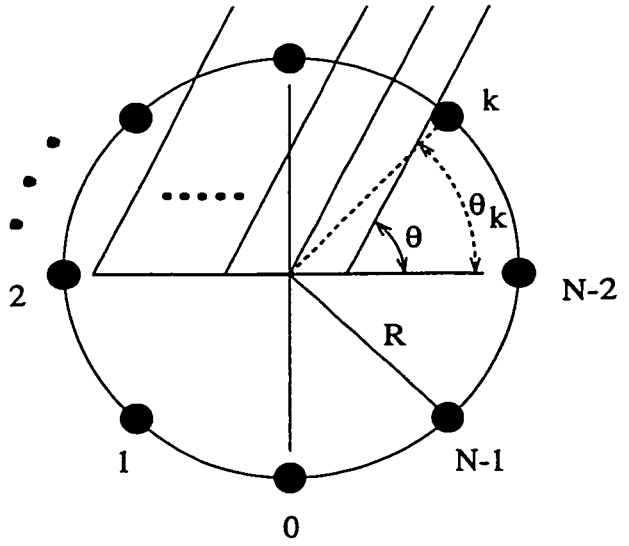

Figure 3.4: Circular array with N elements.

Figure 3.5 is a graph of the outage probability versus pre-combining SNR with the linear and circular array being used for the beamforming. The fast fading model employed is Rician with a strong deterministic component of $l = 0.80$, and a relatively weak deterministic component of $l = 0.30$. The remainder of the system parameters are listed in Table 3.1. With $l = 0.30$, the outage probabilities are almost identical. This is because most of the signal strength is from the multipath components, in which case the array geometry is immaterial. With $l = 0.80$, the linear array outage probability is significantly higher than the circular array outage probability. When most of the signal strength is from the deterministic component, the outage probability becomes more sensitive to the antenna geometry. In case of the linear array, the change in the phase with respect to θ is proportional to $\cos(\theta)$. This means that sources from which the arriving signal is near perpendicular to the array normal do not vary much in their signature. So if the desired station and one or more interfering stations are located near perpendicular to the array normal, the SINR after beamforming is weak. The circular array on the other hand is able to deal with signals originating from any angle equally well, so the SINR after beamforming is better. Figure 3.6 illustrates this point with a polar plot of the smart antenna output power after beamforming with a circular array and a linear array when the desired user is

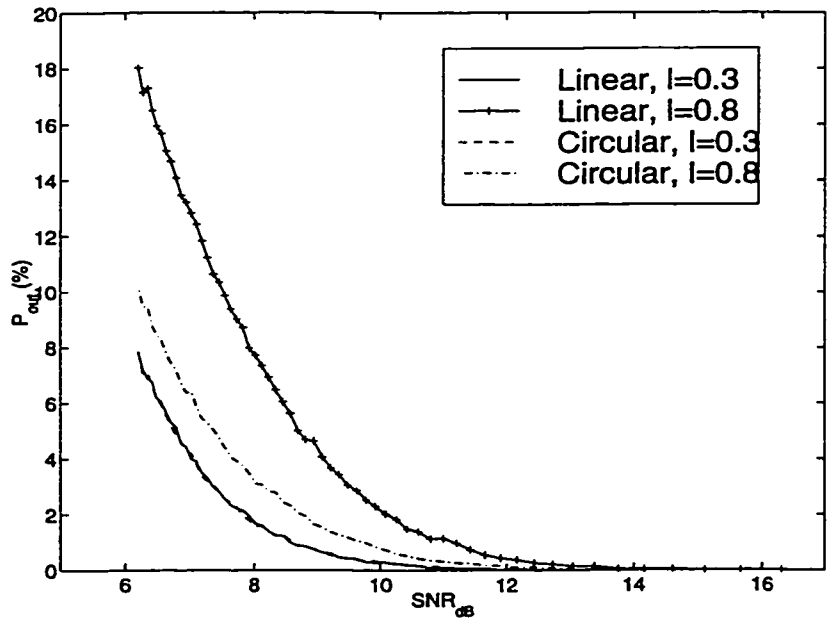

Figure 3.5: Circular and linear array outage probability with Rician signatures. The two overlapping lines correspond to $l = 0.3$.

90° from the array normal, and there is an interferer nearby. It can be seen here that the linear array is not able to put a strong null on the interferer from 115° even though it is 25° away. The circular array is able to null most of the power from this interferer, and hence has a post-combining SINR of 7.9 dB compared to just 2.1 dB for the linear array.

Power Control

The wide fluctuation in received signal strength leads to the capture effect. The capture effect is when a strong signal overpowers a weaker signal. This tends to degrade system performance as the desired signal may be too weak relative to the interferers. Figure 3.7 is a graph of outage probability versus pre-combining SNR for various levels of power control. In this figure exponential power path loss is included using Model 1 from Section 2.7.1 with $n = 3$. Also, lognormal slow fading with 10 dB standard deviation is present.

We now state the values for the probability distribution function of d and P_0 in

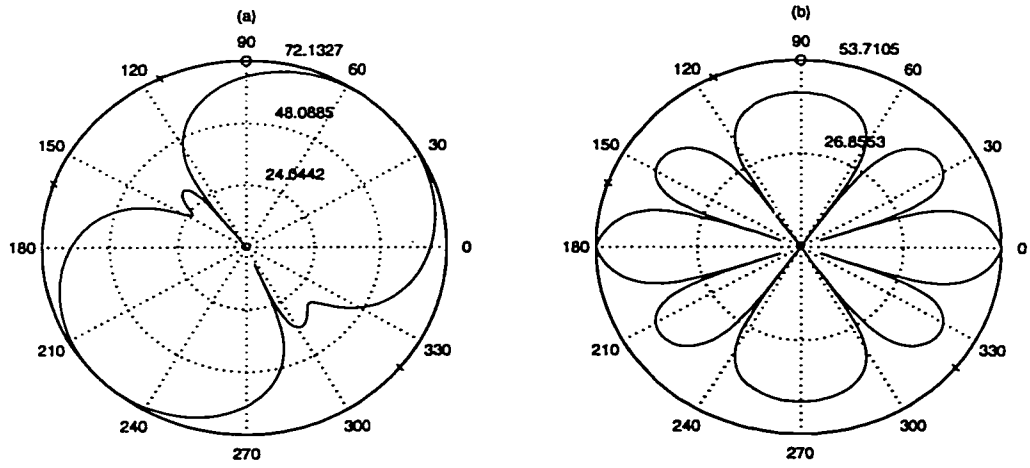

Figure 3.6: Post-combining array output power versus θ using a U-LOS only signature model. $M = 4$ mobiles, $N = 4$, 10 dB SNR, $\theta_d = 90°, \theta_i = 115°, 160°, 320°$. The o indicates the desired station and interfering stations are indicated with an x. (a) Circular array SINR=7.9 dB, (b) linear array SINR=2.1 dB.

Equation (2.2) from Section 2.7.1. Assume that the basestation is at the center of a donut in which portable stations can be located. The inner radius of the donut is R_i, and the outer radius is R_o. Portable stations are uniformly distributed in the donut. The probability density function of d is

$$f_d(r) = \begin{cases} \frac{200}{99} r & , 0.1 \leq r \leq 1.0 \\ 0 & , \text{otherwise,} \end{cases} \tag{3.40}$$

where R_i and R_o have been set to 0.1 and 1.0 without much loss of generality.

The three levels of power control depicted in Figure 3.7 are:

None With no power control the signal exhibits exponential path loss, lognormal slow fading, and Rayleigh fast fading.

Slow With slow power control, the effect of exponential path loss and lognormal fading is eliminated, while Rayleigh fast fading remains.

Full With full power control, the total received power summed across all elements is scaled to be the same for each user through a feedback mechanism. The

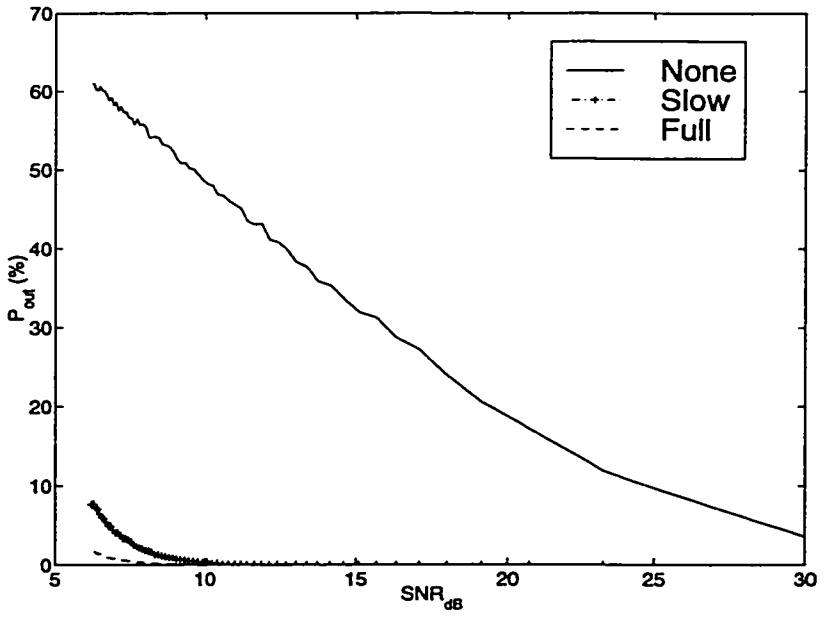

Figure 3.7: Optimum beamforming outage probability for different power control schemes.

signature $\mathbf{v}_m$ is scaled to $\mathbf{v}'_m$ as follows.

$$\mathbf{v}'_m = \frac{\sqrt{N(\mathrm{SNR})}\sigma_n}{\|\mathbf{v}_m\|_2}\mathbf{v}_m. \tag{3.41}$$

Without any power control, the outage probability exceeds one per cent for all depicted SNR levels in the figure. This is because the wide variation in power levels in the presence of noise makes it difficult for the array to mitigate the strong tendency of one station to overpower the others. With slow power control, a SNR of 8.6 dB or higher is sufficient for an outage probability of less than one percent. With full power control, 6.7 dB or higher SNR is sufficient. This important result indicates that with eight elements, with 10 dB SNR an antenna array can almost always receive the signal from a station in the presence of three interferers, providing slow or full power control is exercised.

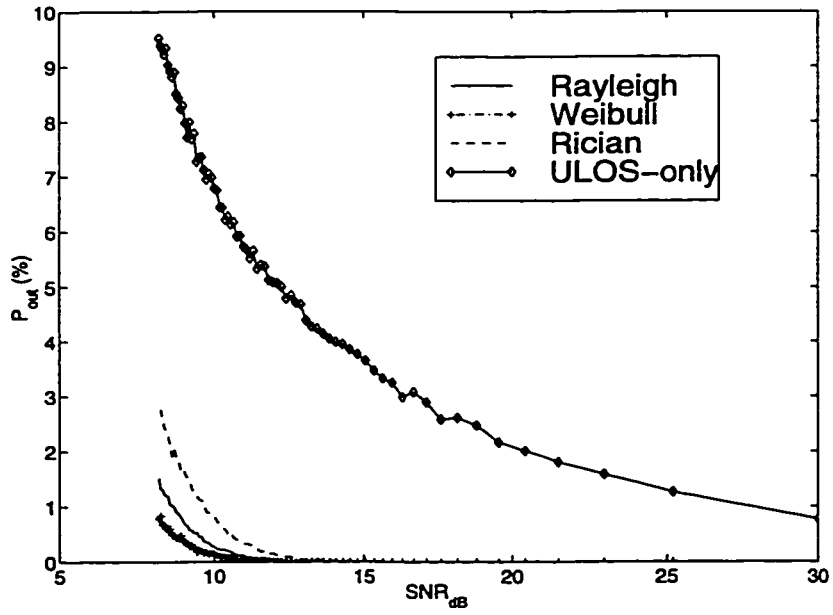

Figure 3.8: Optimum beamforming outage probability for different fast fading models.

Fast Fading Model

The fast fading model can also have an impact on the outage probability. Figure 3.8 is a graph of the outage probability for various fast fading models. The shaping parameter β is set equal to 2.53 for the Weibull distribution, which pertains to Room 112 from Table 2.1. The LOS-factor l for the Rician distribution is 0.80. The important thing to note from this graph is that ULOS-only fast fading, meaning all the signal power is coming from a single direction, fares much worse than the remaining three fast fading models which incorporate multipath. This is because signatures derived from a ULOS-only signature distribution span a smaller signal space. In fact, the entire signature vector can be characterized by 2 degrees of freedom, namely the amplitude and arrival angle.

Mutual Coupling

When a signal impinges upon an antenna output, part of it is reflected onto nearby antennas. This phenomenon is known as mutual coupling. Assuming ideal free space

path loss, the voltage at antenna output j due to mobile m with mutual coupling is

$$\hat{v}_{m,j} = v_{m,j} + \sum_{\substack{i=1 \\ i \neq j}}^{N} v_{m,i} \frac{\alpha}{d_{i,j}} e^{-j\frac{2\pi}{\lambda} d_{i,j}}, \tag{3.42}$$

where $d_{i,j}$ is the distance between antennas i and j, and α is the product of the mutual coupling coefficient and adjacent antenna separation. Therefore, the received voltage due to the reflection of a signal from an adjacent antenna is the mutual coupling coefficient times the voltage of the original signal. In matrix form,

$$\hat{\mathbf{v}}_m = \mathbf{M}\mathbf{v}_m, \tag{3.43}$$

where $\mathbf{M}$ is the $N \times N$ symmetric combining matrix. The elements $m_{i,j}$ of the combining matrix $\mathbf{M}$ are

$$m_{i,j} = \begin{cases} \frac{\alpha}{d_{i,j}} e^{-j\frac{2\pi}{\lambda} d_{i,j}}, & i \neq j \\ 1, & i = j. \end{cases} \tag{3.44}$$

Figure 3.9 is a graph of the outage probability for various degrees of mutual coupling. The values of α have been selected to correspond to a mutual coupling coefficient of 0.0, 0.1, and 0.3. For an α of 0.0 and 0.0195, the outage probability is less than one per cent for an SNR greater than 8.7 and 8.8 dB, respectively. For an α of 0.0585, at least 9.3 dB SNR is required for the outage probability to be below one per cent. Therefore as the mutual coupling increases, a greater SNR is required to have the same outage probability. This result is intuitively satisfying since the mutual coupling reduces the independence between the antenna output envelopes.

3.5 Conclusions

In this chapter smart antennas were considered in detail. Some key developments in the rich 40 year history of smart antennas were cited. Many of the important contributions in the application of smart antennas to packet switched data networks were reviewed. The optimum reverse link beamforming solution for the smart antenna was derived. The forward and reverse link SINRs obtained from the optimal beamforming were given. A few methods for obtaining an estimate of the optimum reverse link weight vector in a practical implementation were examined.

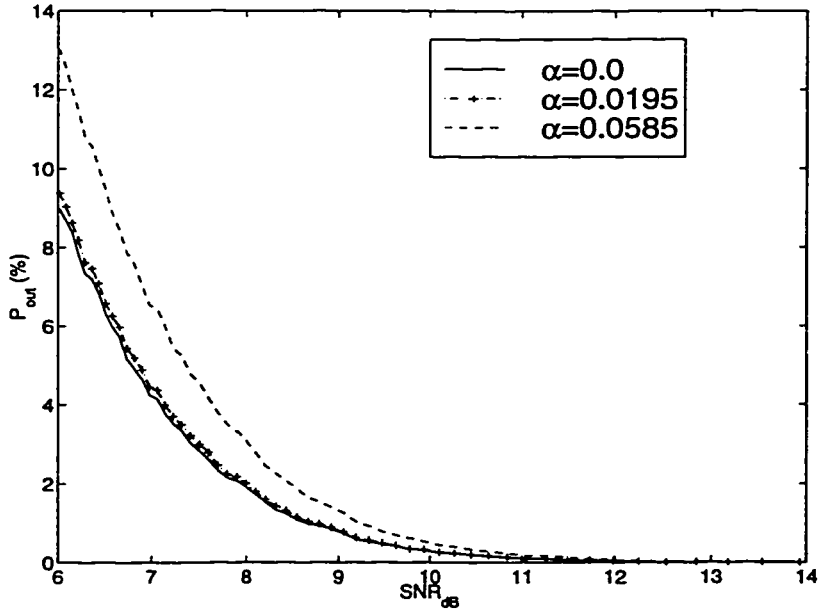

Figure 3.9: Optimum beamforming outage probability for various α's with an 8 element circular array of radius 0.51 m.

Outage probability curves for circular and linear arrays were used to demonstrate the superior performance of circular arrays. Through computer simulation it was determined that power control plays a key role in the outage probability performance of smart antennas. It was also determined that in general, a greater degree of multipath actually improves the performance of the smart antenna. Finally, the phenomenum of mutual coupling was examined. Simulation results showed that mutual coupling between the antenna elements has a negative impact on the smart antenna's output SINR.

Chapter 4

Dynamic Slot Allocation

4.1 Overview

The system considered in this chapter consists of the following entities: a wired network infrastructure, a smart antenna basestation, and a set of portable stations. For the purpose of this thesis, it is assumed that the wired network can reliably deliver packets between any pair of basestations, and the emphasis is on the efficiency of packet transfers between the basestation and the portable stations over a wireless channel. The portable stations are simple lightweight battery operated devices such as a cell phone, pager, or portable computer equipped with a WLAN adapter. For the results presented in this thesis, the portable stations need to be stationary or at most moving at pedestrian speed. The amount of traffic between portable stations within the wireless coverage area of the same basestation is considered minimal. Therefore, in the results considered all packets are exchanged between the basestation and the portable stations. Although various models for the wireless channel are investigated, most of the results correspond to a low SNR situation with heavy multipath.

The primary focus in this chapter is the SDMA/TDMA frame capacity of the system. In the SDMA/TDMA system, the time axis is divided into equal sized time slots in which simultaneous transmissions are possible due to the protection of the smart antenna. The problem of assigning the portable stations to the time slots in which they transmit is called dynamic slot assignment (DSA). The group of

contiguous time slots in which the DSA is done is called the frame. When a smart antenna basestation is used under time-division duplexing (TDD), the vector channel between each active station and the smart antenna basestation can be pre-sampled, and the channel measurement can be used to determine the antenna beamforming at a later time [STSK98, STKL97b]. This technique is called pre-sampled signature acquisition (PSA), and is theoretically possible provided channel coherence times are long compared with the turn-around time. The channel coherence time is the time duration for which the SINR after beamforming is sufficient using antenna weights which are fixed at the start of the frame. In this chapter the issues involved in PSA based SDMA/TDMA DSA are examined in depth. The frame capacity is emphasized over protocol capacity in order to quantify the capacity advantage of using PSA based SDMA/TDMA DSA for a wide variety of packet switched MAC protocols. The PSA based SDMA/TDMA DSA protocol capacity will be examined in detail for various slotted ALOHA protocols in the next chapter.

This chapter is organized as follows. In Section 4.2 the smart antenna basestation which is used to perform the beamforming is discussed. Section 4.3 contains experimental results which demonstrate the feasibility of SDMA in an indoor environment with heavy multipath. The experimental system is an 8 element circular antenna array operating at 1.86 Ghz. This testbed was developed at the Communications Research Laboratory (CRL) at McMaster University. First the ability of the smart antenna to resolve two stations in close physical proximity to each other is examined. This is done for both when an unobstructed line-of-sight (U-LOS) path exists between the smart antenna basestation and portable station and when it does not. Then the performance of the smart antenna is examined when there is pedestrian motion in the channel near the smart antenna, near the portable station, and in between. This is done when just a single portable station is transmitting, and also when an interfering portable station is present.

The remainder of this chapter discusses the DSA algorithms and their capacities under various conditions. Because the problem of performing optimal DSA is NP-complete, simple heuristic DSA algorithms are introduced in Section 4.4. These DSA algorithms dramatically increase SDMA/TDMA frame capacity under non-ideal

propagation situations. The results presented give clear insights into the network capacity possible in such systems and indicate the value of PSA-based DSA. The well known simulated annealing algorithm used for optimization is used to obtain a near upper bound on the DSA capacity in Section 4.5. Indoor vector channel measurements are then used to compare experimental DSA capacity performance with the capacity of the theoretical independent flat-Rayleigh fading model. In Section 4.5.4, the parameters of a first order autoregressive channel coherence time model are fitted to the experimental data, and the maximum length of a frame that can be generated through DSA is examined. Finally, in Section 4.6 a doppler fading model is used to evaluate the protocol capacity of a novel forward link polling based protocol. In this protocol the rapid variations in the channel due to doppler fading are used to actually improve the capacity and delay performance.

4.2 Smart Antenna Basestation

In the system considered, the basestation utilizes a smart antenna with N elements, and communicates with a set of portable stations. The stations are much simpler in design and use single omnidirectional antennas. It is assumed that the system considered uses time division duplexing (TDD). As discussed above, the basestation may be able to determine the correct beamforming for both transmission and reception after first measuring the vector channel response between each station and the array.

Under multiple beamforming SDMA operation, the basestation can attempt to transmit or receive up to n_{bfm} packets simultaneously by forming n_{bfm} antenna beam patterns. This is accomplished by having n_{bfm} parallel beamforming modules operating independently at the basestation. The basestation maintains a different set of weights in each beamforming module and each attempts to optimize the beam performance for one desired station packet transmission.

The system considered is shown in Figure 4.1. For simplicity, the conversion from the passband down to baseband is not indicated. Since the array receiver cannot receive from or transmit to more than N portable stations simultaneously, n_{bfm} is nominally set equal to N. For the reverse link the o denotes a splitter used to send

the signal from each antenna output n to the n^{th} branch of each beamformer. The • is a summer used to add all of the outputs from the beamformer to generate a scalar output. For the forward link, the • denotes a splitter which sends the symbol to be transmitted to all inputs of the beamformer. The o is a summer that adds up all of the signals to be transmitted at the antenna input. The reverse link and the forward link beamforming weights are determined using Equations (3.21) and (3.22), respectively, using the Direct Matrix Inversion (DMI) technique.

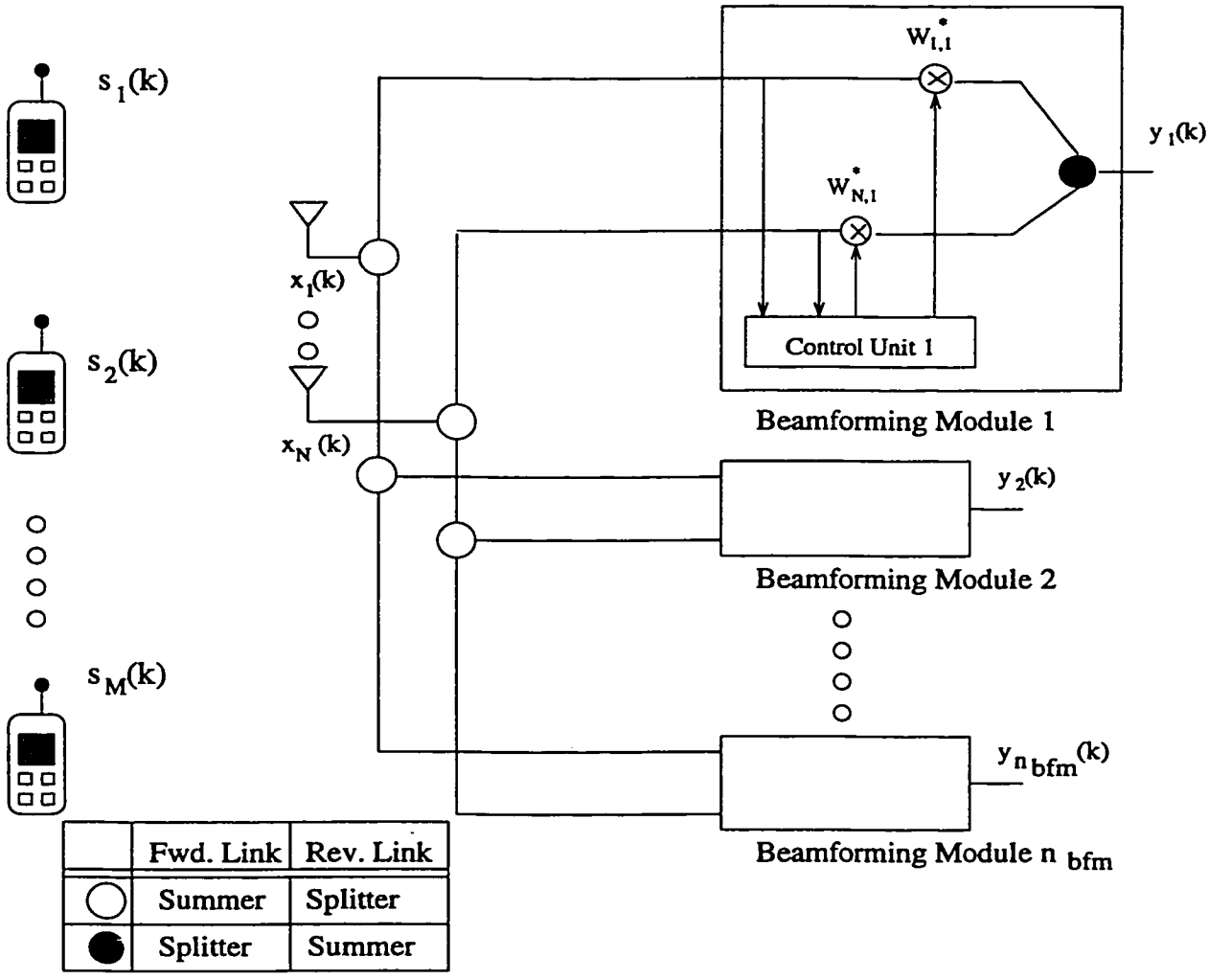

Figure 4.1: Basestation architecture for multibeam dynamic slot assignment.

4.3 Experimental Results

A large set of measurements were taken using the smart antenna constructed at the Communications Research Laboratory (CRL) at McMaster University. Most of the measurements were collected in narrowband directly, but some were taken in wideband and converted to narrowband offline. The method used for the conversion of the wideband samples to narrowband samples is described in Appendix A. Ideally the SNR of the elements of the sampled signature vector $\mathbf{v}$ should be infinity so any SNR can be achieved through offline noise injection. However, due to electrical and atmospheric noise, the SNR of the measurements presented in this thesis was 30 dB or higher. Figure A.7 in Appendix A shows the SNRs obtained from the wideband samples collected in room 103.

A photograph of the testbed used is given in Figure A.1 in Appendix A. Figure 4.2 is an illustration of the portable omnidirectional transmitter and the smart antenna testbed. The antenna used for the results in this chapter was a circular array with a center frequency of 1.86 Ghz. The array consisted of eight 2 dBi vertical dipoles and eight coherent receivers feeding a computer controlled data acquisition system. The array receivers had a noise figure of 5 dB. For the narrowband measurements, the receiver system was configured to have an effective bandwidth of 10 kHz, and the transmitter sent a continuous wave at 1.86 Ghz. For the wideband measurements, which were converted to narrowband, a 5 Mhz baseband pseudo-noise (PN) sequence was modulated by the transmitter. The array diameter for the wideband measurements was 0.20 m, and for narrowband it was 0.51 m. The transmit power was variable between 0 dBm and 30 dBm. Both the array and transmitter were located approximately 1.5 m above the floor.

The array was used to measure station signatures in various locations on the ground floor of the CRL building. The ground floor plan is given in Figure 4.3. Locations of the array and transmitter are marked on the figure for reference.

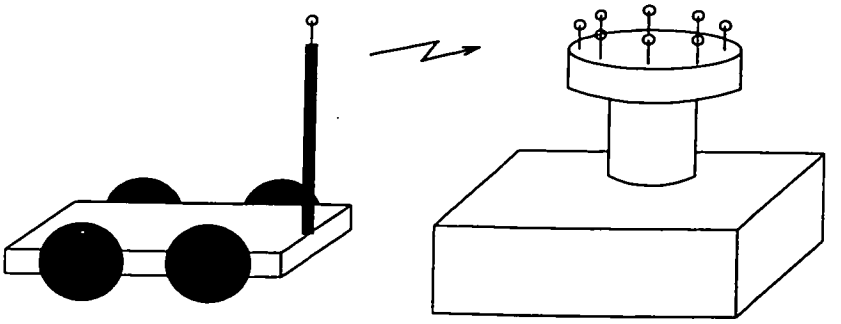

Figure 4.2: Smart antenna testbed.

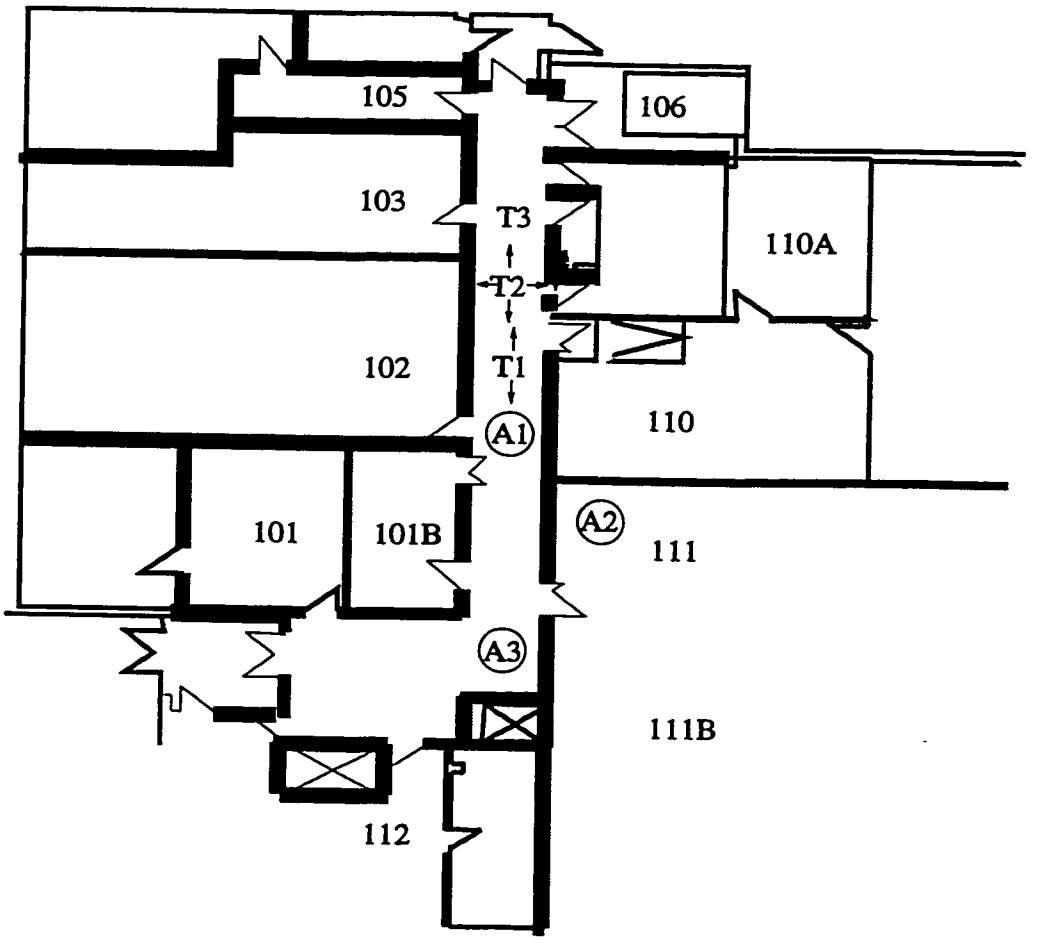

Figure 4.3: CRL ground floor plan.

4.3.1 Spatial Resolution of Stations

In this section the ability of the array to resolve stations in close physical proximity is considered. The resolution is possible because of significant levels of multipath. Information of this nature is useful in that if two or more stations cannot be resolved within distances on the order of several meters, then indoor SDMA operation might be severely limited for that reason alone.

Using the array, station signature measurements were taken at different transmitter locations. The nominal location of the transmitter is shown as position "T2" in Figure 4.3. The measurements were taken by precisely moving the transmitter in 2 cm increments both along and across the hallway as shown. This experiment was performed with the receiving array at location "A3". In this case there was an unobstructed line-of-sight (U-LOS) path between the transmitter and the array. In the second case the array was placed at location "A2" and measurements were taken with the transmitter moved in 1 cm steps along hallway position "T1". In this case the array was in a different room and thus there was no unobstructed line-of-sight (NU-LOS) path between the two.

The results are shown in Figure 4.4. This figure is a plot of the mean SINR, after optimal beamforming, for the desired station in the presence of the interfering one as a function of the distance between them normalized to the carrier wavelength λ. When the stations are separated along the direction of line-of-sight, in the U-LOS case the SINR rises sharply to a maximum at a distance of roughly $\frac{\lambda}{4}$. In this case the SINR shows periodic behavior at distances equal to $\frac{\lambda}{2}$. This is due to the strong line-of-sight components present in this direction. This effect is quite strong and could have an appreciable impact on system performance. Despite this, the overall ability of the array to resolve two stations on the same LOS-path to the array is quite good. This performance is attributed, in part, to different multipath components which allow the two stations to be distinguished by the array. In can be seen that when moving across the hallway perpendicular to the line-of-sight path the periodic effect does not occur. In this case the SINR rises slowly to its maximum value within a distance of roughly one λ. One the same graph the result for the NU-LOS case is shown. The results here are similar to the case just discussed. However in this case

the SINR rises to its maximum value more quickly.

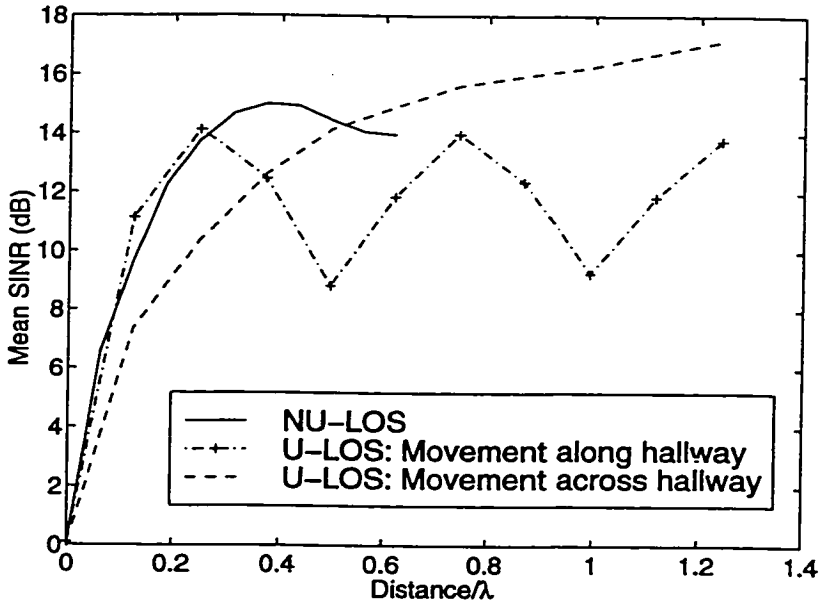

Figure 4.4: Station 1 spatial resolution with 2 stations, 10 dB SNR.

4.3.2 Channel Time Coherence Measurements

A requirement for the use of PSA for DSA is that the channel remain fairly correlated from the time that a station signature is measured until it is used. In this section the effects of finite channel coherence times that were obtained from the testbed measurements are considered. For these results, the desired station signature is first measured. Optimal SINR beamforming is then used to fix antenna weights. Changes in the SINR due to motion in the channel were then evaluated. Typical indoor pedestrian traffic was simulated while these measurements were made. This was done by having various numbers of people moving through the channel while the measurements were made. What follows is a description of an experiment who results are representative of a number that were performed.

In the experiment, the array was placed at location "A3" in Figure 4.3, and the transmitter at location "T3". Both the transmitter and the array were stationary for the duration of the experiment. The diameter of the array was 0.51 m. When the

experiment started, 500 measurements were taken of the received station signatures at 20 ms intervals. Data was collected for the cases where both 2 and 7 people were in motion near the transmitter, the array, and in between. The results are shown in Figures 4.5 and 4.6.

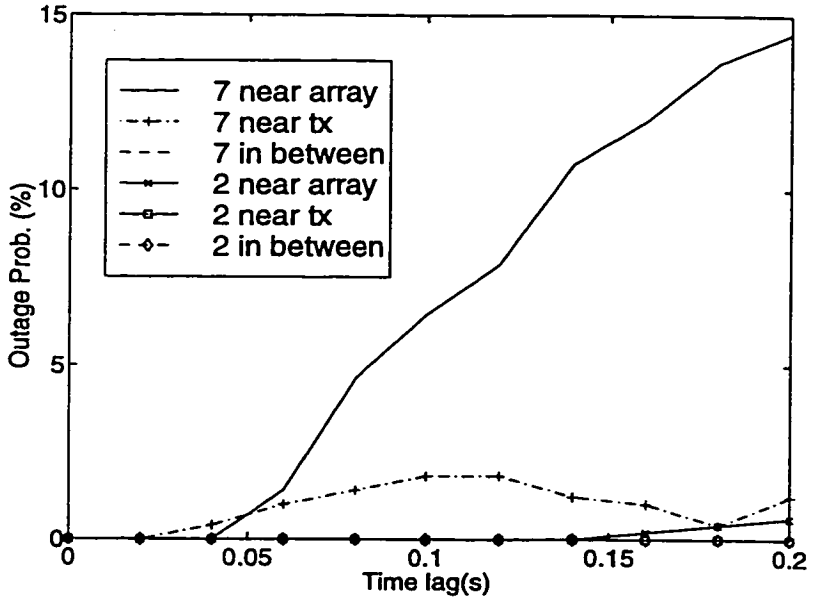

Figure 4.5: Channel coherence time, no interferers, SNR=10 dB. The legend indicates the number of walking pedestrians.

In Figure 4.5, the single station is active with no interferers at an input SNR of 10 dB at each antenna element. $SINR_{min}$ after beamforming is set to 10 dB in these curves. Consequently, at time 0, maximum ratio combining is being done which means that the gain in the presence of white noise is being maximized. The graph shows the increase in outage probability as the time lag increases for the various cases. It can be seen that motion near the array itself has a much stronger effect on channel coherence times. This is because with motion near the array, only some of the multipath components arriving to the array are disturbed, so the relative inter-element envelopes change significantly. This is followed by motion near the transmitter and finally motion in the region between. Motion near the transmitter affects most of the multipath components similarly, so the relative inter-element envelope changes are less significant. Motion in between intercepts fewer multipath components so the

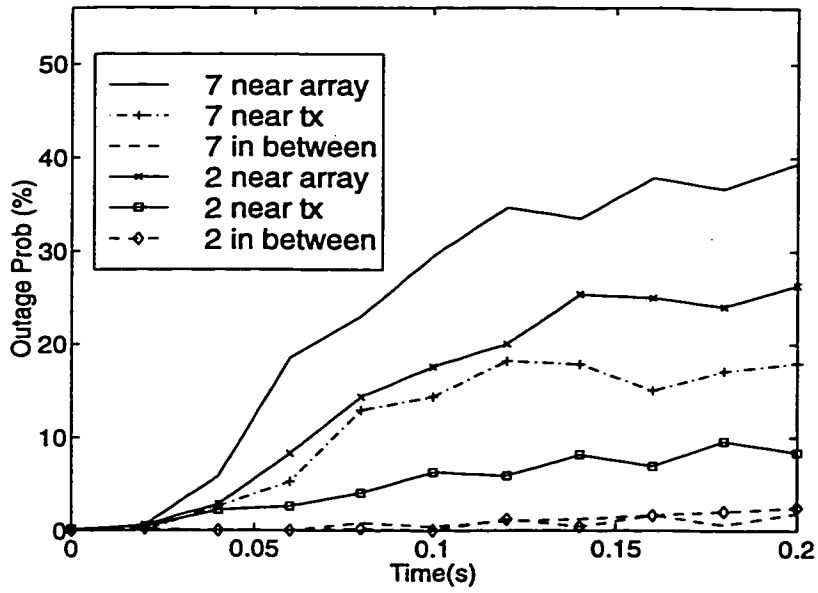

Figure 4.6: Channel coherence time, one interferer, SNR=10 dB.

signature does not change as much. Figure 4.5 suggests that for worst-case pedestrian motion, outages approaching 1 per cent may not occur until time lags of 60 ms or more are reached. Also, the curves suggest that provided human motion is prevented in the vicinity of the array itself, very little degradation in system performance may occur for much longer time intervals.

Figure 4.6 has a similar set of curves where in this case there is one desired station and one interfering station transmitting simultaneously. For the desired signal an additional source with independent Rayleigh fading between this station and each array element was simulated [Win87a]. Over the course of the experiment this received signal remained constant. However, for the interfering station the measured station signatures collected with the array were used. This situation can arise if the channel between the interfering station and the array varies, but the channel between the desired station and the array is time invariant. For example, people could be walking around the interferer, but the desired user could be in an isolated corner of the building where there are no other people. In Figure 4.6, a large number of trials were made with randomly chosen desired station signatures.

The results show a much more heightened sensitivity to movement in the channel. In this case, degradation due to motion in the channel can be very significant even for time intervals well below 100 ms. This is caused by the fact that the beamforming places a very steep null on the interferer so that any change in its signature is strongly felt. For this reason, the protocol design must carefully accommodate these effects. One method for dealing with a rapidly decorrelating channel in an SDMA environment is to increase the value of SINR_{min} in the allocation algorithms to some margin several dB's above the minimum required for adequate demodulation. This technique will be explored Section 4.5.4.

4.4 Multibeam SDMA/TDMA Capacity and Slot Assignment

In smart antenna basestations using TDD, the station signatures can be obtained by polling the active stations before actual user data is transmitted [Aca96, XL94]. Once a set of station signatures is known, the basestation then generates a SDMA/TDMA frame so that transmission can proceed. As in [XL94], it is assumed that these activities occur well within the coherence time of the channel.

In this chapter the focus is on the efficiency of the SDMA/TDMA frame generation process. T is defined to be the batch size, that is, the number of active stations that the basestation considers at a given time. The frame capacity is defined as the ratio of the time it takes to transmit the packets one after the other in omni-directional mode to the time it takes to transmit the packets in SDMA/TDMA mode. It is equal to

$$C_f = \frac{\sum_{k=1}^{n} T}{\sum_{k=1}^{n} L_k}. \tag{4.1}$$

This equation simplifies to

$$\begin{aligned} C_f &= \frac{nT}{\sum_{k=1}^{n} L_k} \\ &= \frac{T}{E[L]}, \end{aligned} \tag{4.2}$$

where $E[L]$ is the ensemble average of the length of the frame. The subscript f is used to emphasize that this is only the frame capacity, meaning the additional protocol overhead incurred due to the use of the smart antenna is not taken into account.

The objective of the frame generation process is to place all T stations into the frame such that $E[L]$ is minimized. This objective is subject to the constraint that the SINR for all stations exceeds an acceptable threshold, SINR_{min}. Since T is fixed for each frame generated, doing this will clearly minimize C_f subject to this constraint. This problem can be shown to be NP-complete. The proof for NP-completeness is given in Appendix B.

4.4.1 SDMA/TDMA Dynamic Slot Assignment Algorithms

In the frame construction process, stations can be allocated to time slots in any fashion as long as

$$\text{SINR}_i \geq \text{SINR}_{min}, \tag{4.3}$$

for each station i. Generally the required SINR_{min} depends on the modulation scheme, acceptable bit error rate, and the channel encoding. For this thesis a relatively conservative value of 10 dB is used. The DSA algorithms are described as follows in increasing order of complexity. In the algorithm descriptions, it is assumed that any station can always be accommodated with the required SINR when assigned to a slot by itself. This is not necessarily the case in practice, but in the results presented, this outage probability is negligible.

Random (or FCFS) SDMA/TDMA : The simplest form of allocation is referred to as Random or first-come-first-served (FCFS). In this scheme, stations are assigned to the current time slot in the order in which they occur. The algorithm begins by adding stations to time slot 1. Each time a station is added to the slot, optimal SINR beamforming is used to test if all stations in the slot satisfy Equation (4.3). The algorithm advances to the next time slot as soon as adding a station violates the constraint. The violating station is the first one placed in the next slot. The problem with this method is that if two consecutive stations are incompatible, the algorithm will advance to the next slot even if an unallocated

compatible station exists. However, the complexity of this algorithm is very low.

Equal Norm SDMA/TDMA : A $T \times T$ compatibility matrix is formed at the start of the frame, where element $T_{i,j}$ is defined as

$$T_{i,j} = \min\left(\frac{\|v_i\|_2^2}{\|v_j\|_2^2}, \frac{\|v_j\|_2^2}{\|v_i\|_2^2}\right). \tag{4.4}$$

The current slot is initialized to time slot 1. The first unallocated station is placed in the current time slot. The algorithm then attempts to add the unallocated station whose minimum compatibility with the stations already allocated to the current slot is maximized. If Equation (4.3) is satisfied for each station, the algorithm continues to search for more stations to add to the same slot. Otherwise, the slot is advanced and the algorithm restarts. Intuitively, this algorithm attempts to place stations with similar power levels in the same time slot.

Orthosigs SDMA/TDMA This is almost the same as Equal Norm SDMA/TDMA DSA, expect that

$$T_{i,j} = 1 - \frac{|\mathbf{v}_i^H \mathbf{v}_j|^2}{\|\mathbf{v}_i\|_2^2 \|\mathbf{v}_j\|_2^2}. \tag{4.5}$$

This algorithm therefore attempts to place stations whose electrical signatures are most orthogonal into the same time slot.

First Fit SDMA/TDMA : The algorithm starts at time slot 1. The first unallocated station is placed into the current time slot. The remaining unallocated stations are searched for the first one where Equation (4.3) is satisfied for all allocated stations when that station is added to the current slot. If one is found, it is added and the algorithm continues. Otherwise, the algorithm advances to the next time slot and starts again.

Best Fit SDMA/TDMA : Initially, the station signatures are sorted in order of ascending power. As before, the algorithm starts with slot 1. The first unallocated station is then placed into the current time slot. The algorithm then

Algorithm	time (ms) with $T = 40$	time (ms) with $T = 50$
Random	0.311	0.388
Random Sorted	0.312	0.390
First Fit	14.3	22.3
First Fit Sorted and Best Fit	14.3	22.3
Equal Norm	0.323	0.407
Orthosigs	0.355	0.457

Table 4.1: Worst case DSA computation time with 1600 MIPS DSP, N=8 antennas.

tests each unallocated station by calculating the SINR_i for each station in the current slot if the candidate station were to be added. The station which would result in the largest minimum SINR_i among the stations already in the current time slot is added, provided that Equation (4.3) is satisfied. If successful, the algorithm continues to search for more stations to add to the current time slot. Otherwise, the algorithm advances to the next time slot.

Note that sorting the signatures in order of ascending power is beneficial since it helps prevent those with higher power from overpowering the others. Also, since lower power signals are also competing with a relatively large amount of noise, it is best to allocate them at the start of the frame where there are more unallocated stations to test. The Random and First Fit TDMA algorithms can also be used with power pre-sorting. The worst case order of the algorithms in terms of the number of floating point operations (FLOPS) is given in Appendix C. Table 4.1 shows the maximum amount of time which it would take to perform the DSA with $T = 40$ and $T = 50$ using a DSP processor capable of 1600 MIPS. With Random allocation, it takes well below 1 ms so the computational complexity is almost negligible. With the stronger DSA algorithms it can become significant so the batch size T should be selected with this in mind. It should be noted that in practice it may take much lesser time to perform the DSA.

4.4.2 SDMA/TDMA Simulated Frame Capacity Results

This section contains a representative sample of the simulated frame capacity curves for the DSA algorithms. In these curves, the channel between each station and basestation antenna element is assumed to have independent Rayleigh fading [Win87a]. As a result, the components of each received station signature vector, $\mathbf{v}_d$, are independent complex Gaussian variates. An $N = 8$ element smart antenna is used. In addition, the vectors are independent from station to station. Each point shown on the graph was obtained via simulation by randomly choosing a large number of station signature sets of size T, and performing the DSA as discussed in Section 4.4.1.

In Figure 4.7 the frame capacity versus the number of stations T is graphed for a relatively low noise situation (20 dB SNR). It can be seen that there is very little distinction between the algorithms. This is because the noise level is so low that the antenna array can almost always null out 7 interferers (i.e., accommodate 8 users per slot). As a result, there is very little to be gained by a more intelligent slot allocation. In the infinite SNR case, the SDMA/TDMA DSA capacity is $\lceil \frac{T}{N} \rceil$ because each of $N - 1$ nulls removes one interferer. Note that the sawtooth drop of the curves is caused when a station is added that must be placed into a new slot by itself.

In Figure 4.8 a similar graph is shown for a higher noise situation (6 dB SNR). It can now be seen that variations between the different algorithms become very significant, especially when a higher number of stations is considered. This is because the more sophisticated algorithms have more stations to consider, so they are better able to generate good slot assignments. In the example shown, the Best Fit algorithm has a capacity roughly 58 per cent higher than the Random algorithm when 50 stations are considered. The trend in this figure is typical of other results that have been found. As the propagation conditions deteriorate, one expects increasing value in performing intelligent slot assignment. Note that the mean frame lengths generated in Figure 4.8 can be calculated using Equation (4.2). Even for 50 stations, the frame length is less than 10 for the best algorithms. In this set of curves the sawtooth drop noted above is less pronounced because the large amount of noise increases the variation in the number of users which are assigned to each slot.

In the previous results it has been assumed that there is sufficient power control

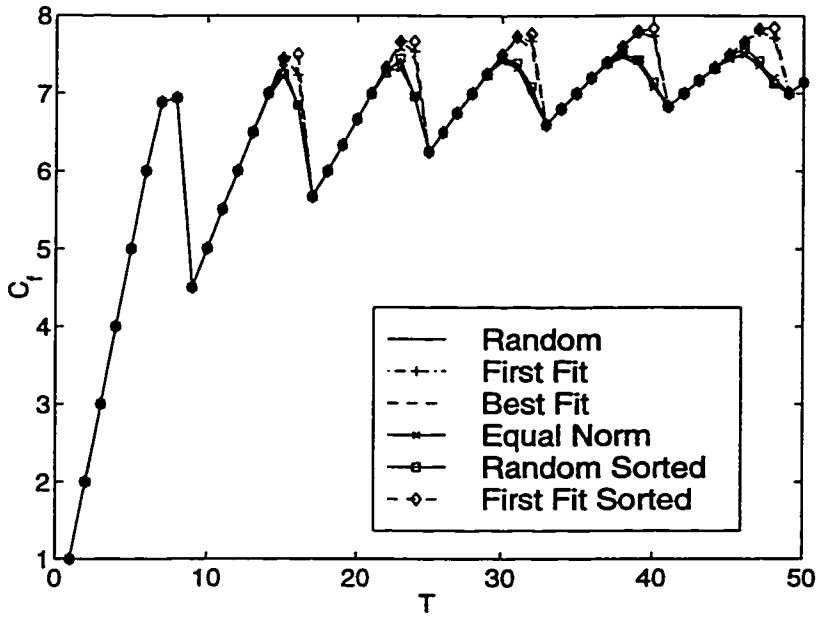

Figure 4.7: Frame capacity with simulated Rayleigh station signatures, 20 dB SNR.

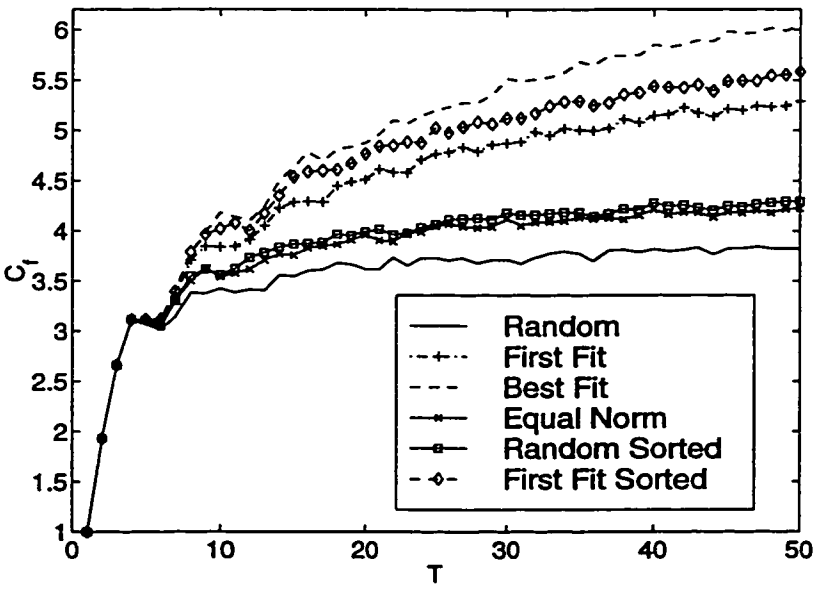

Figure 4.8: Frame capacity with simulated Rayleigh station signatures, 6 dB SNR.

to compensate for any shadowing and exponential power path-loss effects. Under the independent Rayleigh fading assumption, the expected power at the basestation for each portable station is the same. For fixed stations, it may be possible for the system to provide a more strict form of power control by having the station adjust its power through a feedback mechanism so that the total power received from each station summed across all antennas is identical (full power control from Section 3.4.2). As before, Equation (3.41) is applied to normalize the power from each station.

The result of applying this power control is shown in Figure 4.9. Compared to the same scenario without strict power control depicted in Figure 4.8, the Best Fit algorithm now performs about 10 per cent better. It can be seen from a comparison of the graphs that the value of DSA increases as power control becomes less ideal.

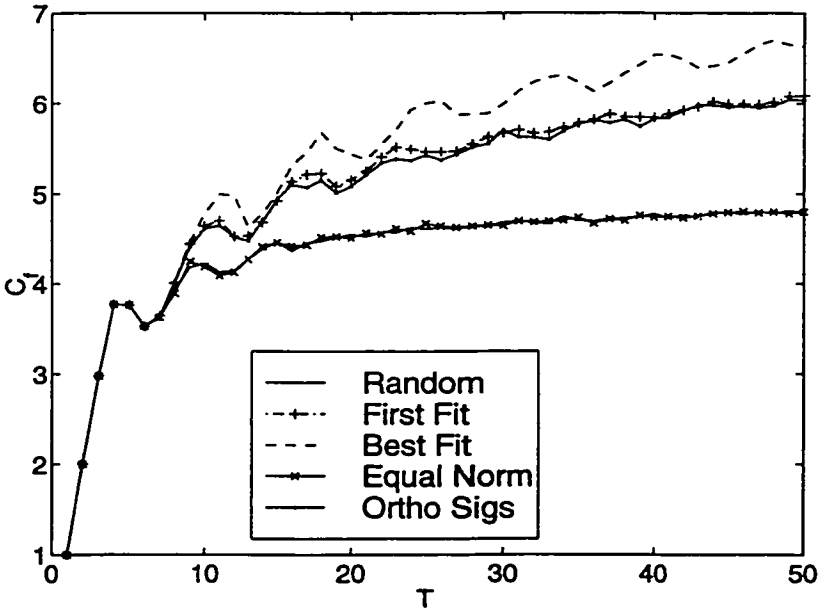

Figure 4.9: Frame capacity with simulated Rayleigh station signatures using full power control, 6 dB SNR.

Figure 4.10 is a graph of the capacity versus the pre-combining SNR. For Random and Equal Norm, the capacity starts to drop very rapidly below 13 dB SNR. For Orthosigs and First Fit, it starts to drop off rapidly below 9 dB SNR. With Best Fit the capacity remains fairly high until 7 dB SNR. This graph indicates that the

difference in the algorithms is most pronounced at low SNRs, and that the stronger algorithms fair much better under harsh operating conditions since they are able to search more extensively for signature compatibility.

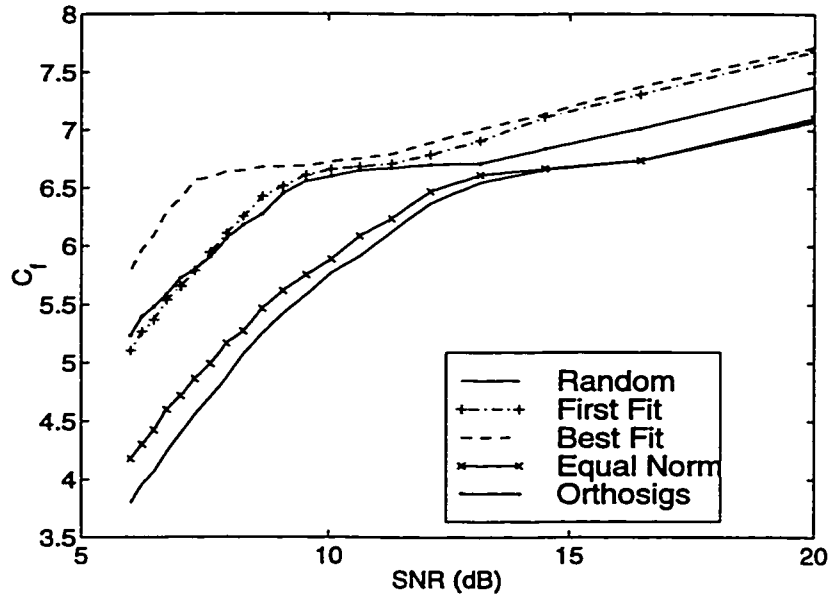

Figure 4.10: Frame capacity versus SNR, $T = 40$ stations.

Figure 4.11 is a graph of the capacity versus the number of antennas N. Initially as the number of antennas increases from 2 to 6, there is a super-linear increase in capacity. This suggests that having fewer than 4 antennas at 6 dB SNR does not provide sufficient gain to allow a capacity which is significantly higher than the omni-directional case. Beyond 6 antennas the increase in capacity is approximately linear with the number of antennas.

In the previous results it was assumed that a power control algorithm was able to remove the effect of exponential power path loss and lognormal shadowing. In the next two figures the influence of these two impairments to the wireless channel is examined. Figure 4.12 is a graph of the capacity versus the exponential power path loss exponent. Beyond a path loss exponent of 2 which corresponds to free space, there is a very dramatic drop in capacity for all of the DSA algorithms. With a path loss exponent of 4, which is often used when the basestation and receiver are

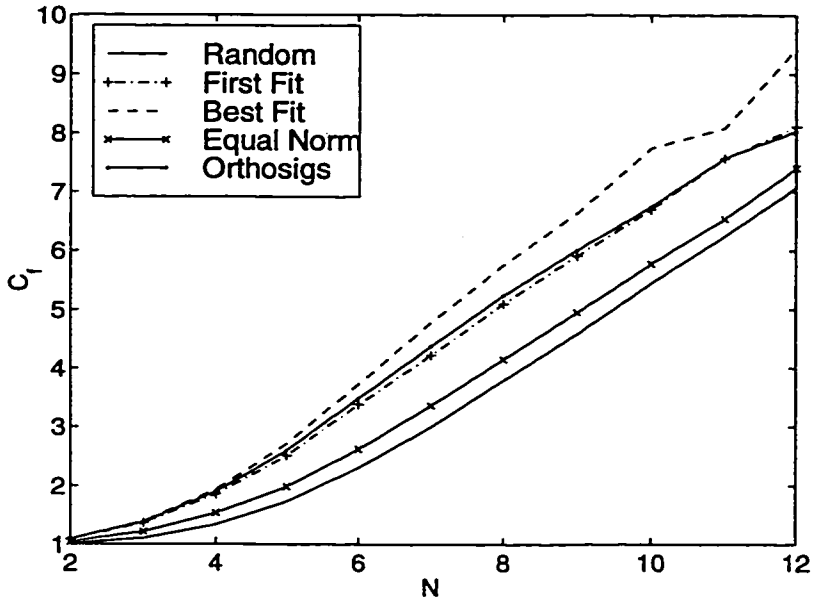

Figure 4.11: Frame capacity versus N, 6 dB SNR, $T = 40$ stations.

close to the ground and there is no U-LOS path between the two, there is almost no capacity gain from using the smart antenna at all. The reason is that power control is extremely important in a low SNR situation since the interferers are never completely removed by the beamformer. With a large path loss exponent, there is a greater variance in received signal strength, and hence stations with lower power levels cannot be accommodated in the same time slot.

Figure 4.13 is a graph of the capacity versus the lognormal shadowing standard deviation in dB's. As the lognormal shadowing increases, the capacity for all of the DSA algorithms falls quickly. With the 8 dB standard deviation that is typically used in literature [Rap94], the capacity is only half of what it is without lognormal shadowing. This result and the previous one indicate that it is very important to implement a power control mechanism to remove the effect of the lognormal shadowing and exponential power path loss if high SDMA capacity is required.

Figure 4.14 is a graph of the capacity versus the required SINR. As expected, the frame capacity drops as the required SINR increases. The largest drop is with the Random and Equal Norm algorithms. The Best Fit algorithm by contrast is

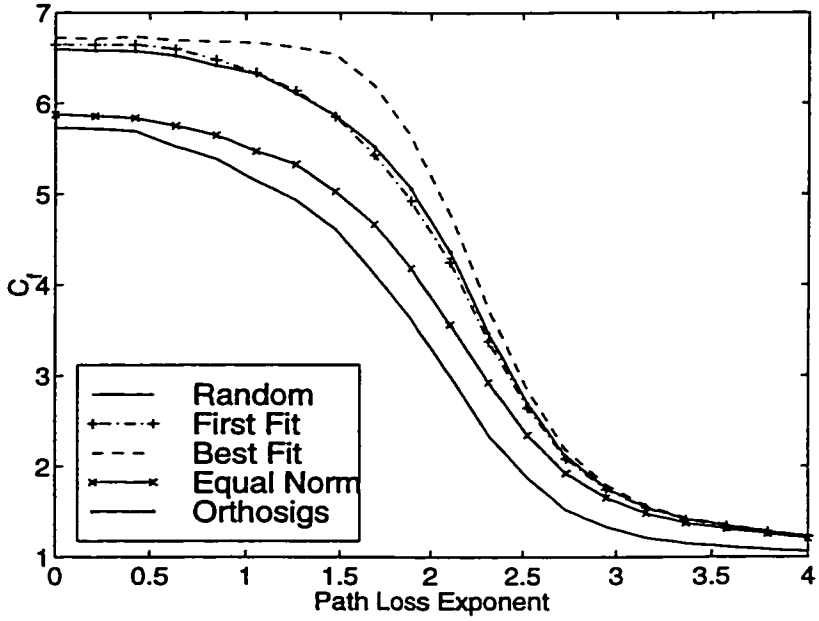

Figure 4.12: Frame capacity versus exponential power path loss exponent, 6 dB SNR, $T = 40$ stations.

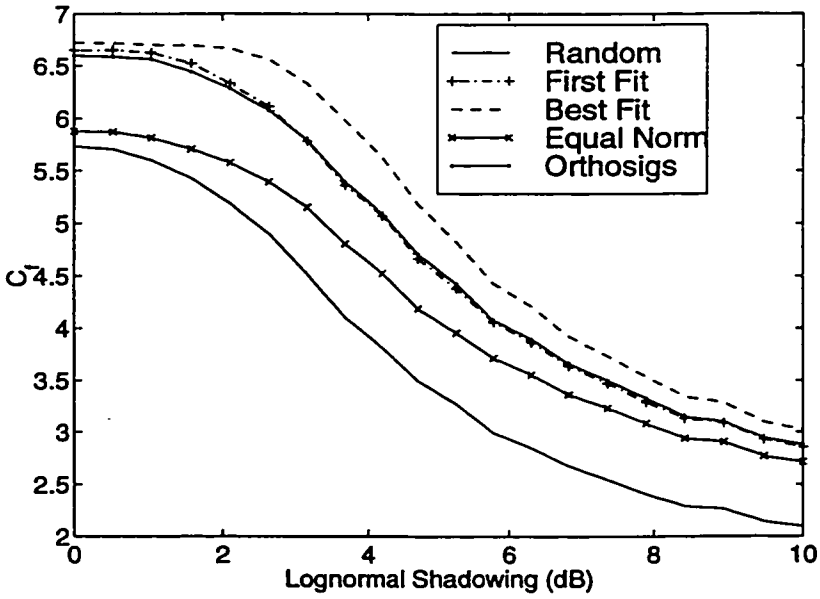

Figure 4.13: Frame capacity versus lognormal shadowing standard deviation, 6 dB SNR, $T = 40$ stations.

remarkably robust to an increasing required SINR.

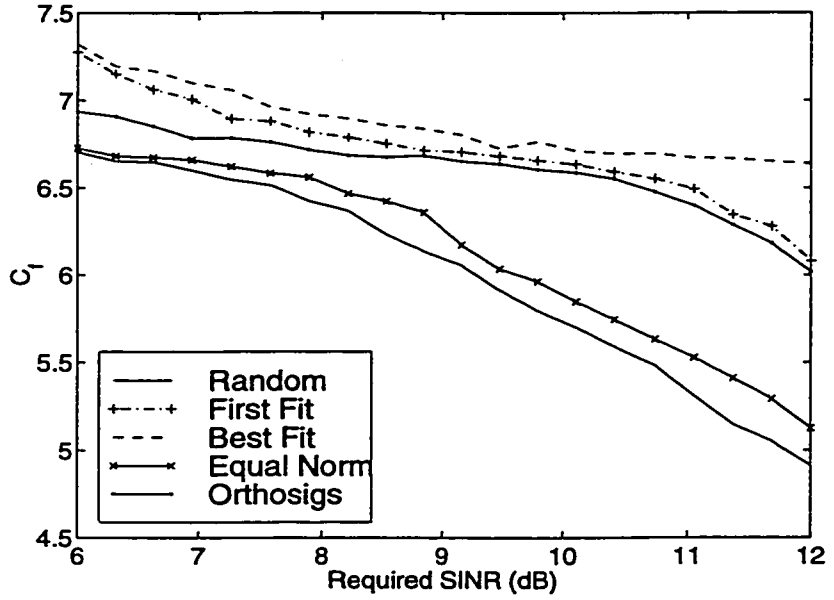

Figure 4.14: Frame capacity versus required SINR, 6 dB SNR, $T = 40$ stations.

In Table 4.2 the capacity is shown for three common propagation models using Random, First Fit, and Best Fit allocation. The results in this table are listed in increasing value of capacity obtained, assuming $T = 50$ and 6 dB SNR. In this chapter the value of l for the Rician distribution has been set to 0.80, which is typical value for indoor radio channels [Bul87]. It is interesting to note from the table that the relative performance is dependent upon the slot assignment algorithm used. For example, with First Fit, the highest capacity is achieved under ULOS-only, followed by Rician and Rayleigh. However, with Best Fit, the order is reversed. This is attributed in part to the fact that Best Fit does a much better job of accommodating stations with a wider variety of power levels. It should be noted that in the Rayleigh case, although each station has the same transmit power, there is more variation in received power than in the other two cases. When this is not the case we generally find that the capacity increases as the deterministic ULOS component diminishes.

Model	Algorithm	Capacity
Rayleigh	Random	3.82
ULOS-only	Random	3.87
Rician	Random	3.99
Rayleigh	First Fit	5.26
Rician	First Fit	5.56
ULOS-only	Best Fit	5.76
ULOS-only	First Fit	5.86
Rician	Best Fit	5.99
Rayleigh	Best Fit	6.03

Table 4.2: DSA frame capacity with $T = 50$ stations, 6 dB SNR

4.4.3 Statistical Slot Assignment

A simpler method of slot assignment is to allocate the stations to the time slots statistically [Win87b]. This means that a fixed number of stations are allocated to each time slot without testing to see if Equation (4.3) is satisfied. The advantage of this is a dramatic reduction in computational complexity and greater robustness under low channel coherence times. The statistical capacity can be defined in one of two ways. One way is to allocate the largest number of stations to each slot so that on average, only o per cent have insufficient SINR after beamforming. To minimize the delay and maintain a reasonably high link quality, we select o to be equal to 1 per cent. The number of stations allocated to each slot with this policy is C_{stat1}. The other way is to allocate the number of stations which maximize the average number of successful transmissions per slot, denoted C_{stat2}. These two capacities can be written as

$$C_{stat1} = \max_n n | P_{out}(n-1 \text{ interferers}) < 1 \text{ per cent}, \tag{4.6}$$

and

$$C_{stat2} = \max_n n(1 - P_{out}(n-1 \text{ interferers})). \tag{4.7}$$

Figure 4.15 is a graph of the frame capacity versus SNR. For a low SNR of 6 dB, the capacity of C_{stat1} is only 1.0, while for C_{stat2} it is at par with the Random DSA. $T = 40$

stations have been used for the Random and Best Fit DSA algorithms. Although C_{stat2} has higher capacity than C_{stat1}, it is also subject to greater delay because many of the packets need to be retransmitted due to a high outage probability. This figure shows that there is significant value in DSA when the SNR is low. However, as the SNR approaches 20 dB, the advantage of DSA over statistical allocation becomes less pronounced.

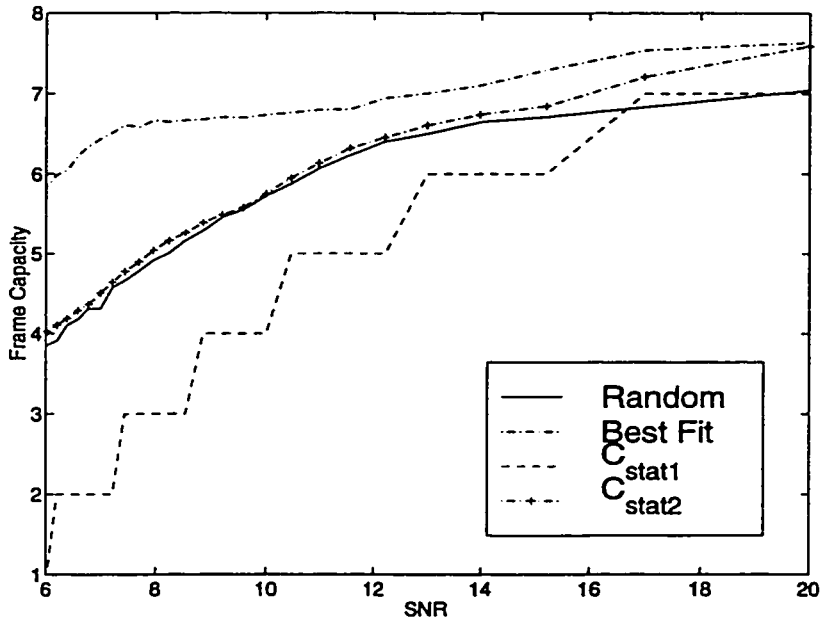

Figure 4.15: Statistical and DSA frame capacity C_f.

4.4.4 Analytic Random DSA Capacity

The Random DSA algorithm "gives up" on the first user that is not compatible. As a result, the correlation between the user signatures remains relatively low throughout the progression of the frame generation process, particularly if the batch size T is small. Hence, it is possible to make the assumption that the user signatures which are not yet allocated are independent. With this assumption, $E[L]$ can be derived using a recursive equation. For the recursive equation, $E[L|r,u]$ is defined as the expected length of the frame given that there remain r unallocated users in the current frame,

and u stations are allocated to the current time slot. Then

$$E[L|r,u] = E[L|r-1,u+1]P_s(u+1|u+1)+(1+E[L|r,0])(1-P_s(u+1|u+1)), \quad (4.8)$$

where $P_s(u+1|u+1)$ is the probability that $u+1$ transmissions are successfully received in the presence of $u+1$ transmissions. These success probabilities are obtained through simulation. The stopping condition for the recursion is

$$E[L|0,u] = 1, \qquad 1 \leq u \leq N. \quad (4.9)$$

$E[L]$, which required in (4.2), is therefore equal $E[L|T,0]$.

Fig. 4.16 shows the simulated and analytic Random DSA capacity versus T, with the running parameter being the pre-combining SNR. The difference in capacity increases as the SNR decreases. The reason is that as the SNR becomes high, C_f approaches the trivial infinite SNR capacity of $\lceil \frac{T}{N} \rceil$, which is independent of signature correlation. However, even for a very low SNR of 6 dB in which case stations allocated near the end of the batch are most correlated, the simulated frame capacity is only 5 per cent higher than the analytic frame capacity.

4.5 Near Upper Bound on SDMA/TDMA Capacity with Simulated Annealing

In order to evaluate the efficiency of the SDMA/TDMA frame generation process, a well known technique for solving complex problems known as simulated annealing can be applied [AK89]. Annealing is a process in which a solid is heated to melting point. It is cooled gradually until it crystallizes to a solid with a perfect lattice. At this state the solid has minimum free energy. This analogy has been shown to work well for combinatorial optimization problems.

The simulated annealing algorithm operates as such. Given the current configuration i, a test configuration j is generated. If the cost of the test configuration, $f(j)$, is less than the cost of the current configuration, $f(i)$, the transition is accepted. However, if $f(j) > f(i)$, the configuration is sometimes accepted. This helps to escape

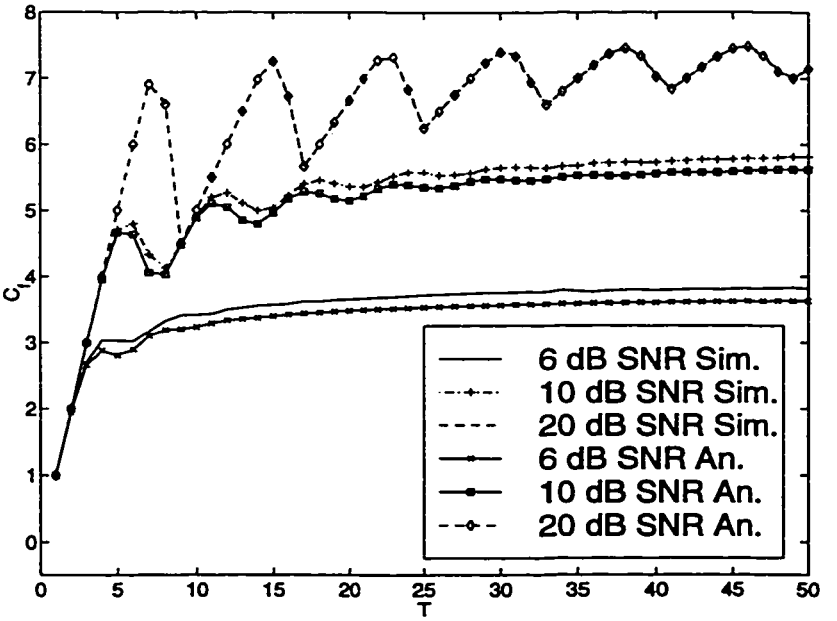

Figure 4.16: Simulated and analytic Random DSA capacity.

local minima. A configuration with a higher cost is more likely to be accepted in the initial stages of the algorithm than at latter stages. A control parameter c, analogous to temperature, determines the probability of accepting the test configuration j. So $P_{ij}(c)$, the probability of going from configuration i to configuration j in a single step is

$$P_{ij}(c) = \begin{cases} 1, & \text{if } f(j) \leq f(i) \\ e^{\frac{f(i)-f(j)}{c}}, & \text{if } f(j) > f(i) \end{cases} . \tag{4.10}$$

4.5.1 Cost function

The cost function f should be such that it is minimal at the optimum configuration k^*. It was found empirically that incorporating the average of the minimum SINR among the users in each slot of the frame into the cost function leads the system towards the optimum solution more quickly. Therefore, the cost function was defined as

$$f(j) = L + \frac{1}{E[\text{Minimum SINR}]}. \tag{4.11}$$

The pseudo code of the simulated annealing algorithm follows:

initialize(c_0,L_0)
$k = 0$
$i = i_{start}$
repeat
    for $l = 1$ to L_k
        Generate test configuration j from i
        if $f(j) \leq f(i)$ then $i = j$
        else
            if $exp((f(i) - f(j))/c_k) >$ uniform [0,1) then $i = j$
    $k = k + 1$
    calculate length L_k
    calculate control c_k
until stopcriterion

k is the total number of test configurations generated so far, L_k is the number of test configurations to be generated at the current control parameter c_k. In the initial configuration, each user was placed in a separate slot. Infeasible test configurations j (i.e. those for which one or more users lacked the required SINR) were not generated.

4.5.2 Finite time cooling schedule

Theoretically, in order to obtain the globally optimal solution, it is necessary to attempt an infinite number of test configurations k. Since this is not practical, a finite-time cooling schedule is required. A cooling schedule specifies

- a finite sequence of values of the control parameter c_k, i.e.
  - an initial value of the control parameter c_0
  - a decrement function for selecting c_{k+1}
  - a final value for c_k (stop criterion)
- a finite number of transitions L_k at each value of c_k

The following conceptually simple cooling schedule, proposed in [KGV83], was used.

Initial control c_0. The initial control parameter c_0 was set so that the maximum possible increase in cost f is accepted 95 per cent of the time.

Decrement of c_k. The control parameter was updated according to the rule $c_{k+1} = 0.99(c_k)$.

Stopcriterion. The stopcriterion was that the simulation would terminate if

1. The cost f remained unchanged for 5 consecutive values of c_k.
2. The index k exceeded 1000.
3. c_k fell below 0.001.

Transitions at each c_k. The number of transitions L_k were limited to the first of

1. 300 accepted transitions.
2. 1000 attempted transitions.

Figure 4.17 shows the frame capacity versus T for relatively low noise 20 dB SNR situation with $N = 4$ antennas. Without a lot of noise even the Random DSA algorithm provides a capacity close to the upper limit of 4. The simulated annealing algorithm yields close to the maximum capacity of 4 users per time slot with 8 or more portable stations. Figure 4.18 shows the capacity versus the number of users for a very high noise 6 dB SNR situation. In this situation the difference in capacity between the various algorithms is more pronounced. For example, with 24 users simulated annealing performs about 43 per cent better than Random DSA, and about 5 per cent better than Best Fit DSA. This important result indicates that Best Fit DSA achieves a frame capacity that is very close to combinatorial optimization through simulated annealing.

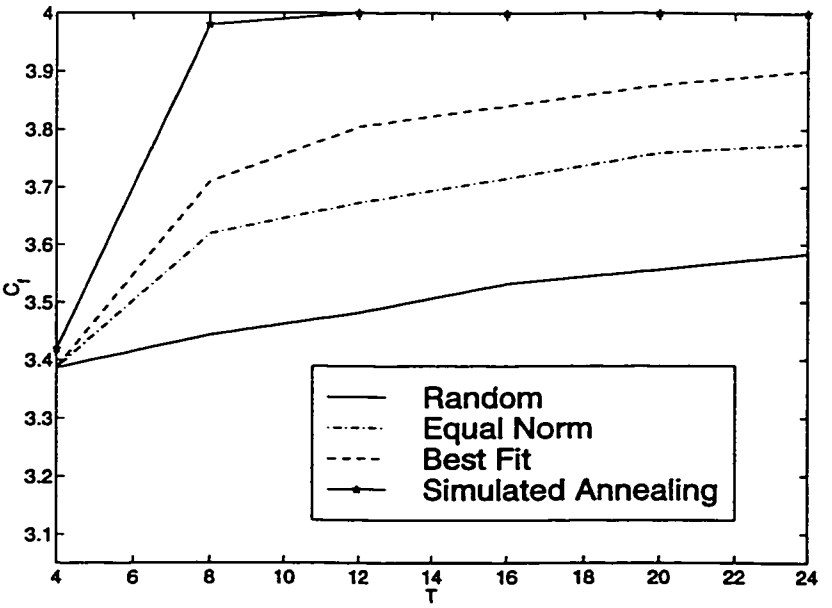

Figure 4.17: Frame capacity 20 dB SNR, $N = 4$ antennas.

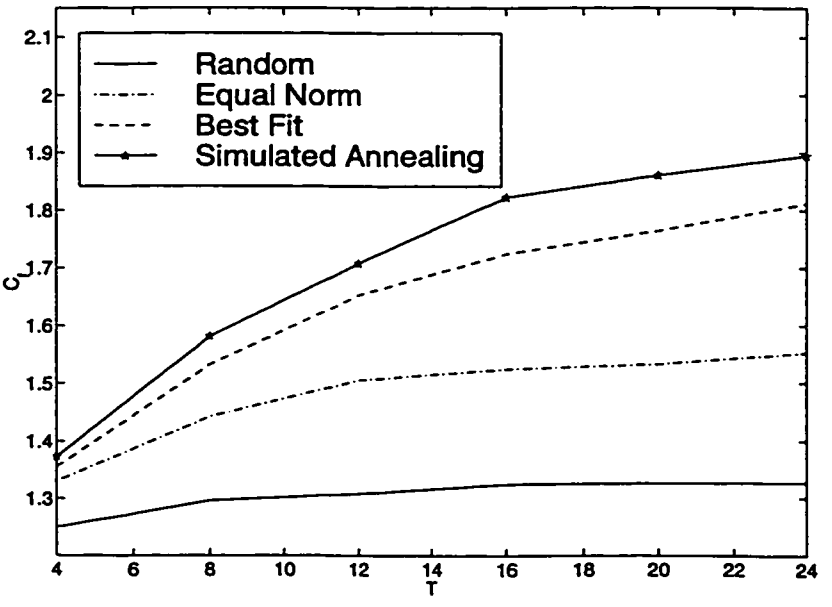

Figure 4.18: Frame capacity 6 dB SNR, $N = 4$ antennas.

4.5.3 SDMA/TDMA Experimental Frame Capacity

Having determined that stations in close physical proximity can indeed be resolved from Section 4.3, the next question of interest is what sort of DSA frame capacities are possible inside a building. Figure 4.19 is a plot of the capacity versus the number of mobiles using the experimental data. This data was collected by placing the array at position A3 in Figure 4.3, and collecting spatial signatures both in Room 103 (for the NU-LOS situation), and in the hallway at T3 (for the U-LOS situation). The diameter of the array was 0.51 m and 1000 samples spaced approximately 0.30 m apart were collected. In the simulation the T station signature vectors for each batch were selected at random with replacement from the 1000 samples. The capacity for the NU-LOS situation is higher than the U-LOS situation, in this case by about 4 per cent for Random DSA. However, when Best Fit DSA is used, the capacity of the NU-LOS situation is roughly 14 per cent higher. Generally it was found that when the level of multipath is higher, larger spatial capacity results when good slot DSA algorithms are used.

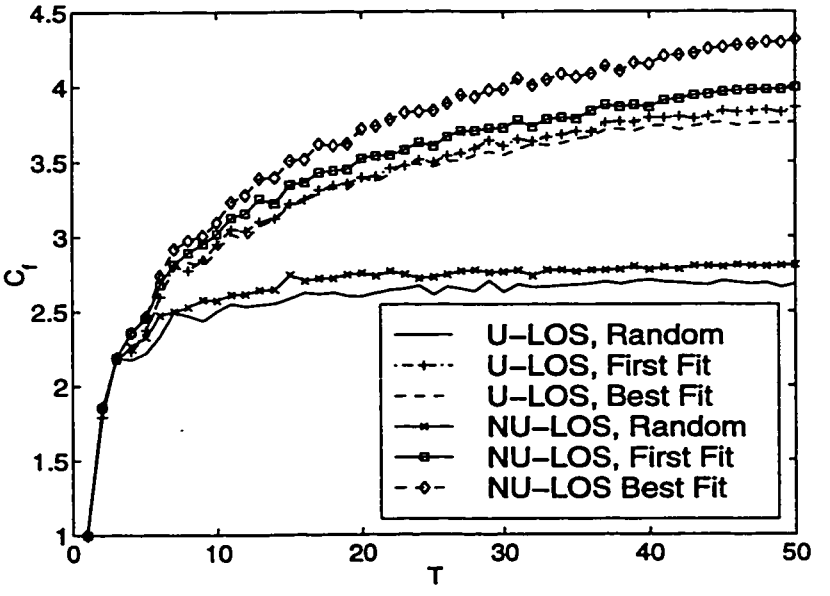

Figure 4.19: Experimental capacity with 6 dB SNR.

The capacity indicated by the NU-LOS experimental data is lower than that obtained with the theoretical Rayleigh fading model. Figure 4.20 emphasizes this point by plotting the experimental and theoretical capacity for NU-LOS and Rayleigh station signatures on the same graph. It can be seen that the theoretical capacity is about 37 per cent higher under Random DSA. Under Best Fit DSA the difference is about the same. The reason for this difference is that the complex envelope which is sampled has a correlation which monotonically decreases as the inter-sample separation and the carrier frequency increase. This gives rise to element to element correlation and also station signature correlation.

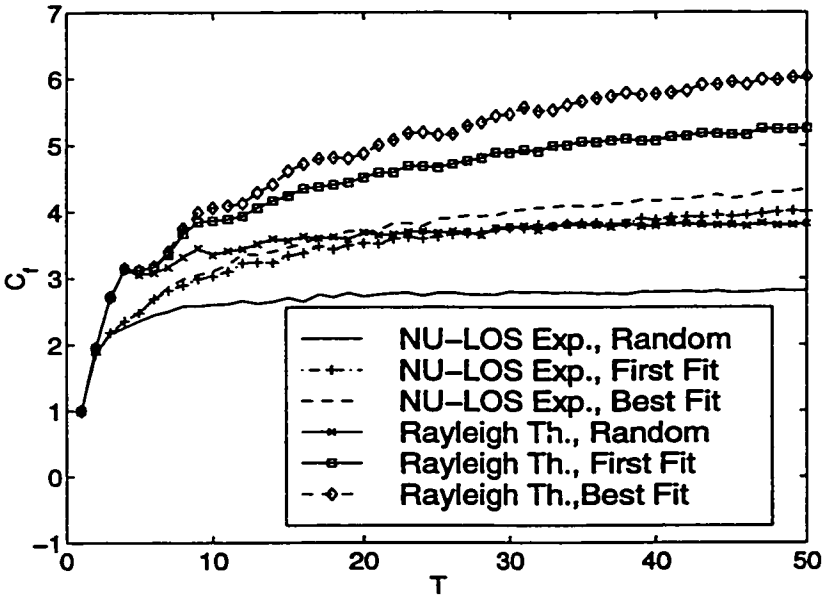

Figure 4.20: Experimental and theoretical frame capacity with 6 dB SNR.

Figures 4.21 and 4.22 are a plot of the frame capacity for Random DSA using the data collected in the various rooms shown in Figure 4.3. The array was at location A1. The antenna diameter was 0.20 m, so the antenna element spacings are a little over one third the previous values. This change is attributed to the general reduction in capacity compared with the previous measurements which were made. The case with independent Rayleigh channels between the transmitter and each array element is also plotted. This is the upper curve in both graphs.

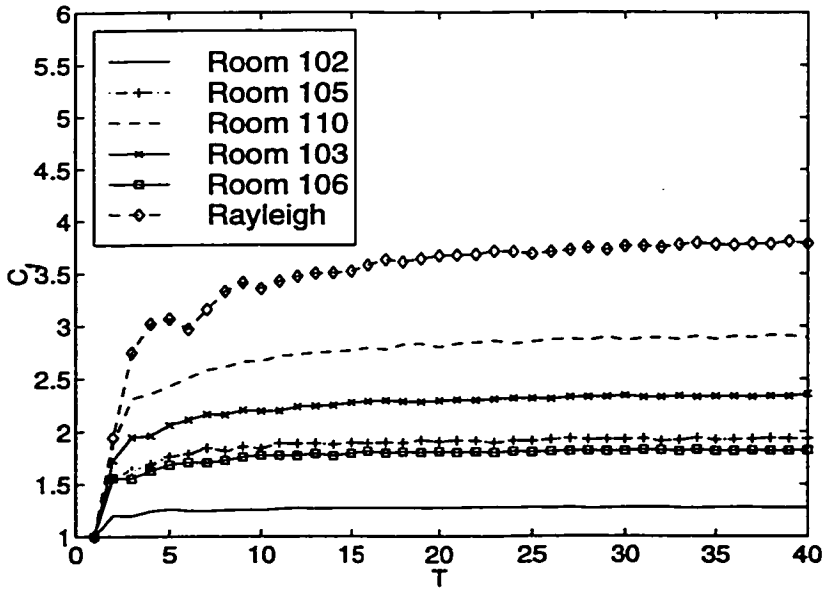

Figure 4.21: Frame capacity for measured station signatures with 6 dB SNR.

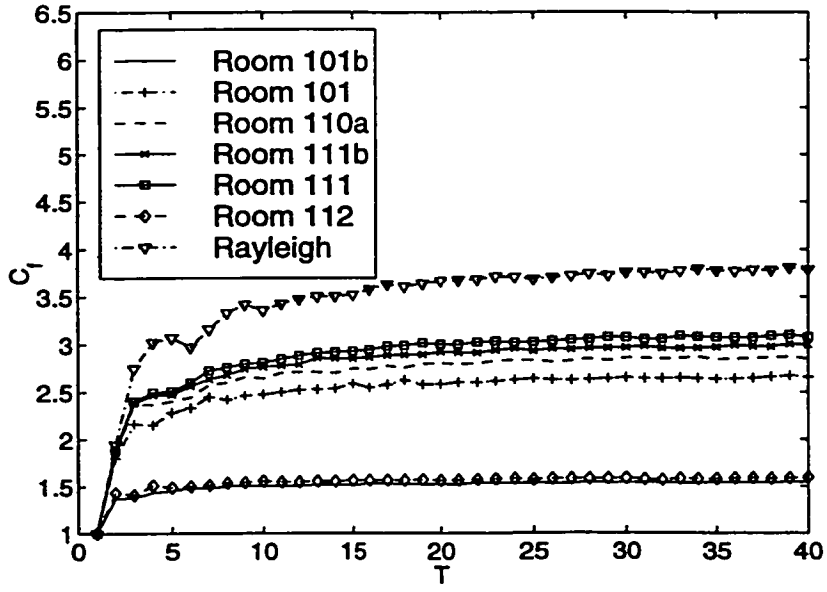

Figure 4.22: Frame capacity for measured station signatures with 6 dB SNR.

It can be seen that the spatial frame capacity varies significantly from one room to the next. This is attributed both to the level of multipath present, and to the azimuth subtended at the array by the positions used. For example, room 111 is known to have strong levels of multipath due to a metal wall and ceiling. For this reason it has a high level of spatial frame capacity. Room 106 has a frame capacity which is about 59 per cent lower than room 110. This is in part because room 110 subtends a greater azimuth by the station signatures collected as compared to room 106 which can be seem from Figure 4.3. It can also be observed that the theoretical capacity is significantly higher than that which was based on measurement. This is caused by non-zero interstation signature correlation and non-zero inter-antenna element correlation. The latter is caused by both the close element spacings and by mutual coupling between elements.

The inter-element correlation can be quantified by the condition number of spatial correlation matrix. The correlation matrix is equal to

$$\mathbf{R}_c = E[\mathbf{v}(t)\mathbf{v}^H(t)], \tag{4.12}$$

where t is the sample index of the transmitter location. The condition number r_{cond} of the matrix $\mathbf{R}_c$ is the largest eigenvalue divided by the smallest eigenvalue. It is a common metric used to measure the correlation between the complex envelopes that make up the signature vector [Rei96]. Table 4.3 shows the Random DSA frame capacity and r_{cond} with $T = 40$ stations for the rooms in Figures 4.21 and 4.22. The capacities are given in descending order. It can be seen from this table that in general, as the condition number increases, the capacity decreases. This indicates that the condition number is a good metric for estimating the DSA frame capacity of a room.

It was determined that another factor which has a strong influence on the frame capacity is inter-element antenna separation. Figure 4.23 is a graph of the capacity with an antenna array diameter of 0.51 m and 0.20 m for two different rooms. With 0.51 m diameter, in room 103 the Random DSA capacity is 19 per cent better, while in 101b it is 72 per cent better. This indicates that if the capacity is to be maximized, the antenna elements should be placed far apart to minimize inter-element envelope correlation. Note however that placing antennas farther apart can increase the level

Room Number	*Random Capacity*	r_{cond}
Rayleigh Fading	3.789	1.12
111	3.080	7.395
111b	2.994	6.807
110	2.894	8.46
110a	2.850	10.45
101	2.658	11.30
103	2.355	17.96
105	1.937	51.87
106	1.825	67.06
112	1.596	96.58
101b	1.544	100.65
102	1.278	323.46

Table 4.3: Random DSA capacity in descending order with 6 dB SNR and $T = 40$ mobiles.

of ISI and create grating lobes in the radiation pattern.

4.5.4 Channel Coherence Time Model

In order for SDMA/TDMA DSA to work when the channel changes due to pedestrian traffic, it is necessary to perform the DSA so that SINR_{min} in Equation (4.3) is a few dB's above the value required for successful demodulation. This is because without signature tracking, the SINR after beamforming will in general be worse near the end of the frame. Figure 4.24 is a graph of some of the DSA algorithms' frame capacity versus the SINR_{margin}, which is the margin above the SINR required for successful demodulation in dB's. For example, with SINR_{margin}=3 dB and a required SINR of at least 10 dB, SINR_{min} is raised to $10 + 3 = 13$ dB's. The first thing to notice is that the stronger DSA algorithms fall in frame capacity faster than the weaker ones as SINR_{margin} increases. As the value of SINR_{min} rises to a point where the channel becomes more noise limited than interference limited, there is little to gain from the stronger search capability of the better DSA algorithms. Therefore, with an SINR_{margin} of 6 dB's or greater, the SDMA/TDMA DSA capacity gain is almost

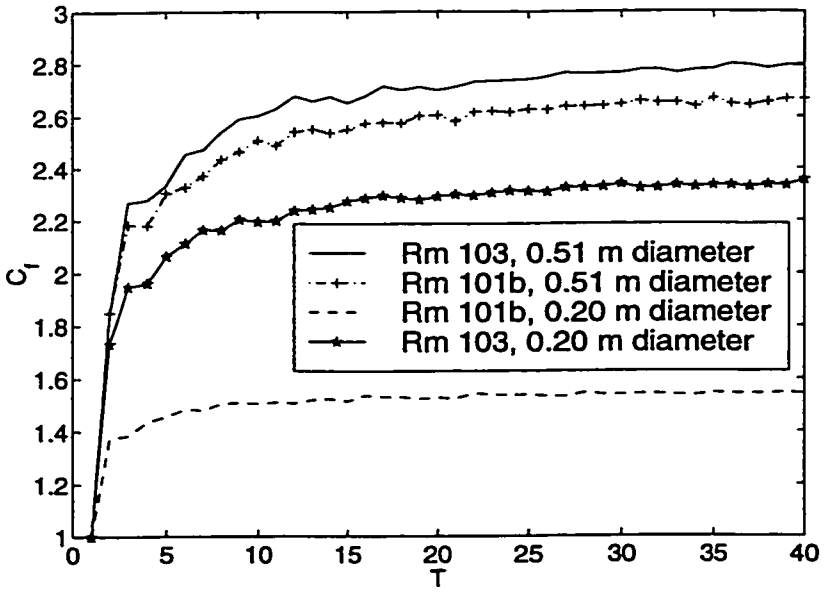

Figure 4.23: Frame capacity for two rooms with 6 dB SNR, Random DSA.

unity.

In an actual MAC protocol the signalling overhead for the signature acquisition is quite significant. Therefore, to maximize the protocol capacity the data slots should be as large as possible. As well, the batch size T should be large so that the DSA protocol efficiency is high. The maximum length of the frame is dictated by how long the SINR with fixed weights remains above 10 dB. This time is called channel coherence time. To determine the channel coherence time a simple first order autoregressive model for the channel variation is employed. The complex envelope of an antenna output can be written as a function of its value one time index prior plus complex Gaussian noise as

$$v(k) = wv(k-1) + n(k), \tag{4.13}$$

where $v(k)$ and $v(k-1)$ are the complex envelopes at times k and $k-1$, respectively, $n(k)$ is the noise, and w is a real number between 0 and 1 which represents the memory. The mean error power to mean signal power ratio γ is equal to

$$\gamma = \frac{\sigma_n^2}{\sigma_v^2}$$

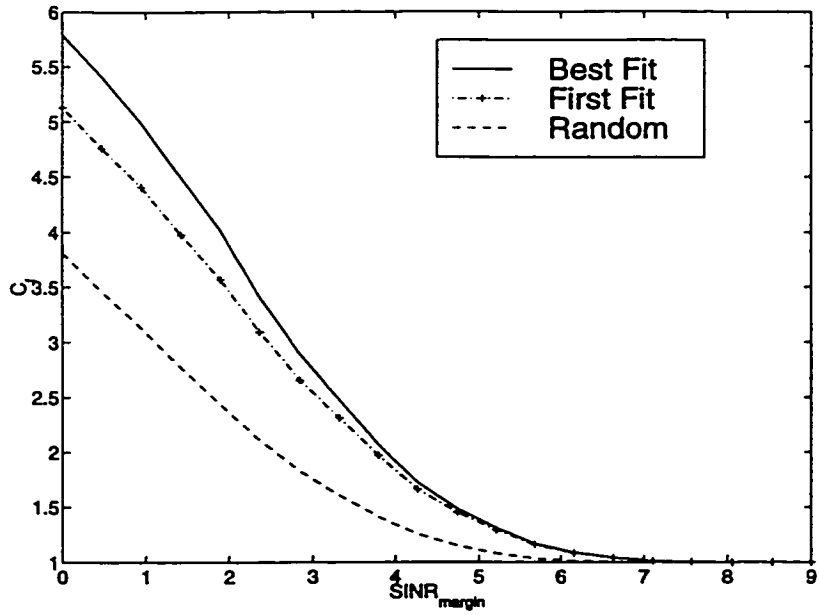

Figure 4.24: Frame capacity for different $\text{SINR}_{margins}$. $T = 40$ stations, 6 dB SNR, SINR_{min}=10 dB+SINR_{margin}.

$$= \frac{\sigma_n^2}{w^2\sigma_v^2 + \sigma_n^2}. \tag{4.14}$$

Without loss of generality, if the mean signal power σ_v^2 at the antenna output is 1 Watt, then

$$w^2 + \sigma_n^2 = 1. \tag{4.15}$$

Solving the two unknowns w and σ_n^2 in Equations (4.14) and (4.15), we get

$$w = \sqrt{1-\gamma}, \tag{4.16}$$

and

$$\sigma_n^2 = \gamma. \tag{4.17}$$

γ is the ratio of the mean error power to the mean signal power at a time index difference of 1 unit. In order to generalize the ratio of the mean error power to the mean signal power to a time index difference of integer t units between the current and reference sample, Equation (4.13) can be written recursively as

$$v(k) = w^t v(k-t) + \sum_{i=0}^{t-1} w^i n(k-i). \tag{4.18}$$

Assuming that the noise errors $n(k-i)$ are independent, the mean error power to mean signal power ratio for a time index difference of t is then

$$\gamma_t = \sum_{i=0}^{t-1} \frac{w^{2i}\sigma_n^2}{\sigma_v^2} = \gamma \sum_{i=0}^{t-1} w^{2i}. \tag{4.19}$$

When the error power is small, w is a number just slightly less than 1, so for small t it can be assumed that $w = 1$. Therefore,

$$\gamma_t = t\gamma. \tag{4.20}$$

From the experimental data used for Figures 4.5 and 4.6, the samples were taken 20 ms apart, so the relationship between γ_t and the time lag is

$$\text{time lag} = (20 \text{ ms})\frac{\gamma_t}{\gamma}. \tag{4.21}$$

Figure 4.25 is a graph of the outage probability versus γ_t. The value of γ corresponding to 0.020 s has been calculated for each of the experiments and is included in the figure caption. In this figure the antenna output envelopes of all portable stations are being altered according to Equation 4.18. If the coherence time is defined to be the time at which the outage probability exceeds $o = 1$ per cent, then the coherence time for First Fit DSA and Best Fit DSA with 3.5 dB SINR_{margin} is around 12, 17, and 28 ms with 7 people moving near the array, transmitter, and in between, respectively. The coherence times drop to 8, 12, and 18 ms when SINR_{margin} is reduced to 3 dB. It should be noted that with the 3 dB SINR_{margin}, the frame capacity is only around one-half of what it is with 0 dB SINR_{margin} which would suffice for the ideal case of a static channel. Nevertheless, with data rates in the range of 1 to 2 Mbps typical of wireless LANs today, this means ten or more 1 kbit time slots can be used in the SDMA/TDMA frame if the coherence time is over 10 ms. This shows that SDMA/TDMA DSA using PSA is practical when the transmitter and array are stationary with some pedestrian traffic in the channel.

4.6 SDMA/TDMA with a Moving Transmitter

In certain situations the transmitter will be in motion, such as when a person is walking with the portable station. For these cases the station signatures will change

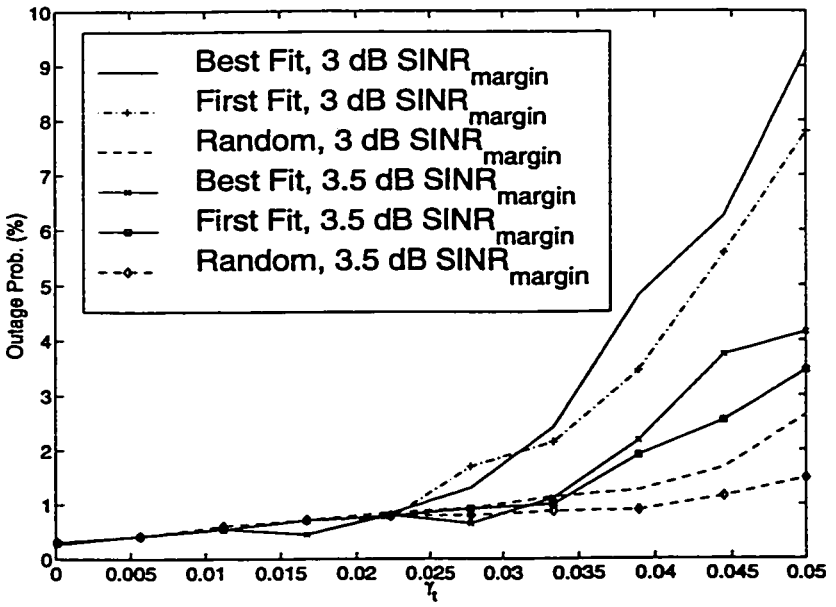

Figure 4.25: Outage Probability versus γ_t for $T = 40$ stations, 6 dB SNR, and 10 dB SINR_{min}. γ is equal to 0.057, 0.038, and 0.024, for 7 people moving near the array, 7 people moving near the transmitter, and 7 people moving in between, respectively.

fairly rapidly. With delay insensitive traffic, this phenomenum can be exploited to improve the system capacity. This is done by withholding transmission until the wireless link between the transmitter and the smart antenna improves. Essentially the correlated fading characteristics of the channel are being observed to time the transmission of the packet. In [CZMV98], the correlated channel fading was used to abort the remainder of the message transmission once an error was detected in one of the packets of the message. As far as the author of this thesis is aware, this is the first time the correlated fading characteristics of the channel are used to time the transmission of new packets. In this section the forward link protocol capacity is considered, although the reverse link would benefit from this as well.

The SDMA/TDMA DSA protocol is modified so that once the basestation polls a batch of T portable stations, only stations for which

$$\| \mathbf{v}_i \|_2^2 > xN(\text{SNR})\sigma_n^2, \tag{4.22}$$

where x is the transmission threshold normalized to the mean signature power, are

selected for DSA in the current frame. The idea is to defer transmission to portables with a weak channel until they go out of the fade. Signals which are rejected in the current frame are polled again in subsequent frames until Equation (4.22) is satisfied. There is also an upper bound m on the number of times which a station is polled before a transmission is forced. This is done to prevent excessive polling overhead and delay. The frame structure of the protocol appears in Figure 4.26. There are T poll/response pairs for the signature acquisition stage. The poll P_i is a 16 bit user identifier spread by a length 3 PN code, making it 48 bits long. This is done to enhance the processing gain against noise to ensure that a portable station does not miss the poll. The basestation's transmit power for the poll could also be increased, but this was not done here to limit cochannel interference to other systems using the same frequency band. The response R_i is a PN sequence of length 63 bits which is used to acquire the user signature $\mathbf{v}_i$. Once the polling is complete, the SDMA/TDMA frame is constructed, and the L data slots are transmitted to the mobiles using optimal beamforming.

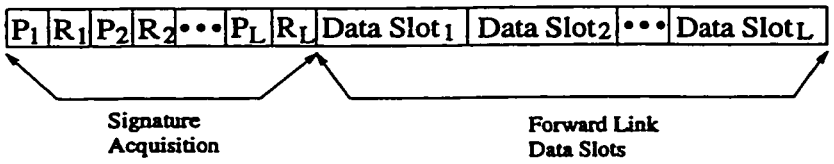

Figure 4.26: Forward link polling protocol frame structure. P_i and R_i are a poll and corresponding response from mobile i.

The doppler fading model employed for the user signatures has been taken from [Jak74]. Each antenna output experiences independent fading. The in phase and quadrature phase envelopes of the signals are equal to

$$v_i(t) = 2\sum_{n=1}^{N_o}\cos(\beta_n)\cos(\omega_n t + \phi_n) + \sqrt{2}\cos(\alpha)\cos(\omega_m t + \phi_m) \quad (4.23)$$

$$v_q(t) = 2\sum_{n=1}^{N_o}\sin(\beta_n)\cos(\omega_n t + \phi_n) + \sqrt{2}\sin(\alpha)\cos(\omega_m t + \phi_m), \quad (4.24)$$

where $N_o = \frac{1}{2}\left(\frac{P}{2} - 1\right)$, $\beta_n = \frac{\pi n}{N_o}$, ϕ_n and ϕ_m are random phases between 0 and 2π radians, $\omega_m = 2\pi\frac{v}{\lambda}$, $\omega_n = \omega_m cos(\frac{2\pi n}{P})$, and $\alpha = \frac{\pi}{4}$. P is the total number of multipaths

arriving at the antenna output such that $\frac{P}{2}$ is an odd integer. $\frac{v}{\lambda}$ is the doppler fading frequency. Intuitively, this time domain doppler fading model is considering P arbitrary signal propagation paths between the transmitter and receiver. In this thesis $P = 34$ paths are considered, which closely approximates a Rayleigh doppler fading channel. A different set of random phases are selected for each smart antenna output in order to make the approximated Rayleigh channels between the portable station antenna input and smart antenna outputs independent.

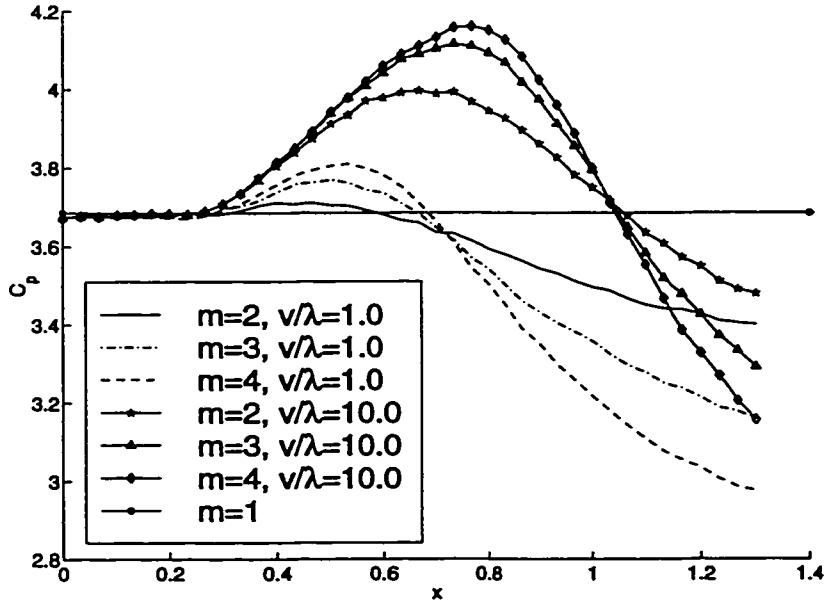

Figure 4.27: Protocol capacity for Random DSA with $T = 30$, l_{data}=8192 bits.

Figure 4.27 is a graph of the protocol capacity versus x for Random DSA. The data rate is 1 Mbps. The value of m ranges from 1 to 4. $m = 1$ means that the packet is always sent after the first poll, and hence no attempt is made to exploit the doppler fading. With $\frac{v}{\lambda} = 1.0$, the Random DSA capacity improves by about 4 per cent with $m = 4$ polls. With $\frac{v}{\lambda} = 10.0$, it improves by about 13 per cent. At a carrier frequency of 1.86 Ghz, this is about 1.6 m/s, which is a typical speed of a person walking indoors. Although the capacity improves monotonically with m, it also becomes more sensitive to the value of x. That is, if the value selected for x is too large, then the protocol will continue to poll until the m^{th} poll, even if the channel is

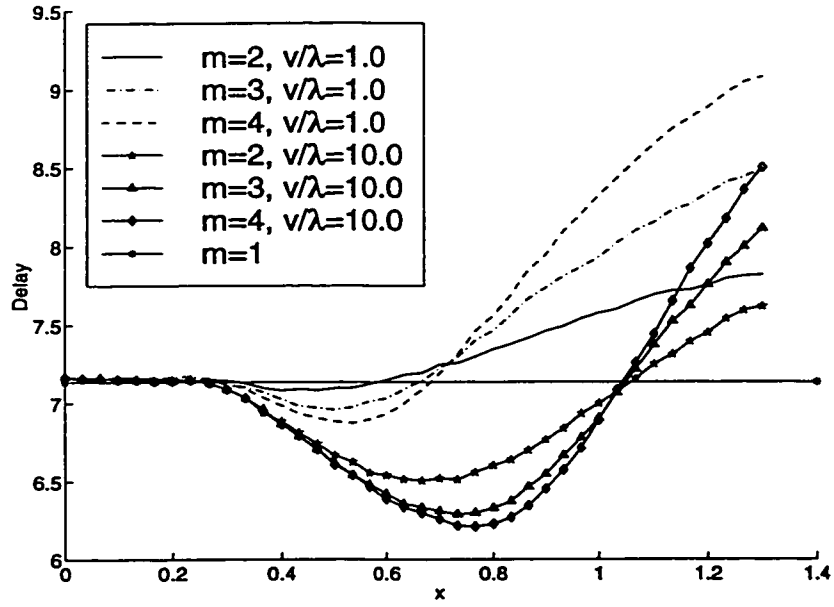

Figure 4.28: Delay versus throughput for Random DSA with $T = 30$, l_{data}=8192 bits.

already very good. So if m and x are too large than the capacity will suffer due to excessive polling overhead.

Figure 4.28 is a graph of the protocol delay for Random allocation as a function of x. The delay is defined as the time it takes for the packet to begin transmission after the first time it is selected for transmission in a batch. This delay is normalized to the size of the data slot l_{data}. With $\frac{v}{\lambda} = 1.0$, the delay is about 7 per cent lower with $m = 4$ as compared to the $m = 1$ case, and with $\frac{v}{\lambda} = 10.0$, it is about 12 per cent lower with $m = 4$. Although with increasing m the protocol overhead increases, the average number of data slots which a packet waits is slightly lower. This is because the capacity is higher, so there are fewer data slots before the desired packet's slot.

Figure 4.29 is the protocol capacity for the First Fit DSA algorithm. With $\frac{v}{\lambda} = 1.0$, the First Fit DSA capacity improves by only 1 per cent with $m = 4$, and for $\frac{v}{\lambda} = 10.0$, it improves by just 5 per cent. The reason that First Fit DSA does not obtain as much benefit from multiple polls is that the capacity with the stronger protocols does not fall off as sharply with decreasing SNR, as indicated by Figure 4.10. This means that sampling the channel multiple times to improve the SNR does not help as much.

Figure 4.30 indicates that the delay is slightly higher than for the trivial $m = 1$ case. Although it does decrease slightly at the optimal choice of x, the increase in delay due to the protocol overhead and not always transmitting in the first frame does not overcome the reduction in delay due to slightly higher frame capacity. This suggests that sampling the channel multiple times is most beneficial to the weaker DSA algorithms.

This protocol benefits the greatest when the channel decorrelation between successive polls is high. This implies that portable stations in a fade with a low doppler fading frequency would need to be polled many times before the signature strength became sufficiently high. The problem with polling too many times however is increased delay and polling overhead. An easy solution for reducing the polling overhead is to poll the user every n^{th} frame, where n is an integer bigger than 1.

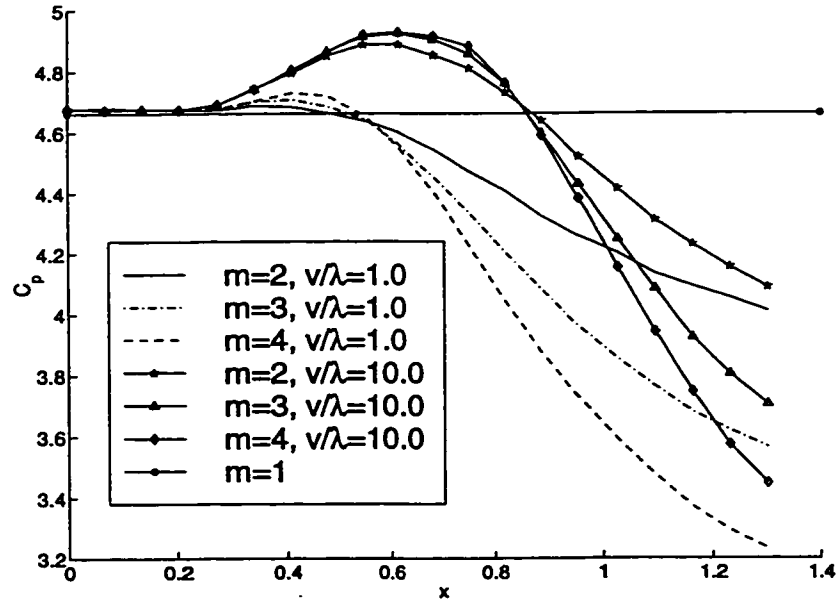

Figure 4.29: Protocol capacity for First Fit DSA with $T = 30$, l_{data}=8192 bits.

In Figure 4.31 the protocol capacity versus x is given for different data slot sizes with Random DSA. From this figure it can be seen that relatively large data slots are necessary to see an appreciable capacity improvement, say at least 4096 bits. The reason is that the protocol overhead for signature acquisition of 111 bits/station is

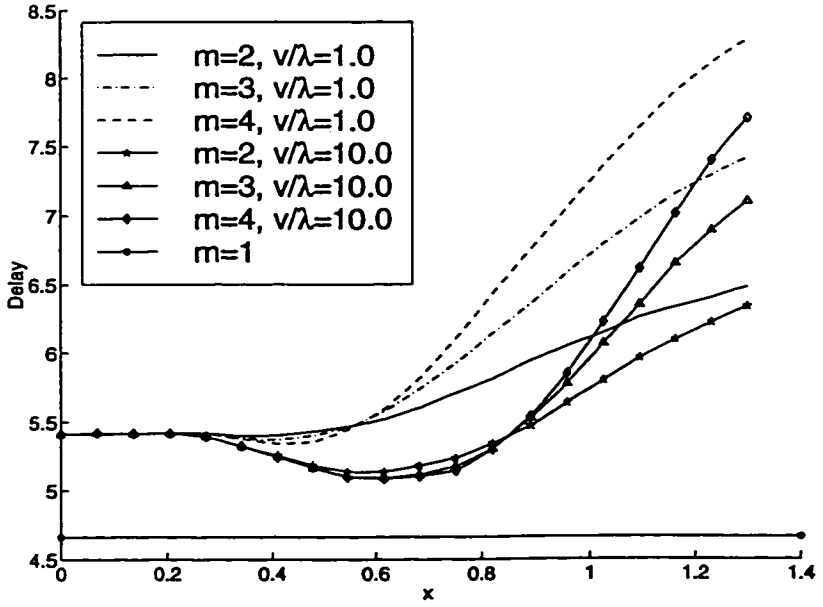

Figure 4.30: Delay versus throughput for First Fit DSA with $T = 30$, l_{data}=8192 bits.

quite significant. So for there to be value in polling a station more than once, the data slots need to be fairly large.

4.7 Conclusions

In this chapter the static SDMA/TDMA capacity of an indoor wireless transmission system was considered. The stations communicate with a basestation which uses a smart antenna operating in SDMA/TDMA mode.

The focus of this chapter was on DSA. In certain smart antenna systems using TDD, the complex station signatures can be obtained by polling the stations before actual user data is transmitted. Following this, the basestation must form a SDMA/TDMA frame so that transmission can proceed. This chapter explored the value of performing dynamic station slot assignment when constructing the SDMA/TDMA frames. Slot assignment algorithms with varying complexity were introduced for this purpose. It was found using both theoretical and experimental data that DSA is capable of increasing static system capacity under non-ideal propagation situations. It

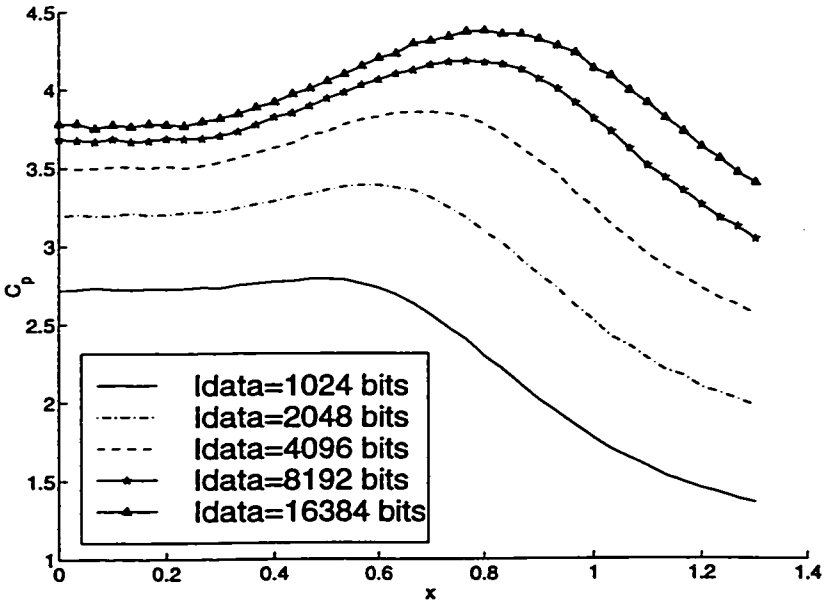

Figure 4.31: Random DSA frame capacity for different data slot sizes with $T = 30$.

was found that the spatial capacity measured can be significantly less than predicted using an independent Rayleigh fading model which is often used in indoor situations. The experimental results were obtained using an 8 element circular antenna array operating at 1.86 GHz.

Also presented were some measurements taken relating to the channel time coherence in the presence of pedestrian traffic in the vicinity of the transmitter, array, and in between. When pre-sampled signature acquisition (PSA) is used under time-division-duplexing (TDD), channel time coherence is essential so that proper beamforming can be applied in the downlink direction. It was found that when the desired signal is undergoing fading in the absence of other interfering stations, significant degradation in performance only occurred when there is significant motion around the array itself. However, when the array is also nulling a single fading interferer, very significant performance penalties may be paid. In this case the SINR may degrade for time lags of much less than 100 ms. In order for the DSA protocols to work with a time varying channel using fixed weight vectors at the beamformers, it is necessary to set SINR_{min} to a value above the minimum required. With an SINR_{margin} of 3 dB, a

channel coherence time of between 8 ms and 18 ms was achievable for the First Fit and Best Fit DSA algorithms.

Finally, a DSA protocol innovation which takes advantage of a user's changing signature due to movement of the transmitter in order to improve the system capacity was considered. It was found that the increase in capacity was the largest when the data packets are large and the transmitter is moving at pedestrian speed. Also, the weaker DSA algorithms benefit more than the stronger ones since they are more sensitive to the SNR at the antenna outputs. This is an important result in that the weaker DSA algorithms are more likely to be employed when channel coherence times are low.

Chapter 5

Indoor Slotted-ALOHA Protocols

5.1 Overview

The original ALOHA system was initially developed for the purpose of efficiently multiplexing a large population of bursty stations on ground-based packet radio networks [Abr70]. In the ALOHA protocol, there is essentially no coordination among stations, and packet transmissions may commence at any point in time. A well known property of ALOHA is that with fixed size packets, the capacity of a system with a large station population is only about 18% [Rob75]. In Slotted ALOHA (S-ALOHA) the capacity attained may be double this value, at the expense of the station synchronization required. Clearly, techniques for increasing these capacities would be very useful. One way of achieving this is to use a multibeam smart antenna at the basestation [WC93], and this is the technique employed in this thesis.

In a study by Ward [WC93], the basestation is permitted to receive multiple packets simultaneously using a smart antenna for reception. It does this by having multiple beamforming modules at the basestation, each pointing its main beam at a desired packet and pattern nulls at interfering transmissions. S-ALOHA protocols are well suited for SDMA operation in indoor systems. This is because unlike conventional LAN protocols such as CSMA, they more readily permit simultaneous station transmission, which is desired when SDMA is being used. It should be noted however that it is possible to exploit carrier-sensing in indoor SDMA, as a mechanism for

synchronizing various basestation antenna operations [ST97].

Due to the stochastic nature of packet transmission, the average number of successful packets per slot using multibeam S-ALOHA reception is much less than the theoretical limit of the number of antennas [Com88]. In theory this problem can be mitigated by the use of a reservation channel composed of minislots used for packet reservations [XL94]. In this approach the reservation channel is configured to consume a relatively small fraction of the channel capacity so that the contention free data channel can operate in a collision free mode.

The previous chapter demonstrated that with PSA based SDMA/TDMA DSA there is a significant capacity increase with just a few antennas. In this chapter we explore the value of DSA by integrating it into the reservation based S-ALOHA protocols. While in the previous chapter the DSA frame capacity was considered, in this chapter the S-ALOHA protocol capacity is evaluated so that the additional overhead associated with smart antenna operation is included. Two slot assignment algorithms are proposed which can be used to dynamically assign portable stations to the data channel time slots. These slot assignment algorithms are similar in concept to the Random and First Fit DSA algorithms given in Section 4.4.1 of the previous chapter. It is shown that significant improvements in system capacity are possible when a more complex slot assignment algorithm is used.

In this chapter six variants of single-beam and multibeam S-ALOHA protocols are considered. The S-ALOHA protocols considered vary widely in the degree of implementation complexity required. In the first two, access to the system is performed directly in the data slots. In the first protocol, single-beam operation is used while in the second, multibeam SDMA operation is required. In the remaining four variants a reservation channel is used to ensure collision free SDMA operation in the data slots. Both single-beam and multibeam SDMA operation is considered for the reservation channel.

Multibeam operation in both reservation minislots and data slots can achieve the highest capacity. However under low SNR, and for long packet lengths, only marginal improvements in capacity are achieved over other methods. This is an important conclusion since operating the system with multibeam minislot contention

is expected to be highly complex, due to the difficulties of dynamic acquisition.

The rest of the chapter is organized as follows. In Section 5.2, the basic system architecture is described. In Section 5.3, the various S-ALOHA protocols are described in detail, and throughput calculations are given. An analytic model is included for the protocols which use data slot contention. In this section two dynamic slot assignment algorithms are proposed. In Section 5.4 the throughput and delay performance of the protocols is evaluated under various conditions. In Section 5.5 the SA-MOB protocol is modified to work in a multicell environment. Delay and throughput results for this protocol are given. Finally, in Section 5.7 some concluding remarks are made.

5.2 Smart Antenna Basestation

In the system considered, the smart antenna basestation with N antennas communicates with a set of portable stations with single omni-directional antennas. The system considered uses time division duplexing (TDD). In a TDD system, it is possible for the basestation to determine the correct beamforming for both transmission and reception after first measuring the vector channel response or station signature vector between each station and the array [STKL97a]. As noted in [STSK98], this technique is only feasible when the coherence time of the channel is long compared to packet transmission times. In [STKL97a], indoor vector channel response measurements were made which include the effects of channel time coherence. In this chapter a narrowband system under relatively heavy multipath conditions is considered, such as that which is typical indoors and in other situations. Accordingly, a flat narrowband Rayleigh channel is assumed between the portable station and each antenna output. This type of model is commonly used in this environment [Win87a], and the results presented in [STKL97a] support its validity. The narrowband assumption is valid for indoor data rates in the low Mbps and below.

A diagram of the system considered is shown in Figure 5.1. Packets which arrive from the wired network for the portable stations are queued at the basestation to await transmission in the forward-link direction. Similarly, packets generated by the portable stations are transmitted on the reverse-link as described in Section 5.3 below.

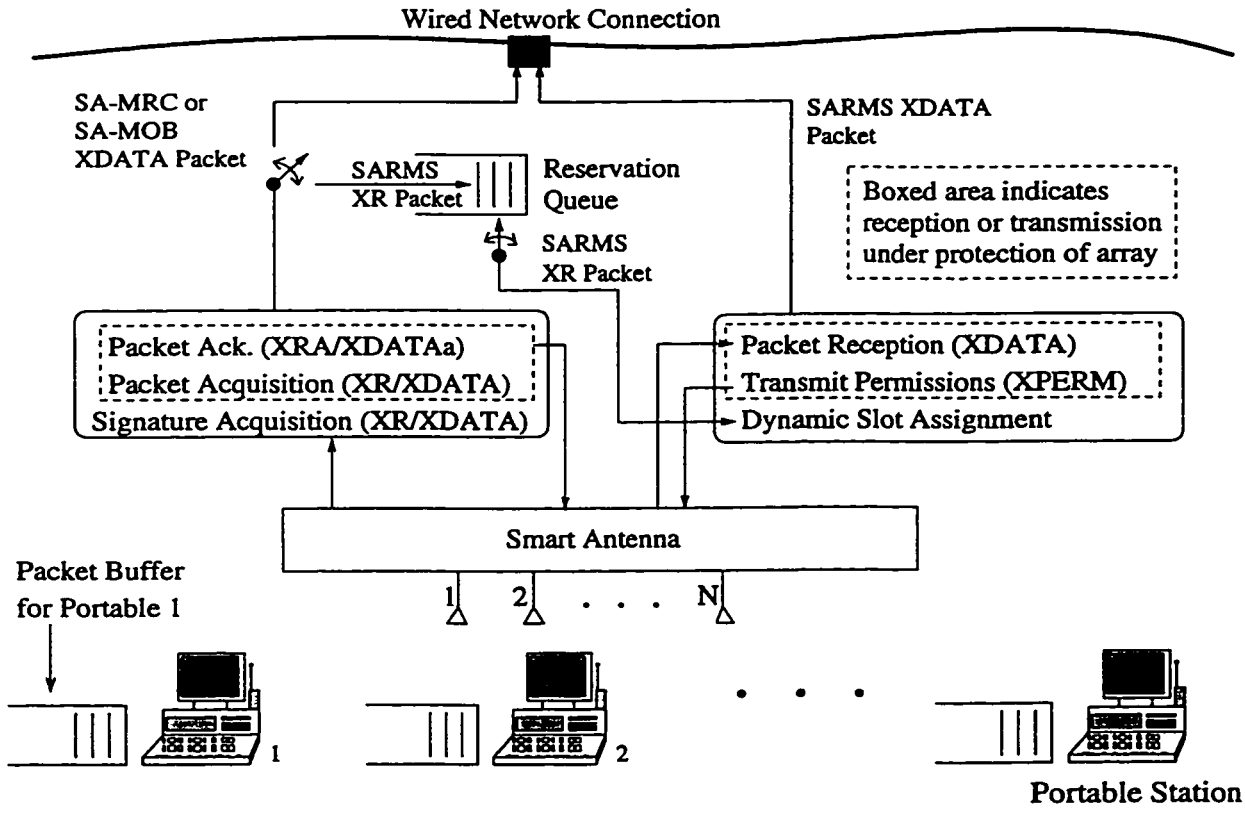

Figure 5.1: Smart antenna basestation S-ALOHA system diagram (Reverse link).

In this chapter the focus is on the latter case, that is, on access to the basestation by the portable stations. The reader is referred to [STSK98] for a discussion of forward-link transmission in this type of system.

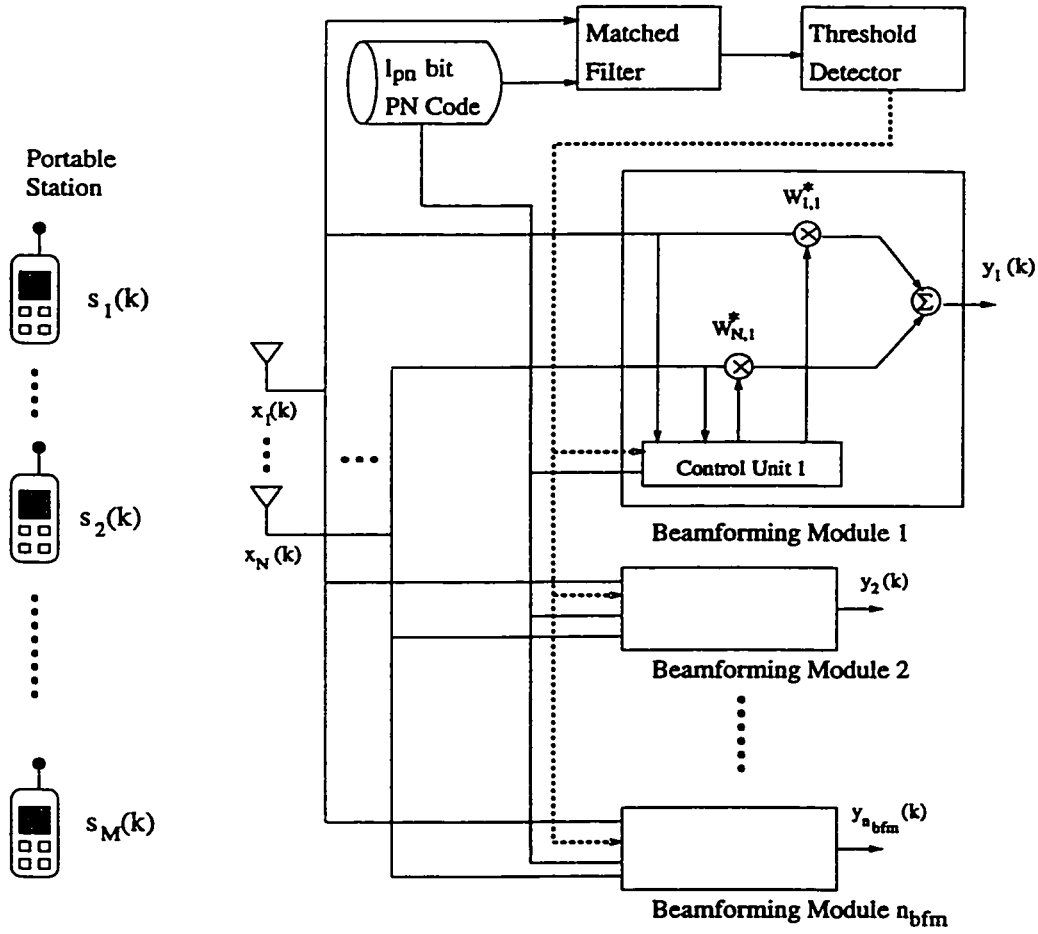

Figure 5.2: Multibeam smart antenna in receive mode.

Under multiple beamforming SDMA operation, the basestation can attempt to transmit or receive up to n_{bfm} packets simultaneously by forming n_{bfm} antenna beam patterns. This is accomplished by having n_{bfm} parallel beamforming modules operating independently at the basestation. The basestation maintains a different set of weights in each beamforming module and each attempts to optimize that beam performance for one desired station packet transmission. The beamforming hardware of the system considered is shown in Figure 5.2. In this chapter the concentration

is on the protocol capacity of the reverse link. A similar analysis can be done for the forward-link direction [LL96]. As before, the optimal weights for reception and transmission are determined through DMI using Equations (3.21) and (3.22). In the ensuing sections the optimal SINR beamforming defined by these equations is used to evaluate the performance of the smart antenna basestation. SNR is defined to be the mean signal power to mean noise power ratio at each antenna output before beamforming.

The systems we consider are packet-based, and therefore acquisition is performed in real-time on a packet by packet basis. The approach taken is to establish the proper antenna beamforming at the start of each received packet, and then use those settings for its duration. This is a reasonable approach for indoor systems operating in the low GHz frequency spectrum, for example the unlicensed ISM bands, since the higher data rates and low doppler ensure that typical channel coherence times are many times longer than packet and frame durations.

Unless otherwise stated, antenna operation is based on optimal beamforming using direct matrix inversion, i.e., Equation (3.19). There are a number of ways that this can be implemented in practice. For example, the desired station signature $\mathbf{v}_d$ can be sampled by correlating against a known pseudo-noise code transmitted at the start of each packet transmission [WC93]. The autocorrelation matrix $\mathbf{R}$ can be estimated in a similar way by sampling the antenna outputs over the same interval. Alternatively, $\mathbf{R}$ can be estimated by using the individual spatial codes obtained from the output of the other basestation beamforming modules.

5.3 Protocol Descriptions

In this section the operation of the S-ALOHA protocols is described. Figure 5.2 indicates the necessary hardware in the most general form. The specific hardware components from this figure which are needed for each protocol will be noted as required. In the protocol descriptions, we use the term "multibeam" to indicate when multiple beamforming modules are active and attempting to receive one packet each. When only a single beamforming module is being used, we refer to this as

"single-beam".

We are interested in the maximum capacity of the systems considered, under a large station population. Accordingly, in our capacity calculations the packet arrivals to the channel are modeled as a Poisson process. This type of model is commonly used to evaluate capacity performance under these circumstances [BG92, Abr70, Rob75]. The channel is assumed to be static in that station signature vectors remain essentially unchanged from the time they are sampled to when the beamforming weights are applied to receive the packet. It should be noted that in [STKL97b], indoor measurements were taken at 1.86 GHz which show that even when there is continuous pedestrian movement in the channel, the coherence times are in the high 10's of ms.

In the protocols discussed below, stations can successfully coexist in the same data slot as long as

$$\text{SINR}_i \geq \text{SINR}_{min}, \tag{5.1}$$

for each station i. The required SINR_{min} threshold depends on the modulation scheme and the bit error rate performance desired [Hay78]. The protocols considered are now described in detail.

5.3.1 S-ALOHA with MRC

In this protocol, a single-beam is used with maximum ratio combining (MRC) antenna beamforming at the basestation [Com88]. Initial access to the channel is done directly in the data slots. An example of the basic frame structure of S-ALOHA with MRC (SA-MRC) is given in Figure 5.3. The XDATA slot includes an l_{pn} bit binary maximum length pseudo-noise (PN) code [SP80], followed by the station identifier, l_{data} bit data slot, and finally a a cyclic redundancy check (CRC) code. It should be noted that in practice a number of repetitions of the PN code would typically be used. The beamforming module correlates against the PN code to obtain the station signature. The reader is referred to [WC93] for a more detailed discussion of the acquisition process. In Figure 5.3 and in those shown below, parts of various packets which are not referred to are shown shaded. Note that the beamforming SINR given in Equation (3.21) cannot be used to determine if the packet was received correctly

because the station signature vectors will be incorrect if two or more stations transmit simultaneously. For this reason a CRC code is necessary to detect errors in reception. For SA-MRC, the basestation is used only to improve the SNR by maximizing the gain against random noise [Win87b]. With MRC, if a single XR packet is sent, it is successfully received and acknowledged by the basestation with a XDATAa packet. Otherwise no packets are successfully received and the XDATAa packet is not sent. With Rayleigh spatial station codes it is possible that a single transmission may not be successful. However, in the results that will be presented, the SNRs are such so that the probability of this is negligible.

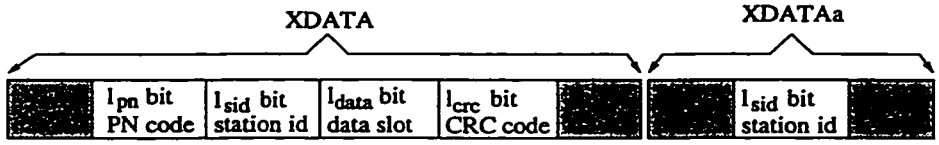

Figure 5.3: Frame structure of SA-MRC protocol.

5.3.2 S-ALOHA with SDMA

In this protocol, multibeam acquisition is performed at the basestation. As before, initial access to the channel is done directly in the data slots. An example of the basic frame structure of the S-ALOHA with SDMA (SA-MOB) protocol is given in Figure 5.4. The uplink XDATA slot consists of a $l_{pn} - 1$ bit randomization interval which sets the starting point of the packet transmission. Following this are three (or more) repetitions of the PN code, the station identifier, the data slot, and finally a CRC code. For SDMA operation, processing is necessary to dynamically acquire more than one packet using multiple beamforming modules. As discussed in [WC93], a matched filter and a threshold detector are required for this, as shown in Figure 5.2. Dynamic packet acquisition is done by using a filter matched to a known PN code. In Figure 5.2, the output of the first antenna is fed into the matched filter. The output of the matched filter is observed by a threshold detector which triggers the next available beamforming module to acquire the desired station signature vector and the autocorrelation matrix. This is done by correlating against the second PN code

in the XDATA packet. The basis for this technique was first suggested in [WC93], where further details are given. The data slots from the desired portable stations are then received using the optimal beamforming weights given by Equation (3.19). Then successful packets are acknowledged by the basestation in the XDATAa slot by using the weights for the reverse link scaled to limit the transmit power and achieve the required SINR_{min}.

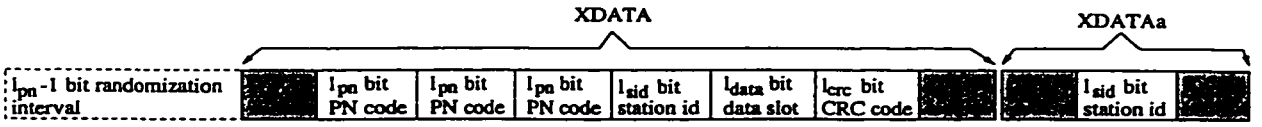

Figure 5.4: Frame structure of SA-MOB protocol.

In Figure 5.2, the output of the first antenna is fed into a matched filter. Since in a heavy multipath situation this antenna could be in a fade, in a practical implementation it may be necessary to feed the outputs of several antennas into different matched filters. The sum of the absolute values of the outputs of these matched filters would then be fed to the threshold detector, and the rest would proceed as before.

5.3.3 SDMA S-ALOHA with Reservation

When reservations are used, the basestation can sample the spatial signatures of those stations which transmit successfully in the reservation subframe. This information is stored at the basestation and used in the beamforming process when the stations transmit in the data slots. The spatial codes can also be used as the basis for dynamic slot assignment as discussed below.

The frame structure of SDMA S-ALOHA with a mini-slotted reservation channel (SARMS) is given in Figure 5.5. Each packet can be viewed as being processed serially by two servers, i.e., first the reservation server (i.e., reservation slots), followed by the data server (i.e., data slots). The reservation server consists of n_{rms} minislots in which stations contend for access to the data server consisting of n_d data slots. New packet arrivals are randomized uniformly over the reservation minislots. The data slots are always operated in multibeam SDMA mode, but the reservation slots can be operated in either single-beam or multibeam SDMA mode. When the reservation slots

use single-beam S-ALOHA with MRC, the protocol is referred to as SARMS-MRC. When it uses multibeam S-ALOHA with SDMA, the protocol is called SARMS-MOB. Use of the former protocol only requires multiple beamforming modules while the latter also requires dynamic packet acquisition using a matched filter and a threshold detector. A variant of SARMS-MOB was proposed in [XL94].

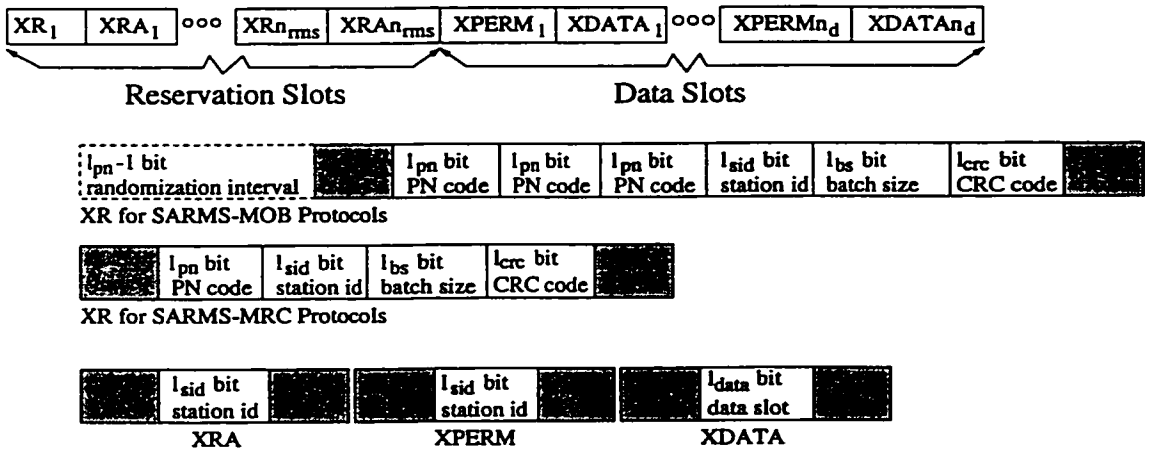

Figure 5.5: Frame structure of SARMS protocols.

Each reservation minislot is composed of a XR and then a XRA. The station identifier, batch size, and then a CRC code are received in the XR part after MRC for single-beam reception or optimal beamforming for multibeam reception has been applied. The batch size indicates to the basestation how many XDATA packets the request is for. The basestation acknowledges all successful XRs in the XRA part. For SARMS-MOB, since only stations which could be successfully resolved in the XR are acknowledged, the XRA is also done in SDMA mode. For SARMS-MRC, the XRA is done in MRC mode.

The data part of the frame contains n_d pairs of transmit permissions (XPERM) and the corresponding data slots (XDATA), both of which take place in SDMA mode. At the start of each data slot, the basestation has to assign packets for transmission. This is accomplished as follows.

Successful XR requests are placed into a reservation queue at the basestation. Each item in the reservation queue contains the station identifier and received spatial signature of the station. This is obtained during the reservation process as discussed

above. Given a set of station spatial codes, there are generally many ways in which the stations can be assigned to the XDATA slots such that Equation (5.1) is satisfied. In this chapter we propose two different slot assignment techniques. The first one is referred to as non-exhaustive, and stops as soon as the next station in the reservation queue cannot be allocated. At this point the basestation proceeds on to allocate the next data slot. The second scheme is referred to as exhaustive, and this technique only stops allocating stations to the current slot when none of the requests in the reservation queue can be added, such that Equation (5.1) is satisfied. It is important to note that this slot assignment is performed in the basestation prior to having the stations transmit into their allocated slots. The two techniques are described in detail as follows.

Non-Exhaustive-MRC and Non-Exhaustive-MOB: The station at the head of the reservation queue is removed from the queue and added to the XDATA slot. Then the next station at the head of the reservation queue is temporarily added to the XDATA slot and optimal SINR beamforming is used to see if Equation (5.1) would be satisfied for each station. If successful, this request is added to the XDATA slot, and the algorithm continues with the next station at the head of the reservation queue. The algorithm terminates once the reservation queue is empty or Equation (5.1) is violated for one or more stations.

Exhaustive-MRC and Exhaustive-MOB: The station at the head of the reservation queue is added to the XDATA slot. Then, starting from the head of the reservation queue, each station in the queue is tested to see if it can be added to the XDATA slot so that Equation (5.1) is satisfied for every station in the XDATA slot. If a successful station is found, it is removed from the reservation queue and added to the XDATA slot, and the algorithm continues with the next station proceeding this one in the reservation queue. The algorithm terminates only when a station cannot be found such that Equation (5.1) is satisfied for all stations in the XDATA slot, or if the reservation queue is empty.

In the rest of this chapter, SARMS-MRC will be used to refer to both Non-Exhaustive-MRC and Exhaustive-MRC, and similarly, SARMS-MOB will refer to both Non-Exhaustive-MOB and Exhaustive-MOB.

Once a XDATA slot assignment is complete, the basestation sends transmit permissions using SDMA in the XPERM slot to all stations which have been selected for the XDATA slot. The stations which receive transmit permission immediately send their data packets in the XDATA slot. Note that in the narrowband indoor environment considered, typical channel propagation delays are at most a few bit times in duration. For this reason, frame pipelining is not needed to ensure small basestation to portable turnaround times.

An important issue is that of the computational complexity of the slot allocation procedures discussed above. This issue was considered in the previous chapters, and also in [Sin97], where slot allocation was discussed in polled systems. It has been shown that for the modest data rates considered, the required computations are well within the current DSP capabilities. It should also be noted that this function is performed in the basestation where it is reasonable to provide the needed computational capability.

5.3.4 Protocol Throughput

In this section simple expressions for system throughput using the classical model [Abr70] are developed. With the SA-MRC protocol, the transmission is successful if and only if a single transmission takes place. Therefore, for SA-MRC the unnormalized throughput S_u is given by the classical S-ALOHA result [Abr70], i.e.,

$$S_u = Ge^{-G}, \tag{5.2}$$

where G is the offered load to the channel. S_u is the average number of successful packet transmissions per XDATA slot, and G is the average number of attempted packet transmissions per XDATA slot. The normalized throughput S which takes into account the protocol overhead is therefore

$$S = \frac{l_{data}}{l_{mrc}} Ge^{-G}, \tag{5.3}$$

where $l_{mrc} = l_{pn} + 2l_{sid} + l_{crc} + l_{data} + l_h$. l_h is defined to be the duration of the shaded packet overheads shown in Figures 5.3, 5.4 and 5.5. For the results in this paper it has been left as 0.

With the SA-MOB protocol, a packet is successfully received only if each packet has selected a different randomization interval and the SINR given by Equation (3.21) is equal to or greater than SINR_{min}. Therefore, for SA-MOB the unnormalized throughput is

$$S_u = \sum_{i=1}^{\infty} \sum_{k=1}^{\min(n_{bfm},N,i)} \frac{e^{-G}G^i}{i!} k p_s(k|i) \frac{(l_{pn})(l_{pn}-1)\cdots(l_{pn}-i+1)}{l_{pn}^i}, \tag{5.4}$$

where $p_s(k|i)$ is the probability of k successful transmissions given that there are i transmissions and each user has selected a unique randomization interval. When optimal SINR beamforming is used, there is no known closed-form expression for these probabilities and hence $p_s(k|i)$ must be evaluated through computer simulation. The fraction to the right of $p_s(k|i)$ in the above formula is the probability that each user has selected a unique randomization interval. The normalized throughput for SA-MOB is then equal to

$$S = \frac{l_{data}}{l_{mob}} \sum_{i=1}^{\infty} \sum_{k=1}^{\min(n_{bfm},N,i)} \frac{e^{-G}G^i}{i!} k p_s(k|i) \frac{(l_{pn})(l_{pn}-1)\cdots(l_{pn}-i+1)}{l_{pn}^i}, \tag{5.5}$$

where $l_{mob} = 4l_{pn} - 1 + 2l_{sid} + l_{crc} + l_{data} + l_h$.

For the SARMS protocols the unnormalized throughput is the minimum of the unnormalized throughput of the reservation and data channels. Therefore, the unnormalized throughput for the SARMS protocols is equal to

$$S_u = \min(\frac{n_{rms}S_r}{n_d}, S_d), \tag{5.6}$$

where S_r is equal to S_u from either Equation (5.2) or Equation (5.4) depending on whether the reservation channel is run in single-beam or multibeam mode, respectively, and S_d is the unnormalized throughput of each data slot. An analytic expression does not exist for S_d, so it is obtained through computer simulation of the exhaustive or non-exhaustive dynamic slot assignment scheme. The normalized

throughput for the SARMS protocols is equal to

$$S = \frac{n_d l_{data}}{n_d(l_{data} + l_{sid}) + n_{rms} l_{saloha}} \min(\frac{n_{rms} S_r}{n_d}, S_d), \tag{5.7}$$

where $l_{saloha} = l_{mrc}$ for SA-MRC, and $l_{saloha} = l_{mob}$ for SA-MOB. The optimal design of the system involves setting the integers n_d and n_{rms} so as to maximize the peak value of S as a function of G, i.e, the capacity. This optimization depends upon the S-ALOHA protocol, l_{data}, and the SNR. In this chapter the values of n_d and n_{rms} have been optimized manually to maximize the capacity results.

5.3.5 Analytic Delay Model for SA-MRC and SA-MOB Protocols

A simple analytic delay model for the SA-MRC and SA-MOB protocols is now considered. It is assumed that we have a finite population of M portable stations. To obtain an analytically tractable model, we will also assume that the channel is independent between successive transmissions from the same portable station. This assumption will be validated by computer simulation.

Referring back to Figures 5.3 and 5.4, at the start of a XDATA slot, a station is either blocked or unblocked. An unblocked station transmits its packet with a probability of p_o, where $p_o = \lambda/M$, where λ is the rate at which new packets are generated by active stations. Successful packets are immediately acknowledged in the subsequent XDATAa slot. If a packet is not acknowledged, the station becomes blocked. Under low load, in order to clear blocked packets quickly, a blocked station retransmits its packet with a probability of p_r, which is greater than p_o. Under medium to high load from a capacity point of view it is best to limit p_r to a value much less than one so that the channel is not saturated after a collision. This does, however, compromise the delay performance. It is assumed that packets which arrive to blocked stations are discarded. This type of model is commonly used to approximate the performance of large populations where there is infinite queueing available at each station [BG92]. Formulas for the mean throughput using a discrete time finite state Markov chain are now derived.

Let the state n be the number of blocked portable stations at the start of a time slot. Each of these stations will retransmit a packet in the slot with a probability p_r. Each of the $M - n$ unblocked stations will transmit a new packet with a probability of $p_o = \lambda/M$.

Let $P_r(l, n)$ be the probability that l blocked stations retransmit given that there are n blocked stations. Let $P_o(l, n)$ be the probability that l unblocked stations transmit, given that there are n blocked stations, i.e.,

$$P_r(l, n) = \binom{n}{l} p_r^l (1 - p_r)^{n-l}, \tag{5.8}$$

$$P_o(l, n) = \binom{M - n}{l} p_o^l (1 - p_o)^{M-n-l}. \tag{5.9}$$

For SA-MRC, n increases by the number of new transmissions by unblocked nodes, less one if a transmission is successful. A transmission is successful if one unblocked node transmits and no blocked nodes transmit, or vice-versa. Therefore, the state transition probability of going from state n to $n + i$ is given by

$$P_{n,n+i} = \begin{cases} P_o(i, n), & 2 \leq i \leq (M - n) \\ P_o(1, n)[1 - P_r(0, n)], & i = 1 \\ P_o(1, n)P_r(0, n) + P_o(0, n)[1 - P_r(1, n)], & i = 0 \\ P_o(0, n)P_r(1, n), & i = -1. \end{cases} \tag{5.10}$$

Figure 5.6 is a diagram of the corresponding Markov chain.

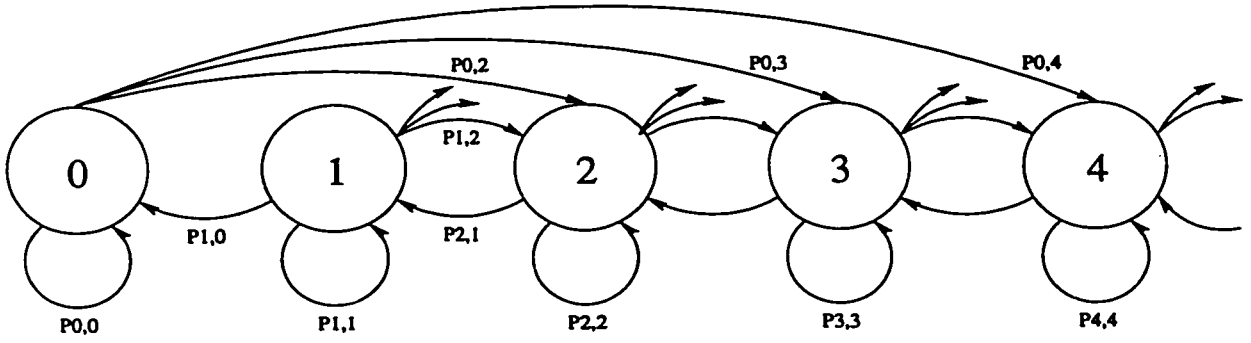

Figure 5.6: Markov chain for SA-MRC.

For SA-MOB, the multibeam capability of the smart antenna permits up to $\min(n_{bfm}, N, n)$ blocked packets to be successful at once. The probability of having l successful packets in the presence of k transmissions after multibeam optimal beamforming has been determined by simulation. For more than one packet to be successful, it is also necessary for each portable station to select a different randomization interval. Therefore, the probability of having l successful users given k transmissions is

$$P_s(l|k) = \begin{cases} p_s(l|k)\frac{(l_{pn}-k+1)\cdots l_{pn}}{l_{pn}^k}, & 0 < l \leq k \\ p_s(0|k)\frac{(l_{pn}-k+1)\cdots l_{pn}}{l_{pn}^k} + (1 - \frac{(l_{pn}-k+1)\cdots l_{pn}}{l_{pn}^k}), & l = 0. \end{cases} \tag{5.11}$$

For the backlog to decrease by i, at least i backlogged users need to transmit. Therefore the state transition probability of going from state n to $n-i$ is,

$$P_{n,n-i} = \sum_{k=i}^{n} \sum_{l=0}^{M-n} P_r(k|n) P_o(l|n) P_s(i+l|k+l),\ i \leq n \leq M \text{ and } 1 \leq i \leq \min(n_{bfm}, N, n), \tag{5.12}$$

where k is the total number of backlogged transmissions and l is the number of new transmissions. For the backlog to increase by i, at least i unblocked users need to transmit. Therefore the state transition probability of going from state n to $n+i$ is

$$P_{n,n+i} = \sum_{k=0}^{n} \sum_{l=i}^{M-n} P_r(k|n) P_o(l|n) P_s(l-i|k+l), 0 \leq n \leq M \text{ and } 0 \leq i \leq M-n. \tag{5.13}$$

The $(M+1)\times(M+1)$ matrix $\mathbf{P}$ defined by the state transition probabilities, given in Equation (5.11) for SA-MRC or Equations (5.12) and (5.13) for SA-MOB, is used to find the steady state probability distribution vector $\underline{\pi} = [\pi(0), \pi(1), \cdots, \pi(M)]$, where $\pi(i)$ is the probability of i blocked users in steady state. The solution to this is given by the usual linear system of equations defined by

$$\underline{\pi} = \underline{\pi}\mathbf{P}, \tag{5.14}$$

subject to the constraint

$$\sum_{i=0}^{M} \pi(i) = 1. \tag{5.15}$$

For SA-MRC, since a transmission is successful if and only if a single transmission takes place, the unnormalized throughput conditioned on the state is

$$S_u(n) = P_r(1,n)P_o(0,n) + P_r(0,n)P_o(1,n). \tag{5.16}$$

For SA-MOB, it is possible for up to N packets to be successful. The unnormalized throughput conditioned on the state is

$$S_u(n) = \sum_{s=1}^{\min(N,n_{bfm})} sP(s \text{ successful users}), \tag{5.17}$$

where $P(s$ successful users$)$ is obtained by conditioning on the total number of transmissions as

$$P(s \text{ successful users}) = \sum_{l=s}^{M} P_s(s|l)P(l \text{ transmissions}). \tag{5.18}$$

$P(l$ transmissions$)$ is obtained by conditioning on the number of retransmissions from blocked users as

$$P(l \text{ transmissions}) = \sum_{k=\max(0,l-M+n)}^{\min(l,n)} P_r(k|n)P_o(l-k|n). \tag{5.19}$$

Then the unnormalized throughput is

$$S_u = \sum_{n=0}^{M} S_u(n)\pi(n). \tag{5.20}$$

The normalized throughput is then equal to

$$S = \frac{l_{data}}{l_{saloha}} S_u. \tag{5.21}$$

The average number of blocked users is

$$B = \sum_{n=0}^{M} n\pi(n). \tag{5.22}$$

Using Little's Theorem [TK84], the average delay normalized to the size of a data slot is

$$D = \frac{l_{saloha}}{l_{data}} \frac{B}{S_u}. \tag{5.23}$$

The load line $S_{in}(n)$, defined as the average number of new packets offered to the system per data slot, is

$$S_{in}(n) = (M-n)p_o. \tag{5.24}$$

Suppose that $S_{in}(n)$ intersects $S_u(n)$ three times. Then the second point of intersection, say state n_u, is called an unstable equilibrium. Once the number of blocked

users reaches n_u, the system can quickly drift to the third point of intersection where it remains in a state of low throughput and high delay for a long time. Hence, the mean time to failure (MTTF) is defined as the average time it takes for the number of blocked users to reach n_u, assuming that the system starts with zero blocked users. Then, using a first step analysis technique described in [TK84], the MTTF is the first element of the $n_u \times 1$ column vector

$$\mathbf{v} = (\mathbf{I} - \mathbf{P}_u)^{-1}\mathbf{1}, \tag{5.25}$$

where $\mathbf{I}$ is the an $n_u \times n_u$ identity matrix, $\mathbf{P}_u$ is an $n_u \times n_u$ matrix composed of the upper left quadrant of $\mathbf{P}$, and $\mathbf{1}$ is a $n_u \times 1$ column vector composed entirely of ones. It is also possible for $S_{in}(n)$ to intersect $S_u(n)$ only once. In this case if the intersection is at a point of high throughput and low delay, then the MTTF is defined to be infinity. If it is at a point of low throughput and high delay, then the MTTF is defined to be zero.

5.4 Performance Comparisons

A large number of performance comparisons have been made for the protocols. In this section some representative examples of the results obtained are given. Table 5.1 shows the default parameters used for the results presented. The first set of results are throughput versus applied load for the SA-MOB system at various SNRs. In these curves the system capacities can be compared with that of SA-MRC. The delay-throughput performance of these systems are then compared using the analytic model presented in Section 5.3.5. Close agreement is seen between the capacities obtained using the analytic model and those obtained in the delay results. Simulation results for mean delay are also presented which serve to further validate the analytical model. Then the effect of varying n_{bfm} for SA-MOB are examined. Following this the SARMS protocols are examined and compared with SA-MOB and SA-MRC for different XDATA slot sizes and SNRs. Throughput results are presented for a variety of operating conditions. Increases in system capacity using more sophisticated dynamic slot assignment is also considered. Improvement in the throughput of the SARMS

protocols due to requests for multiple packets with each XR are then examined. Finally, mean delay simulation results for all of the protocols using two different data slot sizes are given.

Parameter	Value
Antennas (N)	8
SINR_{min}	10 dB
SNR	6 dB
Num. beamforming modules (n_{bfm})	8
Length of PN code (l_{pn})	63 bits
Length of station id. field (l_{sid})	8 bits
Length of batch size field (l_{bs})	8 bits
Length of CRC field (l_{crc})	32 bits
Size of XDATA slot (l_{data})	1024 bits
Batch size (b_s)	1 (constant)

Table 5.1: Default simulation parameter values

Figure 5.7 is a graph of the throughput versus the offered load for the SA-MRC and the SA-MOB protocols for different values of noise power. The throughput is the average number of successful transmissions per XDATA slot and is normalized to take protocol overheads into account. The offered load is the average number of packet transmissions per XDATA slot. The capacity for SA-MRC is about 0.33, which is slightly less than the 0.36 for infinite population single channel S-ALOHA due to the protocol overhead. For SA-MOB, the capacities are 1.98, 2.54, and 2.83 for 6 dB, 10 dB, and 20 dB SNR, respectively. This means that under high SNR, SA-MOB actually performs over N times better than SA-MRC. However, the SA-MOB capacity is still much less than N under high SNR because of the large variance in the number of transmissions per XDATA slot.

Figure 5.8 is a graph of mean delay versus S for the SA-MRC and SA-MOB protocols using the finite population analytic model with $M = 30$ active portable stations. For SA-MRC the capacity obtained is 0.34, and for SA-MOB, the capacities are 2.04, 2.64, and 2.95 for 6 dB, 10 dB, and 20 dB SNR, respectively. These capacities

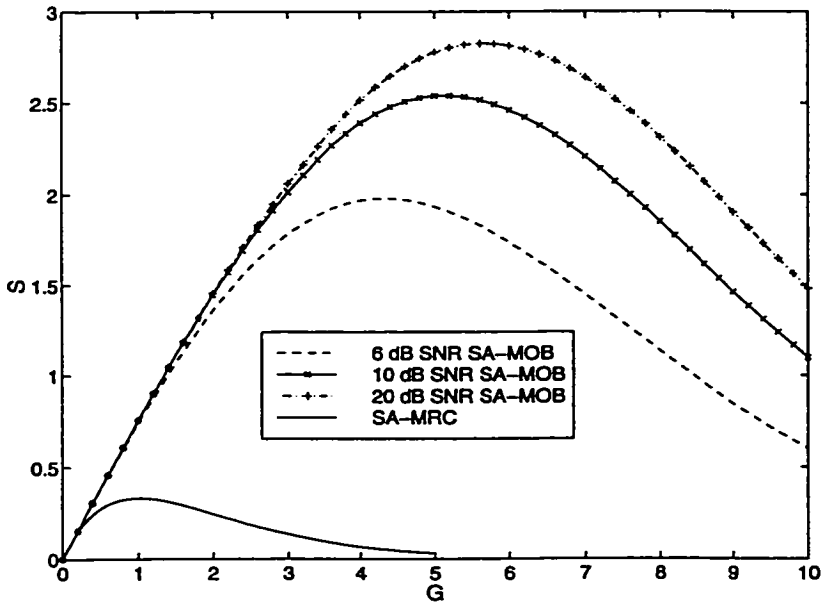

Figure 5.7: SA-MOB and SA-MRC throughput for different values of SNR.

are very close to those which were obtained with using the Poisson channel arrival model given in Figure 5.7. In Figure 5.8 we have also included simulation results of the two systems. In the simulation results the signature of the data packet remains the same until the packet is cleared because the channel is assumed to be static. It can be seen that there is reasonable agreement between the analytical and simulation results which further helps to validate the usefulness of the analytical model. The agreement between simulation and analysis is least for the smallest value of SNR. Under these conditions it is more difficult for the basestation to achieve successful multibeam operation, and the independence assumption used in the model is less valid than under lower noise conditions.

With the fixed value backoff probability p_r, a system with an unstable equilibrium can saturate as discussed before. Figure 5.9 is a graph of the MTTF for the SA-MOB protocol with 6 dB, 10 dB, and 20 dB SNR. A o on the graph indicates the peak throughput. It can be seen that the SA-MOB protocol can be driven very close to system capacity without failure. In results not presented here it was discovered that when p_r is made larger, the system needs to be driven at values slightly lower than

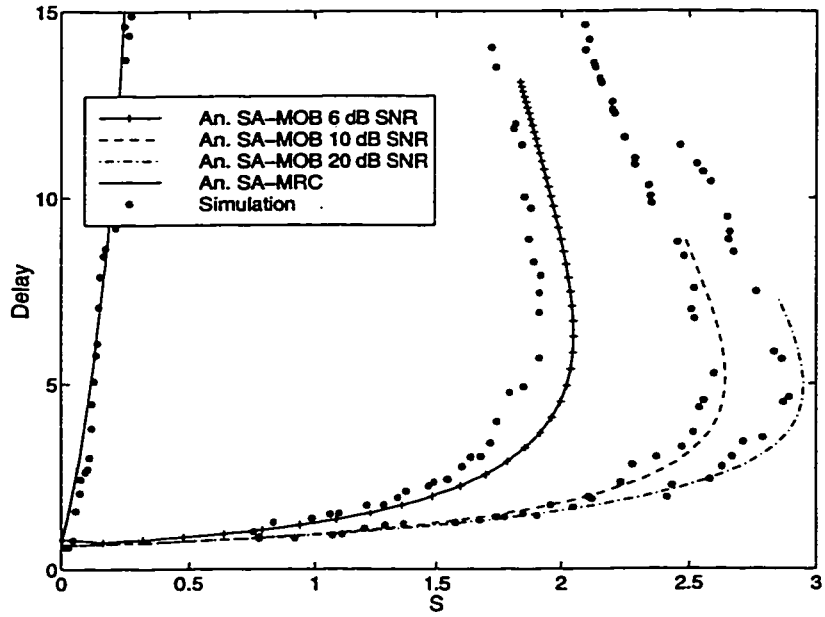

Figure 5.8: SA-MOB and SA-MRC delay and throughput for different values of SNR using the analytic finite population model.

peak throughput in order for the system to remain stable.

In [CR98], a novel technique for improving the throughput and delay performance under high load is proposed in which the array only accepts packets from certain angles at any given time slot. This technique is possible with a LOS-only wireless propagation channel. The admissible angles are shifted every K time slots so that in the long run 360 degree coverage is achieved. This technique improves performance under high load by effectively reducing the finite population size. However, under low load the delay is higher and the throughput lower because packets become backlogged when their signature space is not being serviced. We propose a technique in which mobile stations withhold packet transmission altogether until their associated time slot appears. When a mobile transmits its very first packet, it selects this time slot and every subsequent $p_{sf}{}^{th}$ time slot as one in which it can access the channel, where p_{sf} stands for population splitting factor. This way, on average the number of stations which contend for the channel in each time slot is M/p_{sf}. Figure 5.10 is a graph of the SA-MOB delay versus S with population splitting. Under low load, the delay is

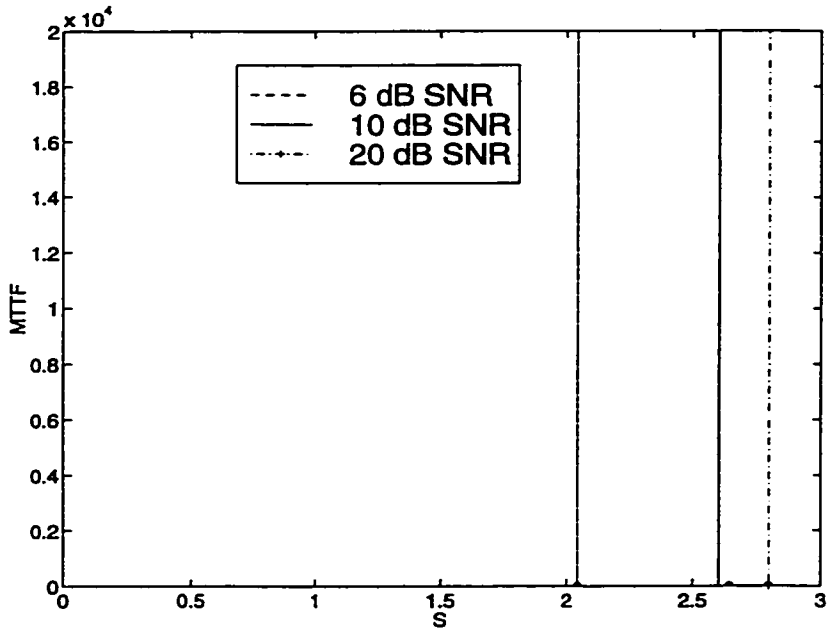

Figure 5.9: SA-MOB MTTF for different SNRs.

lower without population splitting because a station in general successfully transmits in the next slot. With population splitting, it needs to wait for its assigned slot before transmitting. With $p_{sf} = 1, 2, 3$, and 5, the capacity is equal to 2.05, 2.12, 2.21, and 2.46, respectively. This indicates that there is significant capacity advantage with population splitting. The penalty for this is higher delay at low throughput and the fact that the highest sustainable data rate of a station is reduced to $1/p_{sf}$ packets per time slot.

The number of beamforming modules in Figure 5.2 can be changed from the nominal value of N. Figure 5.11 is a graph of the S versus the offered load G for various values of n_{bfm}. It can be seen that in this high noise region the value of n_{bfm} can be reduced to 5 without significant degradation in performance. Increasing n_{bfm} to a value beyond $N = 8$ had negligible gain.

Figure 5.12 is a graph of the S versus G for various protocols with a 424 bit data slot. The values of n_{rms} and n_d are optimized to maximize the capacity. Exhaustive-MOB performs the best with a capacity of 2.08, followed by SA-MOB with a capacity of 1.49. Next is Non-Exhaustive-MOB, with a capacity of 1.46. Exhaustive-MRC and

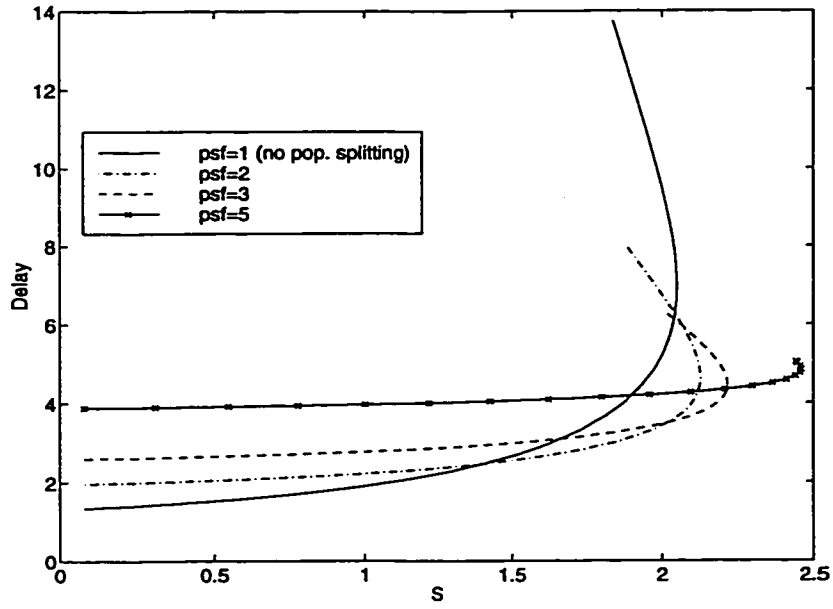

Figure 5.10: SA-MOB delay versus throughput with population splitting.

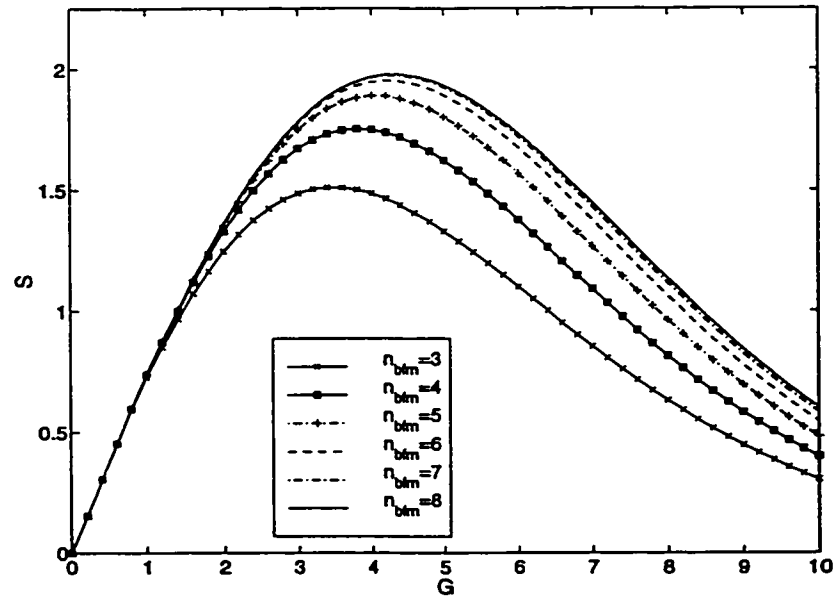

Figure 5.11: SA-MOB throughput for different n_{bfm}.

Non-Exhaustive-MRC have a capacity of 1.03 and 0.94, respectively. SA-MRC has the lowest capacity of just 0.29. Therefore, when data packets are in the ATM cell size range, having an SDMA random access channel is the best. When the data packets are small, it is very important to maximize the throughput of the random access channel since it consumes a significant fraction of the frame. Using an SDMA reservation channel to feed a contention free data channel works the best, especially when the data channel is run using the more sophisticated Exhaustive-MOB slot assignment scheme. However, the SARMS-MRC protocols still have about three times higher capacity than SA-MRC.

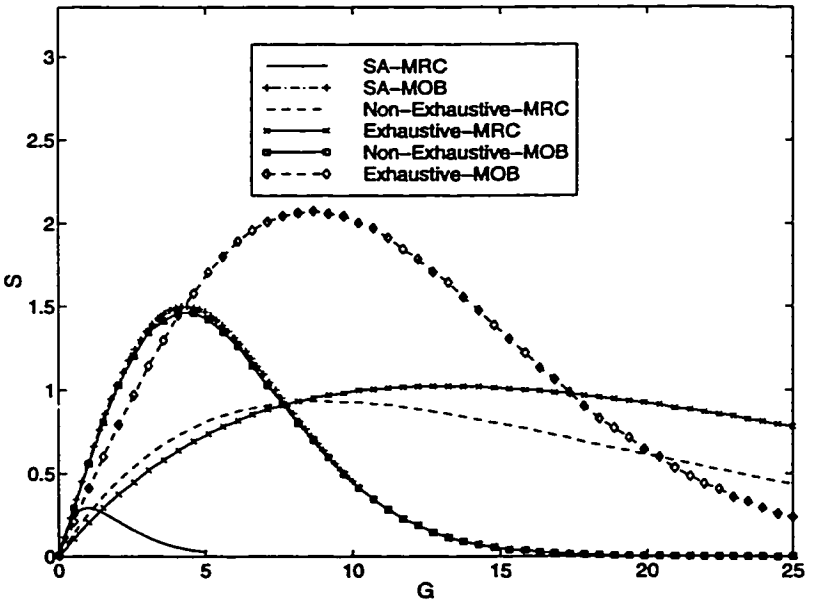

Figure 5.12: Throughput for the different protocols with $l_{data} = 424$ bits.

Figure 5.13 is a graph of the throughput versus offered load for the protocols with a 1024 bit XDATA slot. In this case, the results are similar, except that all capacities are higher due to lower protocol overhead. Also, Exhaustive-MRC is about as good as SA-MOB, indicating that for data packets roughly 1 kbit or larger, a single-beam reservation channel gives comparable performance to using SDMA in the reservation channel directly when XDATA slot assignment is done efficiently. This result is important to note, since implementing dynamic SDMA acquisition in the

reservation channel is highly complex. The throughput obtained in this figure is the minimum of the throughput of the reservation and data channels. The "flattening" of the curves for the Non-Exhaustive-MRC and Non-Exhaustive-MOB protocols is due to the data channel reaching a peak throughput before the reservation channel due to integer effects. Recall from Equations (5.6) and (5.7) that when reservation slots are used, the capacity is the minimum of the capacities of the data and reservation channels. In the optimization that is performed, an integral number of reservation and data slots per frame is chosen. As a result, the total capacity is sometimes prevented from increasing with applied channel load since the data slot throughput has become a bottleneck.

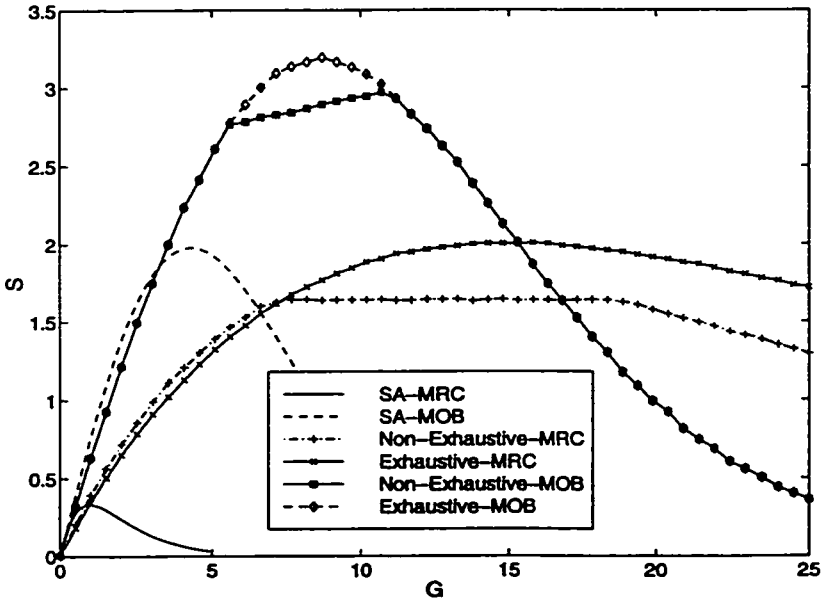

Figure 5.13: Throughput for the different protocols with $l_{data} = 1024$ bits.

Figure 5.14 is a graph of the throughput versus offered load for the protocols with an 8192 bit data slot. In this figure the strong capacity advantage of the Exhaustive DSA over Non-Exhaustive DSA in the SARMS protocols is very evident. Exhaustive-MOB for example has a capacity 35 per cent higher than Non-Exhaustive-MOB. Under the low SNR conditions presented, these results indicate that intelligent DSA

is very important for improving the overall system capacity. For both of the SARMS-MOB protocols, the flat part of the graph has a gradual upslope. For Non-Exhaustive-MOB, the upslope is because there is less chance of the reservation queue being empty at higher loads, and hence the dynamic slot assignment algorithm tends to terminate only when the station being tested has an incompatible spatial signature. For Exhaustive-MOB this is also because with more stations in the reservation queue, the dynamic slot assignment algorithm has a greater number of stations to search for signature compatibility.

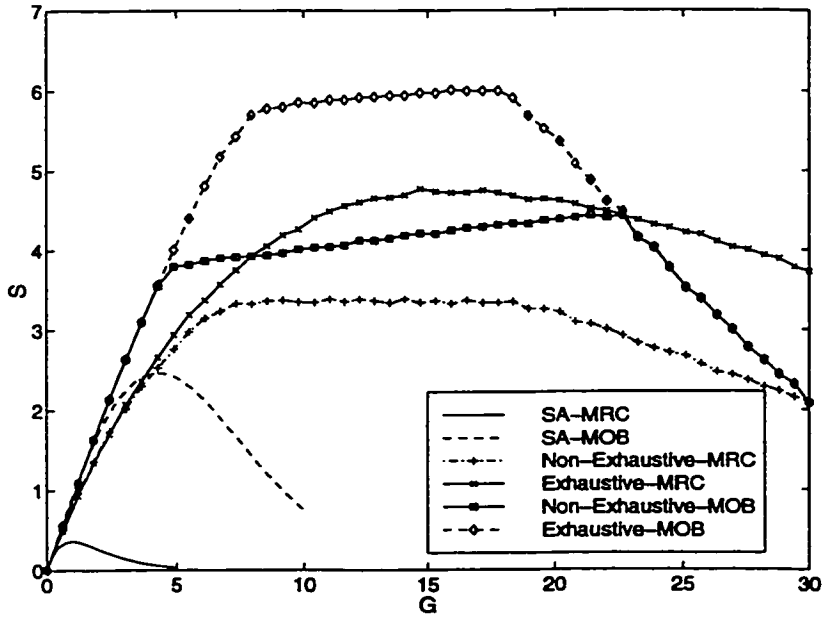

Figure 5.14: Throughput for the different protocols with $l_{data} = 8192$ bits.

Table 5.2 shows a summary of the capacity for various values of l_{data} and SNR. For the SARMS protocols the number of reservation minislots was selected to maximize the capacity. Exhaustive-MOB performs the best in all regions. For small l_{data}, SA-MOB performs better than SARMS-MRC because the extra capacity of the data channel cannot make up for the low capacity of the reservation channel. However, as the size of the XDATA slot increases, the single-beam reservation channel of SARMS-MRC is able to provide sufficient capacity with a low enough overhead to outperform SA-MOB. At 6 dB SNR, SARMS-MRC outperforms SA-MOB for data slots equal to

or larger than 2048 bits, and at 20 dB SARMS-MRC outperforms SA-MOB with a 2048 bit or larger data slot.

For small l_{data}, SARMS-MOB works much better than SARMS-MRC because the SDMA reservation channel is very bandwidth efficient and thus does not require many minislots to provide a sufficient load to the data channel. For large l_{data}, the advantage of SARMS-MOB over SARMS-MRC is marginal because even with many reservation minislots the reservation channel overhead is small. In fact, for 6 dB SNR with an 8 kbit data slot, Exhaustive-MRC actually performs better than Non-Exhaustive-MOB because of the stronger XDATA slot assignment of the former.

Until now the value of b_s in the SARMS protocols has been left as 1. In certain applications such as packetized voice, the packets are generated in batches. If the data is not delay sensitive, batch arrivals can be machine generated by enqueuing packets at the portable station before making a XR. In these situations there is value in making a request for several XDATA slots simultaneously in that a smaller proportion of the frame is required for the reservation channel. Figure 5.15 is graph of the Non-Exhaustive-MOB throughput for different values of b_s. The capacity with a constant batch size of 1 is only around 2.97. With a uniformly distributed mean batch size of 2 and 10, it increases to 3.55 and 4.25, respectively. With SARMS-MRC the capacity gain should be even higher because of the lower efficiency of the reservation channel.

As mentioned earlier, in this chapter the values of n_{rms} and n_d for the SARMS protocols are set to maximize the capacity. Figure 5.16 is a graph of the throughput versus offered load for the Non-Exhaustive-MRC and Non-Exhaustive-MOB protocols. The optimal value of n_{rms} is annotated in the legend with an asterisk (*). It can be seen from this graph that as n_{rms} is increased to a value that is larger than the optimal, the protocol achieves higher throughput under high load at the cost of a small reduction in capacity. This is because the random access channel is effectively given a lesser per minislot load for the same offered load, and hence saturates at a higher level.

Figure 5.17 shows the mean delay results with a 424 bit data slot. For these simulation results the binary exponential backoff algorithm is employed, and the

l_{data}	Protocol	6 dB SNR	20 dB SNR
424 bits	SA-MRC	0.29	0.29
	SA-MOB	1.49	2.14
	Non-Exhaustive-MRC	0.94	1.08
	Non-Exhaustive-MOB	1.46	3.04
	Exhaustive-MRC	1.03	1.08
	Exhaustive-MOB	2.08	3.04
1024 bits	SA-MRC	0.33	0.33
	SA-MOB	1.98	2.83
	Non-Exhaustive-MRC	1.64	2.22
	Non-Exhaustive-MOB	2.97	4.60
	Exhaustive-MRC	2.01	2.25
	Exhaustive-MOB	3.20	4.60
2048 bits	SA-MRC	0.35	0.35
	SA-MOB	2.21	3.19
	Non-Exhaustive-MRC	2.31	3.41
	Non-Exhaustive-MOB	3.40	5.37
	Exhaustive-MRC	2.92	3.48
	Exhaustive-MOB	4.50	5.50
8192 bits	SA-MRC	0.36	0.36
	SA-MOB	2.45	3.52
	Non-Exhaustive-MRC	3.38	5.87
	Non-Exhaustive-MOB	4.44	6.98
	Exhaustive-MRC	4.77	6.00
	Exhaustive-MOB	6.01	7.16

Table 5.2: Capacity at different operating regions.

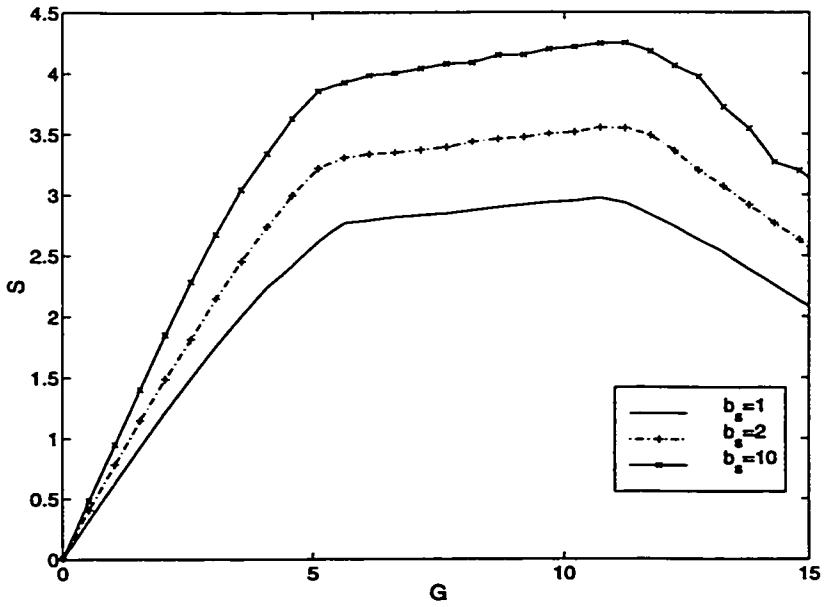

Figure 5.15: Non-Exhaustive-MOB throughput S for different b_s.

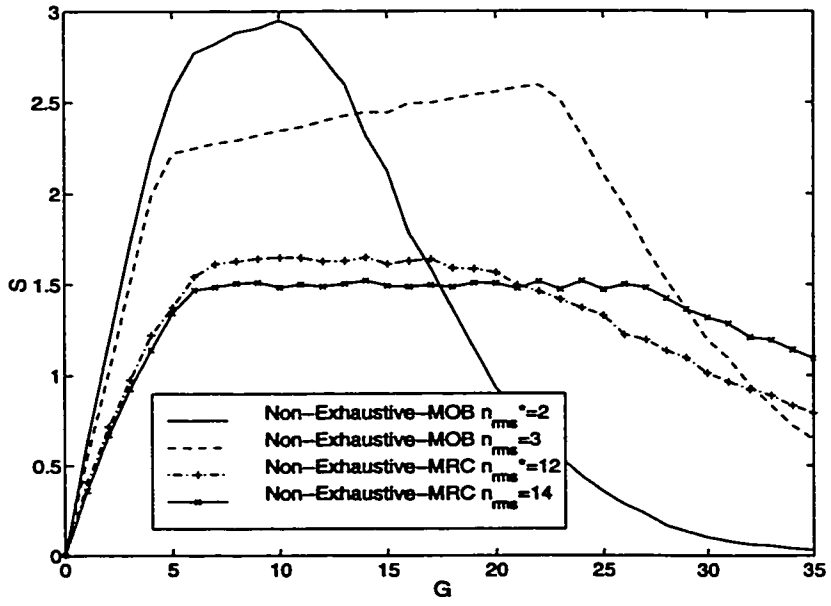

Figure 5.16: SARMS protocol throughput S for different n_{rms}. The value of n_{rms} which maximizes capacity is indicated with an asterisk (*).

delay is normalized to the length of one data slot. For low arrival rates the delay of SA-MRC and SA-MOB is less than 1 data slot, and for the SARMS protocols it is between 2 and 3 data slots. The delay is higher for the SARMS protocols because each packet needs to pass through both the reservation and data channels. In the following discussion we note the delay at 90 per cent of the peak throughput for the protocols. For SA-MRC and SA-MOB, this delay is about 50 and 25 data slots, respectively, indicating a significant advantage in delay performance of SA-MOB over SA-MRC. The delay for Non-Exhaustive-MRC, Exhaustive-MRC, Non-Exhaustive-MOB, and Exhaustive-MOB is about 27, 29, 17, and 17, respectively. This indicates that the delay at this point is about one-half for the SARMS-MOB protocols as compared to SARMS-MRC, and that is it not particularly sensitive to the data slot assignment strategy. The reason for this is that even a relatively small number of SDMA reservation slots operating well below capacity can provide ample traffic for the data channel. Therefore, most of the delay for the SARMS-MOB protocols is from the data channel only.

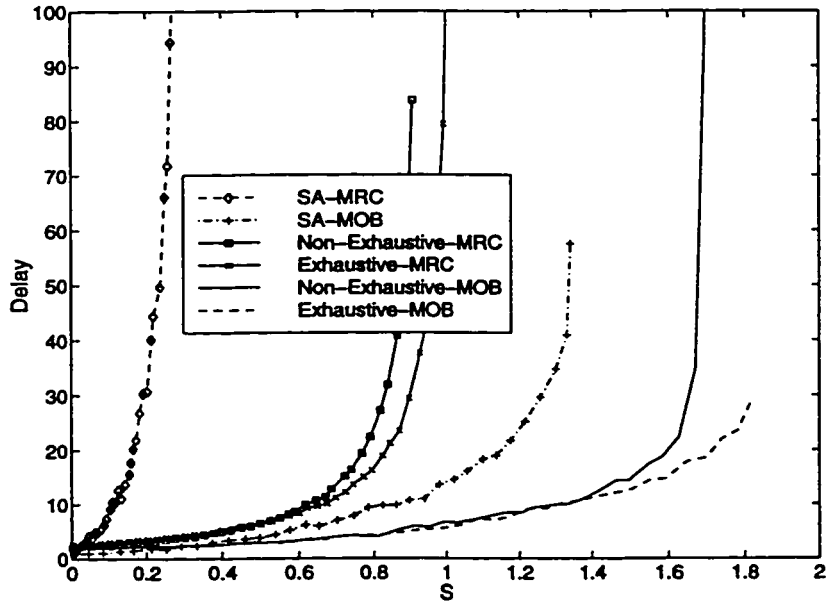

Figure 5.17: Delay results with 424 bit data slot.

Figure 5.18 is a graph of the mean delay results for a larger 1024 bit data slot. At

low load the SA-MRC and SA-MOB delay is roughly the same as for the 424 bit data slot, but the SARMS protocol delays are now between 1 and 2 XDATA slots. This is lower than the 424 bit data slot because in relation to the size of the data slot, the reservation channel is narrower and in general it operates farther from saturation. At 90 per cent of the peak throughputs the delay for SA-MRC and SA-MOB is about 58 and 18, which is similar to the previous case. For Non-Exhaustive-MRC, Exhaustive-MRC, Non-Exhaustive-MOB, and Exhaustive-MOB, the delay is equal to 12, 15, 5, and 8. As before, the delay performance of SARMS-MOB is significantly better than SARMS-MRC. This shows that delay performance improves as packets become larger.

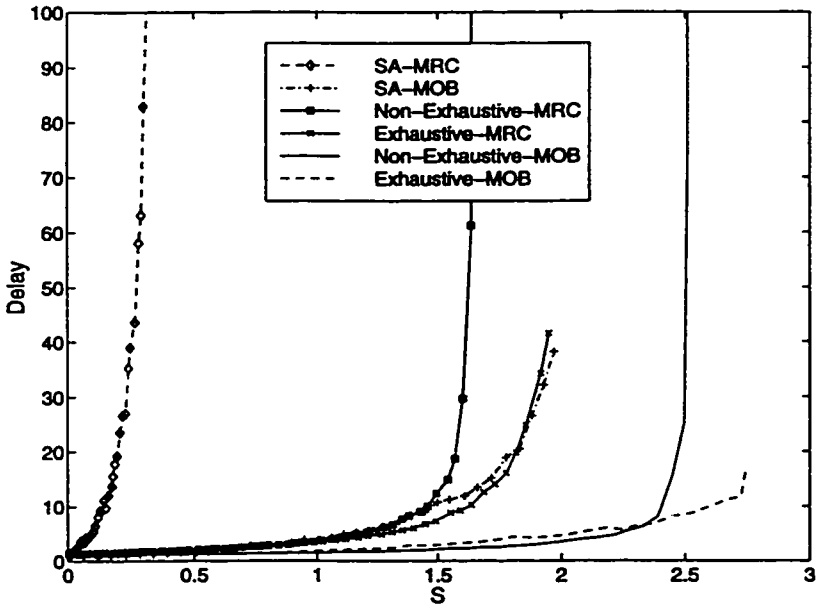

Figure 5.18: Delay results with 1024 bit data slot.

5.5 Multicell SA-MOB protocol

In some cases it may be necessary to use multiple basestations in a picocellular (100 meter diameter) architecture. Reasons for this include the need for greater capacity, lower transmit power, and larger coverage area. Several researchers have examined the use of smart antennas for increasing the capacity of multicell networks [NPK94, YL97,

NP96, SBEM90, TGM96]. In the remainder of this chapter the SA-MOB protocol considered earlier in Section 5.3 is modified to work in a multicell environment with a large degree of coverage area overlap.

As before, the system is TDD, and the concentration is on the reverse link capacity of the protocol. A flat narrowband Rayleigh channel is assumed to exist between the portable station antenna and each smart antenna output. This channel is also subject to lognormal shadowing and exponential power path loss. The frequency is reused in every cell. Basestations are synchronized against a common clock, which could be derived from the Global Positioning System (GPS). This is necessary to prevent the catastrophic interference which can arise if forward and reverse link transmissions coincide. The reverse link configuration of the smart antenna basestation is given in Figure 5.19. The basestation is the same as for the single cell SA-MOB case shown in Figure 5.2 except that it now contains one of several unique PN codes, and the control unit is now also able to transmit the assigned PN code. The portable stations in this system are designed with the necessary functionality for nearest basestation acquisition. More will be said on the issue of basestation acquisition later.

The remainder of this chapter is organized as follows. First the multicell architecture is described. Then the forward and reverse link channels are characterized and modeled. Next the multicell SA-MOB protocol is explained. The additional protocol overhead incurred from the multicell implementation of SA-MOB is examined. Then the throughput and delay performance of the multicell SA-MOB protocol is studied under various system parameters.

5.5.1 Multicell System Architecture

Figure 5.20 indicates the architecture of the multicell system considered in this chapter. There are a total of M mobiles in each cell. N_o is the number of outer cells from which the signature of interfering mobiles is explicitly used. This model for the channel has been taken from [MM97]. If the first two tiers around the center cell are considered for this, as indicated by the larger hexagon in Figure 5.20, then N_o is 18, and the radius R_o of this cluster is $\sqrt{19}$ when the radius of a single cell is equal to 1.

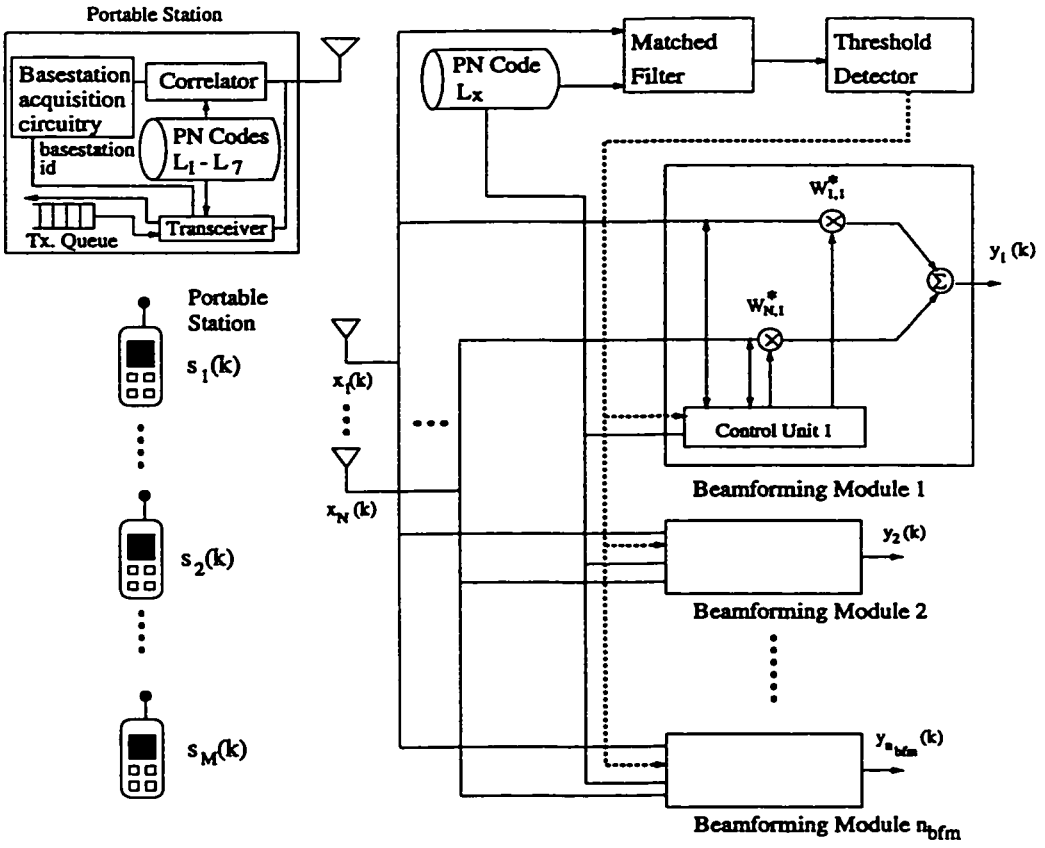

Figure 5.19: Multicell smart antenna basestation in receive mode.

The radius is defined as the distance from the basestation to the vertex.

5.5.2 Multicell SA-MOB Reverse Link

For the reverse link the basestation receives signals from the transmitting mobiles. The basestation which attempts to receive from the desired mobile is the one "closest" to it, and it is located in the center cell. Closest is used here to refer to the basestation which has the strongest link between itself and mobile station. Because of the log-normal shadowing and exponential power path loss, it is not necessarily the one closest in straight line distance. The received $N\times 1$ baseband signal vector $\mathbf{x}(k)$ at the center cell basestation at time sample k is

$$\mathbf{x}(k) = t(d)\mathbf{v}_d s_d(k) + \sum_{\substack{i=1 \\ i\neq d}}^{M} t(i)\mathbf{v}_i s_i(k) + \sum_{o=1}^{MN_o} t(o)\frac{1}{r_o^2}10^{\frac{l_o}{20}}\mathbf{v}_o s_o(k) + \mathbf{n}(k). \qquad (5.26)$$

$t(\cdot)$ in Equation (5.26) is equal to 1 if the corresponding mobile is transmitting, 0 otherwise. $\mathbf{v}_d$ is the complex baseband signature vector of the desired mobile at the center cell basestation, and $s_d(k)$ is the transmitted desired signal. Similarly, $\mathbf{v}_i$ is the complex baseband signature of interferer mobile i at the center cell basestation, where mobile i is located in the center cell. $\mathbf{v}_o$ corresponds to the signature of mobile o from one of the outer cells to the center cell basestation before it is scaled for path loss and lognormal fading. Due to the basestation acquisition process in the protocol which will be discussed in Section 5.6, the mobiles are able to perform power control to remove the effect of exponential path loss and lognormal fading between themselves and the basestation which is receiving from them. The signatures from the interfering mobiles from other cells are subject to lognormal fading $10^{\frac{l}{20}}$ and path loss $\frac{1}{r_o^2}$, where l_o is a normally distributed random variable with a standard deviation of $\sigma_l = 8$ dB [Vit95], and r_o is the distance from the center cell basestation to the basestation in which the interfering mobile is located.

$\mathbf{n}(k)$ is an $N\times 1$ noise vector which is generated from independent identically distributed complex Gaussian samples. It is composed from two sources, and equal to

$$\mathbf{n}(k) = \mathbf{n}_n(k) + \mathbf{n}_i(k). \qquad (5.27)$$

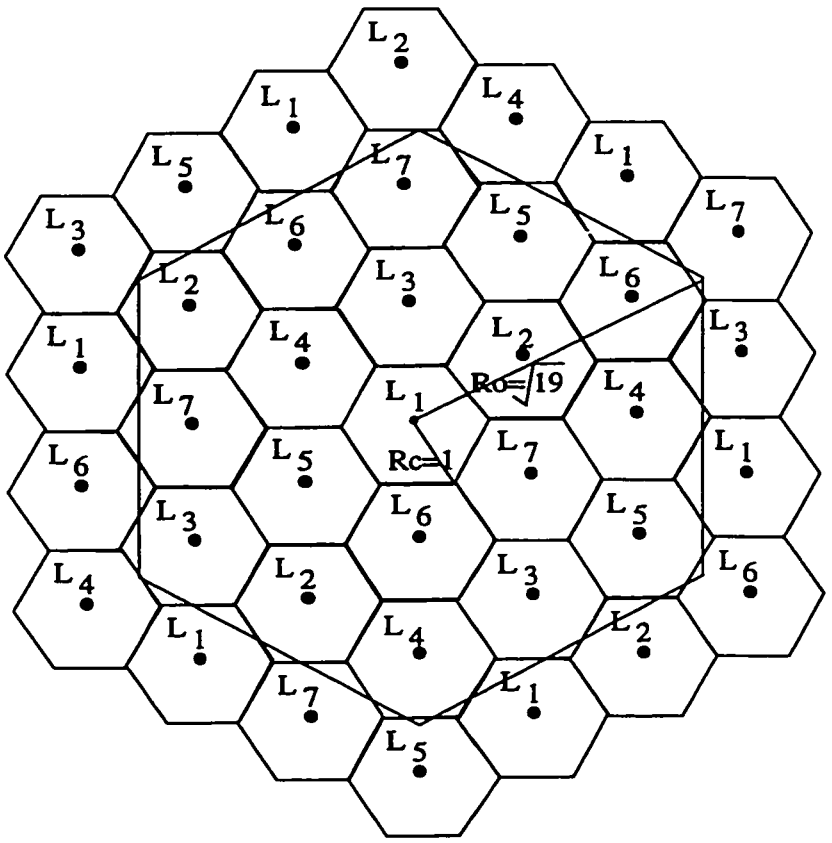

Figure 5.20: Multicell structure with reuse factor seven. The large hexagon has the same area as the center cell plus the first two tiers.

$\mathbf{n}_n(k)$ is the Gaussian noise vector which determines the signal to noise ratio (SNR) at each antenna output, and $\mathbf{n}_i(k)$ is the Gaussian noise that is used to approximate the effect of the interfering mobiles outside of the N_o outer cells. The variance of the zero mean Gaussian noise process is therefore

$$\begin{aligned}\sigma_n^2 &= \sigma_{n,n}^2 + \sigma_{n,i}^2 \\ &= \sigma_{n,n}^2 + \int_{r=R_o}^{\infty} C_m \sigma_v^2 r^{-4} 2\pi r dr, \end{aligned} \tag{5.28}$$

where C_m is the average number of mobiles transmitting per unit area, and σ_v^2 is the average received signal power per smart antenna output from a mobile in the center cell. As before, optimal reverse link beamforming is used to determine the antenna weights.

5.5.3 Multicell SA-MOB Forward Link

For the forward link the basestations transmit to the mobiles. As for the reverse link, the signal is sent to the mobile by the electrically closest basestation. The received baseband signal $x(k)$ at the desired center cell mobile d is

$$x(k) = t(d)\mathbf{w}_d^H \mathbf{v}_d s_d(k) + \sum_{\substack{i=1 \\ i \neq d}}^{M} t(i)\mathbf{w}_i^H \mathbf{v}_d s_i(k) + \sum_{o=1}^{MN_o} t(o)\frac{1}{r_o^2} 10^{\frac{\iota_o}{20}} \mathbf{w}_o^H \mathbf{v}_o s_o(k) + n(k). \tag{5.29}$$

$t(\cdot)$ in Equation (5.29) is equal to 1 if the basestation is transmitting to the corresponding mobile, 0 otherwise. For the forward link, the same weight vector as the reverse link optimal weight vector is used. However, it is scaled so that the forward link SNR at the mobile is a constant 20 dB. This ensures that the system is interference limited. $\mathbf{v}_d$ is the signature of the desired mobile to the center cell basestation, and $s_d(k)$ is the transmitted symbol. The first summation in Equation (5.29) corresponds to the interference generated by transmissions to other mobiles in the center cell. $\mathbf{w}_i$ is the complex weight vector used to transmit to center cell mobile i. The second summation corresponds to transmissions by basestations in the outer cells. $\mathbf{w}_o$ is the complex weight vector used by the outer cell basestation to transmit to mobile o, and $\mathbf{v}_o$ is the signature from the basestation transmitting to mobile o to the desired mobile d.

The variance of the zero mean Gaussian noise $n(k)$ at the desired mobile is equal to

$$\begin{aligned} \sigma_n^2 &= \sigma_{n,n}^2 + \sigma_{n,i}^2 \\ &= \sigma_{n,n}^2 + \int_{r=R_o}^{\infty} C_b P_t r^{-4} 2\pi r dr, \end{aligned} \tag{5.30}$$

where C_b is the average number of basestation transmissions per unit area, and P_t is the average transmit power per mobile at the basestation.

5.6 Multicell SA-MOB Protocol Description

In this section the frame structure of the SA-MOB protocol is motivated and discussed. Figure 5.21 is the structure of the frame. The shaded areas in the protocol indicate the additional header and tail overhead bits which encapsulate packet transmissions. For the sake of simplicity, only the reverse link capacity is considered. Further, the propagation delay is assumed to be negligible compared to the duration of a bit. The basestations and mobiles share a common clock and the timing of the frame is identical at each basestation. The first part of the frame consists of the basestation acquisition phase. In the basestation acquisition phase, the mobiles listen to the channel to determine which basestation they will communicate with. The second part is composed of n_d data slots in which mobiles are permitted to transmit information using the SA-MOB protocol which was discussed earlier.

In the basestation acquisition phase the active mobiles listen in order to locate the electrically closest basestation. Each basestation is statically assigned one of seven pseudo-noise (PN) sequences according to the pattern shown in Figure 5.20. That is, if the term L_x lies in the basestation's cell, then the basestation uses the PN sequence number L_x. The PN sequences are selected from a set of sequences which have a highly peaked autocorrelation and low cross correlation, such as Gold sequences [SP80]. A reuse factor of seven yields a processing gain of 18 dB against the other basestations using the same PN sequence [Lee86]. All basestations assigned the same PN sequence transmit simultaneously. The basestations which are assigned different PN sequences transmit in different time slots. This is done so that a single correlator at the mobile

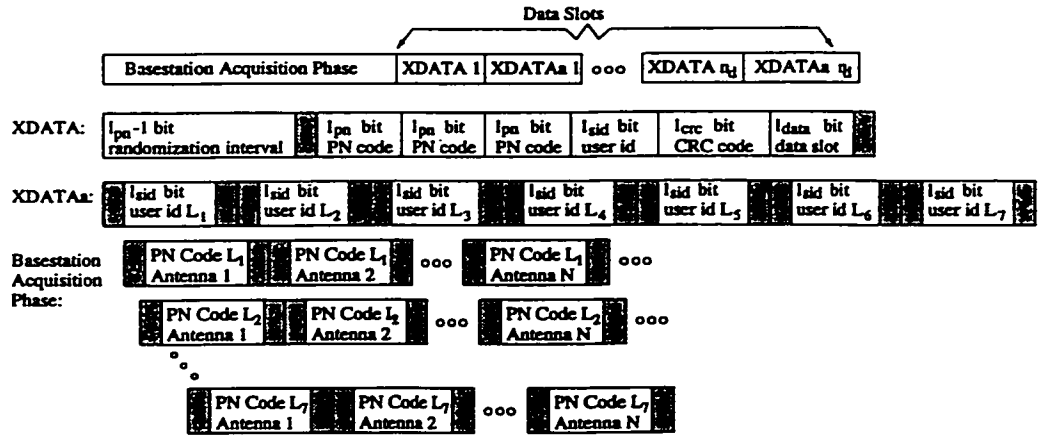

Figure 5.21: Frame structure of multicell SA-MOB protocol.

can be reprogrammed to use different PN codes. The PN code is repeated by the basestation one antenna at a time. This timing structure can be seen in the basestation acquisition phase part of the frame structure of the multicell SA-MOB protocol given in Figure 5.21. The mobile station contains the list of all 7 PN sequences. A single correlator at the mobile correlates against the current PN sequence, and sums the absolute value of the correlation across the transmissions received from all antennas of the basestation. At the end of the basestation acquisition phase, the PN sequence which gives the highest total absolute value correlation indicates to the mobile the PN sequence associated with the closest basestation. This PN sequence is flagged by the mobile as the one to use for the dynamic packet acquisition stage. Since the fast fading is largely averaged out over the N antennas, the mobile station is able to estimate the slow fading and exponential power path loss from the closest basestation. In subsequent communication with this basestation, each mobile adjusts its transmit power so that the average received power at its assigned basestation is the same as every other mobile which is transmitting to that basestation.

The basestation acquisition overhead A_o is the fraction of time the channel is used for the purpose of basestation acquisition. It is equal to

$$A_o = \frac{7N(l_{pn})}{l_{frame}}, \tag{5.31}$$

where

$$l_{frame} = 7N(l_{pn}) + n_d(4l_{pn} - 1 + 8l_{sid} + l_{crc} + l_{data}). \quad (5.32)$$

l_{pn} is the length of the PN sequence, n_d is the number of data slots, l_{sid} is the length of the user identifier, and l_{crc} is the length of a CRC code used to determine if the packet is correctly received by the basestation, and l_{data} is the length of the data packet. The number of overhead bits given by the shaded region in Figure 5.21 is set equal to 0 in this chapter. If the basestation needs to be acquired at least every t_a seconds and the data rate is R, then

$$A_o = \frac{7N(l_{pn})}{7N(l_{pn}) + \lfloor \frac{t_a R - 7N(l_{pn})}{4l_{pn}-1+8l_{sid}+l_{crc}+l_{data}} \rfloor (4l_{pn} - 1 + 8l_{sid} + l_{crc} + l_{data})}. \quad (5.33)$$

The specific value of t_a depends on parameters such as user mobility, the degree of shadowing, and the size of the cells. Figure 5.22 is a graph of A_o as a function of $\log_{10}(R)$ for different values of t_a using the default parameters given in Table 5.3. A_o for $t_a = 1.0$ sec and $R = 1.0$ Mbps is only 0.0035. However, with $t_a = 0.1$ sec and $R = 100$ kbps, A_o increases to 0.41. Therefore A_o can become quite significant for a system with a low data rate and frequent basestation acquisition.

Once the basestation is acquired, mobile stations transmit packets to the basestation using SA-MOB. A mobile transmits a packet in the XDATA slot as soon as one becomes available. If the packet is not immediately acknowledged in the XDATAa slot, the packet becomes backlogged. Backlogged packets are cleared using the binary exponential back-off algorithm [BG92]. In this algorithm the time which a backlogged station waits before retransmission is doubled after each collision. Packets which arrive to the mobile transmitter when it is backlogged are added to a first-in first-out (FIFO) queue. The size of this queue is limited to 100 packets. Packets are acquired in multibeam SDMA mode in a fashion very similar to the single cell SA-MOB protocol given earlier. As already mentioned, the first difference here is that each basestation is assigned one of seven different PN codes. The mobile selects the best one to use for the XDATA packet in the basestation acquisition phase. The other difference is that a reuse factor of 7 is employed for the XDATAa slot, so each basestation sends the XDATAa in its assigned section of the XDATAa slot. This way, the outer cell

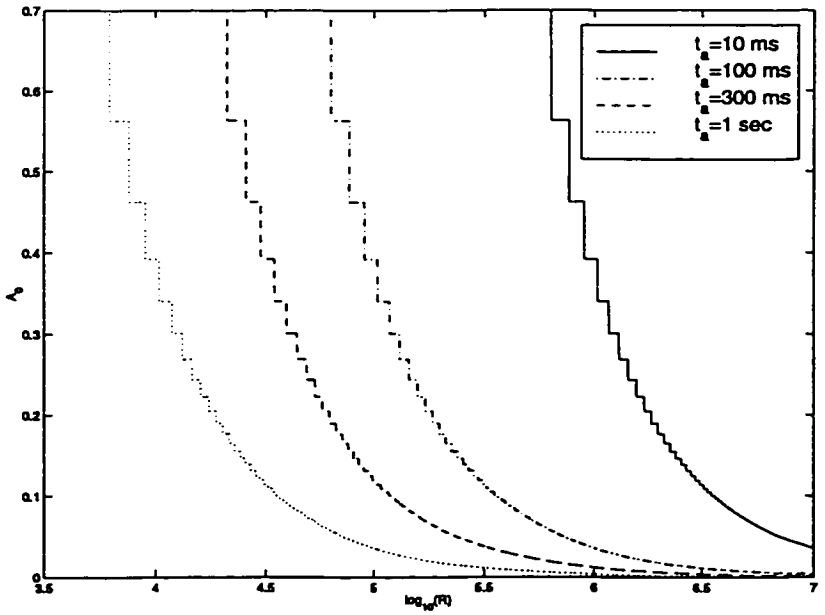

Figure 5.22: Basestation acquisition overhead for multicell SA-MOB.

interference is minimized. The interference due to acknowledgement of packets in the same slot is minimal since the XDATAa packet is sent under the protection of the array. If k XDATA packets are successfully acquired in the reverse link, the number of packets which are successfully acknowledged may be fewer than k since in general the forward link SINR is different than the reverse link SINR.

5.6.1 Multicell SA-MOB Protocol Performance Results

All results presented in this section are generated using a computer simulation. An 8×8 cellular grid with edge wrap-around is used. The edge wrap-around technique allows the use of a finite number of cells to approximate an infinite plane. If the cellular grid is reasonable large, then the interfering transmissions are roughly independent. The wrap-around is necessary to remove the edge effects. The mobile station signatures from the first two tiers around the center cell are used explicitly in calculating the SINR, so N_o is 18 in Equations (5.26) and (5.29). Packets arrive to the mobile stations with an exponentially distributed inter-arrival time. If the mobile is backlogged, they are held in a queue until transmission is successful. The mean throughput S, which

Parameter	Value
Antennas (N)	8
Number of mobiles per cell (M)	30
SINR_{min}	10 dB
SNR (reverse link)	6 dB
SNR (fwd. link)	20 dB
Num. beamforming modules (n_{bfm})	2
Length of PN sequence (l_{pn})	63 bits
Length of station id. field (l_{sid})	8 bits
Length of CRC field (l_{crc})	32 bits
Size of data slot (l_{data})	1024 bits
Std. Devn. of lognormal fading (σ_l)	8 dB
Exponential power path loss exponent (n)	4.0
Data Rate (R)	100 kbps
Basestation acquisition period (t_a)	1.0 sec

Table 5.3: Default multicell SA-MOB system parameters

is the average number of successful packets per XDATA slot, is normalized to take into account the protocol overhead. It is equal to

$$S = \frac{n_d l_{data}}{l_{frame}} S_u, \tag{5.34}$$

where S_u is the unnormalized throughput per XDATA slot. Similarly, the mean delay, which is the average time between when a packet arrives to a portable station to the time it starts to be successfully received by the basestation, is normalized to l_{data}.

Table 5.3 indicates the system parameters used for the multicell SA-MOB protocol. All of these parameters are the same as the ones which were used for the single cell S-ALOHA protocols, except that n_{bfm} has been changed from 8 to 2. It was determined from the simulations that using more than 2 beamforming modules gave negligible capacity improvement.

Figures 5.23 and 5.24 are graphs of the throughput S and the delay for the multicell SA-MOB protocol for different SNR levels. λ is the rate at which new packets are generated at each cell. Note that under high load this is not the rate at which they are transmitted since packets which arrive to a mobile whose transmit queue is full are

discarded. The delay at the peak throughputs is less than 5 data slots. However, the peak throughput, even with a very high SNR of 20 dB, is only 0.32. The reason for this relatively low capacity is that in the multicell case, with a frequency reuse factor of 1 stations have to transmit very infrequently to limit the number of simultaneous transmissions. This suggests that S-ALOHA in a multicell environment without a greater than 1 frequency reuse plan is feasible, but the per cell capacity in this case is much lower than the single cell case.

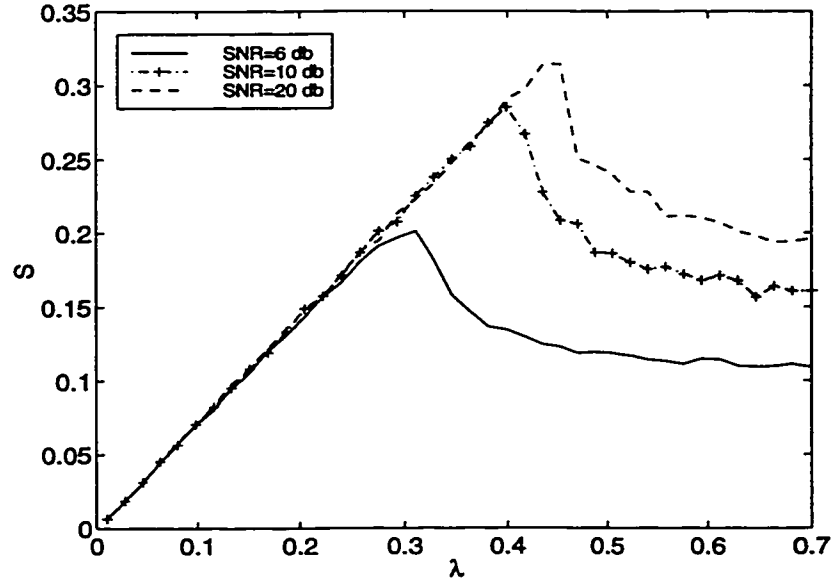

Figure 5.23: Multicell SA-MOB throughput S for different SNRs.

Figure 5.25 is a graph of the throughput S for different number of beamforming modules n_{bfm}. Since the throughput is fairly low, the system can get away with just 2 or 3 beamforming modules without significant loss in system capacity. Figure 5.26 is a graph of S for a different number of antennas N at the basestation. It is interesting to note that the per antenna throughput increases with the number of antennas. With the low throughputs observed with this protocol, there are typically at most one or two successful transmissions per data slot. So the increase in the throughput is mainly due to the diversity gain from having many antennas, and also the increased ability of the array to null the many interferers which are present even under a light

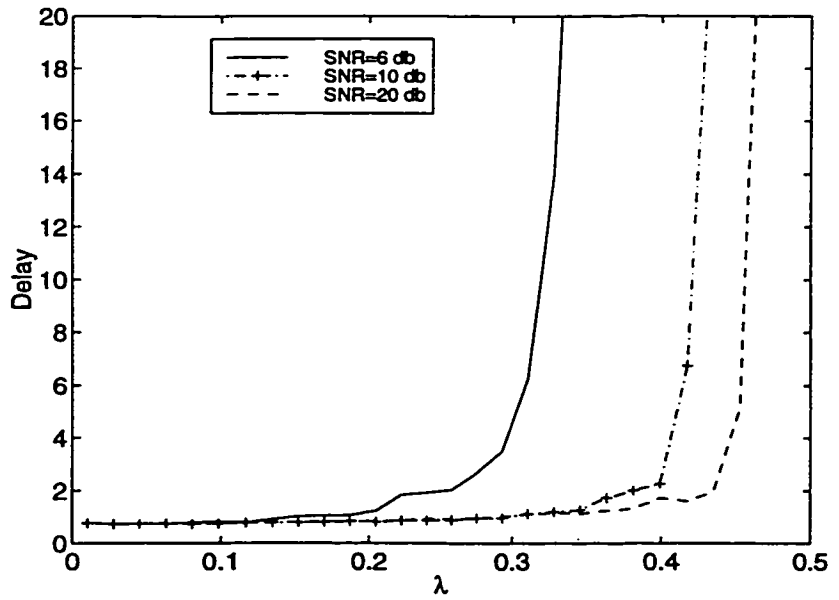

Figure 5.24: Multicell SA-MOB delay for different SNRs.

load.

5.7 Conclusions

In this chapter the capacity performance of S-ALOHA protocols which use a smart antenna at the basestation was considered. A narrowband Rayleigh fading environment is used to model heavy indoor multipath conditions [Win87a]. Versions of the system were considered where random access occurs in the XDATA slots directly, and when a minislotted reservation channel is used. In addition, both multibeam and single-beam operation was considered in the reservation minislots.

With the reservation protocols, the basestation pre-samples the spatial signatures (or codes) of successful stations during the reservation minislots. Based on this, two DSA algorithms were proposed. The exhaustive algorithm was found to be superior to non-exhaustive because it performs a more thorough search for stations with compatible spatial codes. Although the performance of Exhaustive-MOB is the highest under all conditions, Exhaustive-MRC works almost as well when the packets are

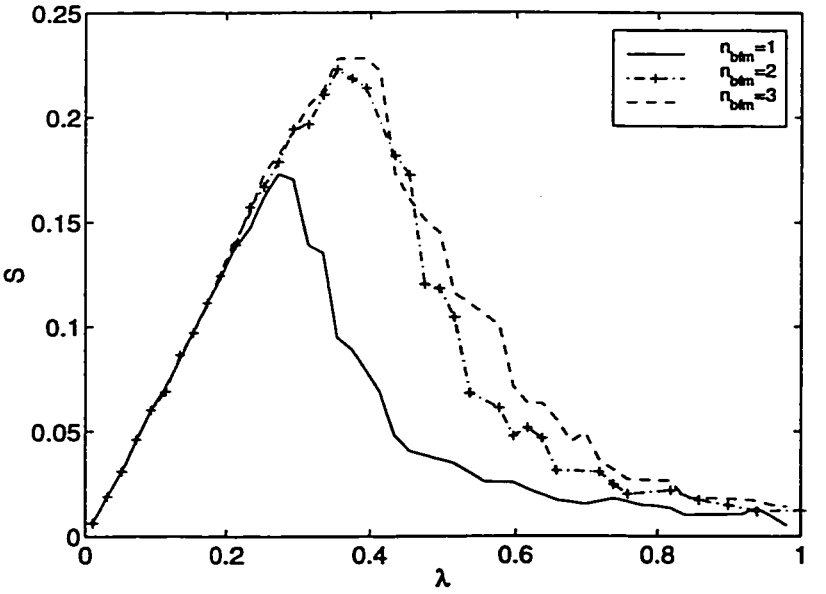

Figure 5.25: Multicell SA-MOB S for different n_{bfm}.

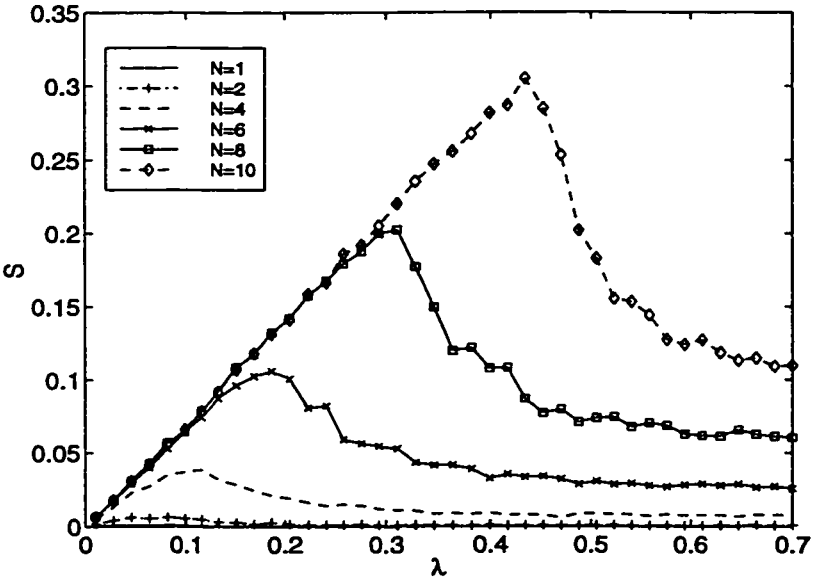

Figure 5.26: Multicell SA-MOB S for different number of antennas N at the basestation.

long and the SNR is low. For very large packets Exhaustive-MRC even outperforms Non-Exhaustive-MOB. This is important to note because operating the system with multibeam minislot contention is expected to be highly complex, due to the dynamic packet acquisition which must take place. At 6 dB SNR, for data packets less than 1024 bits, there is no advantage of SARMS-MRC over SA-MOB. Therefore for small sized packets it is best to perform contention in the data slots directly.

In this chapter a variety of throughput and mean delay results were presented. An analytic mean delay model was presented for the data slot contention systems and results were in agreement with the capacity models and with simulation results. Mean delay simulations were also presented for all the systems which show that at low load the SARMS protocols had significantly higher delay than SA-MRC and SA-MOB. Near the channel capacity the delay of the protocols using a SDMA contention channel was much lower than without, particularly when initial station access occurred in the contention channel directly.

SDMA S-ALOHA performance was also examined for a situation with multiple cells. The primary modification which was made to the protocol was the addition of a basestation acquisition phase to the protocol in which the portable stations listen to the channel to acquire the PN code associated with the nearest basestation. The protocol overhead associated with the basestation acquisition was determined to be negligible with a 1 Mbps data rate and a 1 sec acquisition period. The normalized per cell throughput was determined to be between 0.2 and 0.3. Although this is lower than the single cell case, it is quite good considering that the same frequency is being used in every cell. Furthermore, the delay at capacity is only about 5 data slots.

Chapter 6

Multicell Dynamic Slot Assignment

6.1 Overview

In the previous chapter a multicell situation was examined with the S-ALOHA protocol in its most basic form. In this chapter we explore some of the additional capacity gains which can be realized when dynamic data slot assignment is combined with varying degrees of real-time exchanges of information between the basestations. A network which consists of multiple smart antenna basestations that are connected to a wired backbone through a switch is considered. The basestations are in close proximity to each other, for example in different corners of a building floor. The advantage of having multiple basestations over one is greater capacity, larger coverage footprint, and lower transmit power.

The Best Fit algorithm initially given in Section 4.4.1 is adapted for operation in a multiple basestation network. The basestations can coordinate the DSA procedure among each other to maximize capacity. A system with network wide coordination however requires the network to be fast enough to exchange the packets needed for synchronization well within the channel coherence time. In situations where coordination among the basestations is not feasible, it is necessary to perform the DSA independently at each basestation. Both of these scenarios are considered in this

chapter. Two versions of the Best Fit DSA protocol are examined in which coordination between the basestations is not needed. In the first version each basestation is given an equal number of packets to transmit. In the second version basestations select packets with the highest link gain for transmission. Two versions are also proposed for when it is possible to have coordination between the basestations. In one version each packet is allocated to the basestation with the highest pre-combining link gain. In another version the optimal beamforming SINR of the packet is calculated at each basestation before allocation.

Although the protocols work with any number of basestations, the computer simulation experiments presented here are for a two basestation network. The SDMA/TDMA frame capacity is examined under different degrees of shadowing and path loss in a low SNR environment. The feasibility of using A basestations to effectively form a single smart antenna basestation with $A \times N$ times as many antennas is considered. Finally, some protocol enhancements to improve system performance with variable sized packets are developed.

6.2 Multicell Smart Antenna Architecture

The system studied in this chapter is given in Figure 6.1. Two basestations are shown in the figure, although the system can be scaled to any integer number of basestations A. Each basestation, equipped with an N element smart antenna basestation, attempts to communicate with a set of portable stations that have an omni-directional antenna. The basestations communicate with each other through a wired local area network (LAN). A switch with enhanced functionality necessary for the protocols connects the LAN to the rest of the wired infrastructure. When all smart antennas are combined to make an $A \times N$ element antenna, a clock which feeds all basestations is also necessary for implementation reasons that will be explained later.

The exchange of packets between the portables and basestations is scheduled in time-division duplexed (TDD) reverse and forward link TDMA frames. It is assumed that the basestations have a mechanism to synchronize their frames to within a fraction of a bit interval. This is necessary in a TDD system to avoid excessive interference

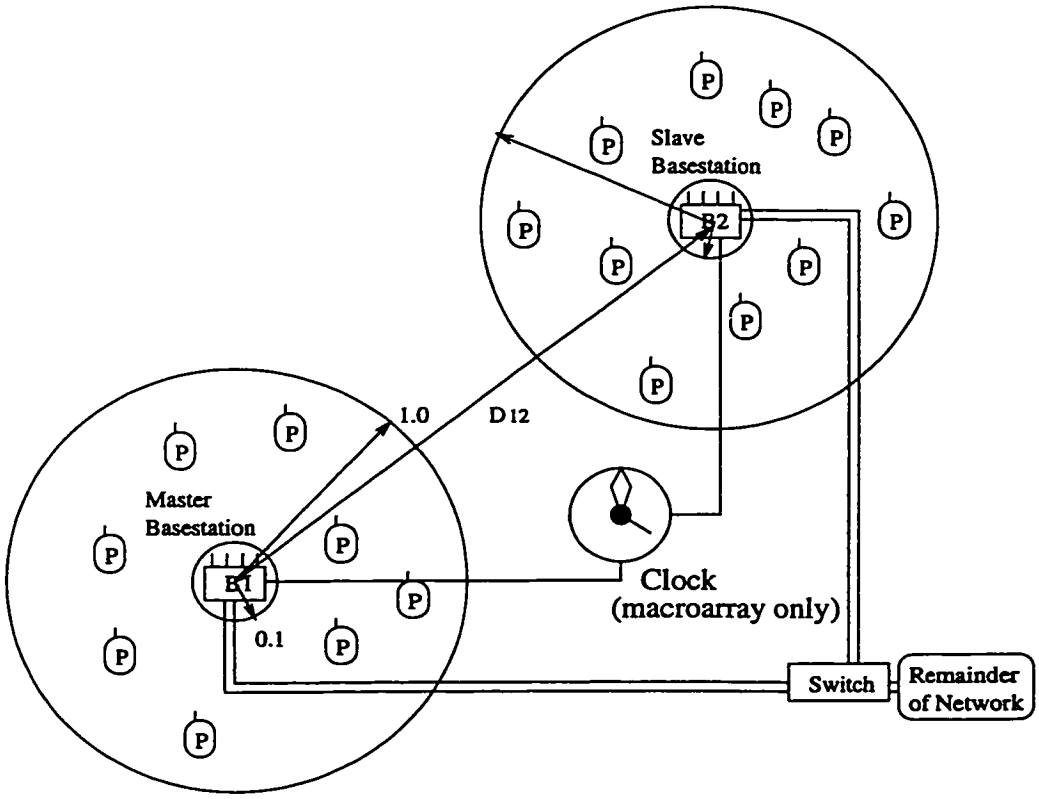

Figure 6.1: Two cell network architecture.

at the mobile station due to the near-far effect. The near-far effect can arise if there are two mobile stations close to each other, and one is receiving while the other is transmitting. For simplicity, the propagation delay is assumed to be zero. One of the basestations is designated the master basestation, while the others are the slave basestations. For the forward link (basestation to mobile) frame, the master basestation polls a batch of T portable stations. Each poll consists of a small packet transmission made by a single antenna of the basestation which contains the identifier of the polled portable, followed by the transmission of a known pseudo-noise (PN) code response by the solicited portable, as suggested in [Aca96]. In a real implementation of this protocol it may be necessary to repeat the PN code a few times. Similarly, it may be necessary to transmit the polling packet consecutively over several antennas or spread it by a PN sequence [Sin97]. All basestations correlate against the PN code to acquire the $N \times 1$ electrical signature vector of the polled portable. Once all T signatures have been obtained, the SDMA/TDMA frame is constructed at the basestations, and the packets are sent to the portables. The reverse link frame is generated in a similar method except that after the SDMA/TDMA frame is constructed, the basestations send the time slot assignment schedule to the portable stations one at a time using maximum ratio combining (MRC), after which the packets are sent by the portables and received in SDMA mode by the basestations. It is assumed that the duration of a single frame is well within the coherence time of the channel.

The indoor narrow band channel model used in this chapter incorporates Rayleigh fast fading, lognormal shadowing with standard deviation σ_l, and exponential power path loss of order n. This type of model is commonly used to model the indoor and picocellular multipath propagation environment [Has93]. $\mathbf{v}_{b(l),l}$, which is the electrical signature of portable station l at its associated basestation $b(l)$, is a complex valued N dimensional vector representing the estimate of the phase shift and attenuation at each antenna output. The Rayleigh fading is assumed to be independent at each antenna output, and the lognormal shadowing is independent among the basestations. As shown in Figure 6.1, each basestation is at the center of a donut in which portable stations can be located. The inner radius of the donut is R_i, and the outer radius is R_o. Portable stations are uniformly distributed in the donut, and are equally likely

to be in any donut. D_{ij} is the ratio of basestation i to basestation j separation to the outer radius of the donuts R_o.

The exponential power path loss associated with a portable station a distance R away from the basestation is

$$\text{Path Loss} = P_0 R^n, \tag{6.1}$$

where P_0 is the path loss at a distance of 1 meter. The probability density function of R is

$$f_R(r) = \begin{cases} \frac{200}{99} r & ,0.1 \leq r \leq 1.0 \\ 0 & ,\text{otherwise,} \end{cases} \tag{6.2}$$

where R_i and R_o have been set to 0.1 and 1.0. R_i cannot be equal to 0 because this would saturate the receiver. R_o cannot be too large because this would give too low an SNR or it would increase the dynamic range requirements of the receiver.

6.2.1 Multicell Smart Antenna Beamforming

For SDMA/TDMA operation, multiple beamforming modules are needed to communicate with the portable stations. For every time slot, each assigned portable station is paired up with a beamforming module belonging to one of the basestations. Since there cannot be more than N successful transmissions in a time slot [Com88] at the basestation, the number of beamforming modules n_{bfm} at each basestation is nominally set to N. The detailed diagram of each of the two basestations in Figure 6.1 was given in Figure 4.1.

For the reverse link, the output of a beamformer is the complex inner product of the weight vector with the antenna output. The weight vector is optimal if the signal to interference plus noise ratio (SINR) is maximized. The optimal weight vector for the reverse link of desired station l, scaled to unity power, is

$$\mathbf{w}_l = \frac{1}{\| \mathbf{\Phi}_{b(l)}^{-1} \mathbf{v}_{b(l),l} \|_2} \mathbf{\Phi}_{b(l)}^{-1} \mathbf{v}_{b(l),l}, \tag{6.3}$$

where $b(l)$ is the index of the receiving basestation, $\mathbf{\Phi}_{b(l)}$ is the correlation matrix at the receiving basestation, and $\mathbf{v}_{b(l),l}$ is the signature of portable station l at the

receiving basestation $b(l)$. Note that this is essentially the same result as the single cell case given by Equation (3.19), except that the signatures and correlation matrices now include the basestation index. If there are a total of M portable stations transmitting in the time slot, the reverse link SINR of desired portable station l is

$$\text{SINRrev}_l = \frac{|\mathbf{w}_l^H \mathbf{v}_{b(l),l}|^2}{\sum_{\substack{i=1 \\ i \neq l}}^{M} |\mathbf{w}_l^H \mathbf{v}_{b(l),i}|^2 + \sigma_n^2}, \tag{6.4}$$

where σ_n^2 is the noise power, and $\mathbf{v}_{b(l),i}$ is the signature of interferer i at the basestation receiving from l.

For the forward link, the output of the smart antenna is the forward link weight vector multiplied by the transmit symbol. If Equation (6.3) is also used as the weight vector for the forward link, then the forward link SINR at portable station l is

$$\text{SINRfwd}_l = \frac{|\mathbf{w}_l^H \mathbf{v}_{b(l),l}|^2}{\sum_{\substack{i=1 \\ i \neq l}}^{M} |\mathbf{w}_i^H \mathbf{v}_{b(i),l}|^2 + \sigma_n^2}, \tag{6.5}$$

where $\mathbf{v}_{b(i),l}$ is the signature of portable station l at the basestation transmitting to interferer i.

Although we have defined no explicit optimization criteria for the forward link weights, the outage probability is equal for both the reverse and the forward link because of the symmetry of Equations (6.4) and (6.5). This symmetry can be observed by making the substitution for the weight vector given by Equation (6.3) in the SINR equations.

For the reverse link, the SNR is the mean signal to mean noise power ratio at each smart antenna output. For the forward link it is N times the mean signal power to mean noise power ratio at the portable station antenna output when only a single antenna of the smart antenna is transmitting.

6.3 Multicell SDMA/TDMA Dynamic Slot Assignment Algorithms

As before, the objective of the SDMA/TDMA frame generation process is to maximize the frame capacity defined by Equation (4.2). The Best Fit algorithm introduced in

Chapter 4 has been used as a basis for new algorithms which exploit the fact that most portable stations are capable of communicating with two or more basestations.

In this section the operation of the protocols is described in detail. First a relatively simple technique in which there is no coordination among the basestations is described. Then some protocols where the basestations exchange user signatures are explained. Finally, some enhanced protocols designed to deal with variable sized packets are developed.

For all of the algorithms, all forward link traffic needs to originate at the switch. A duplicate of each packet is sent to both basestations. For the reverse link, all packets recovered at the basestations are sent to the switch.

6.3.1 Uncoordinated Transmission

With uncoordinated transmission, there is no exchange of station signatures among the basestations. This type of system is needed when the channel coherence time is relatively small compared to the delay involved in exchanging packets between the basestations, and when the computational performance is limited. Since the basestations are not permitted to exchange station signatures after the polling is complete, it is impossible for one basestation to know the slot assignment at the other basestation. In order to prevent collisions, the basestations never transmit or receive simultaneously. Therefore, first the master basestation transmits its SDMA/TDMA frame, followed by an end-of-frame (EOF) transmission in omni-directional mode. Upon hearing the EOF transmission, the slave basestations transmit their frames one after the other with an EOF signal indicating the end of each frame. The following two uncoordinated multicell DSA algorithms are proposed:

Uncoordinated Equal Split As the name implies, the T portables designated to transmit in the batch are split equally among the A basestations. Note that for the reverse link, after the polling is complete, each basestation is aware of the value of T so the appropriate number of portable stations can be allocated to each basestation. That is, the first basestation is assigned the first T/A portable stations. The second basestation is assigned the next T/A portable stations,

and so on until all portable stations are allocated to exactly one basestation. For example, if there are $T = 50$ portable stations in the batch, and $A = 5$, then each basestation is allocated a unique set of 10 portable stations. Following this, the SDMA/TDMA DSA is done independently at each basestation using the algorithm called Best Fit SDMA/TDMA from Chapter 4. It is repeated here for convenience.

Best Fit SDMA/TDMA Initially the station signatures are sorted in order of ascending power. The algorithm starts with slot 1. The first unallocated station is placed into the current time slot. The algorithm then tests each unallocated station by calculating the SINR_l for each station l in the current slot if the candidate station was added. SINR_l is calculated using Equation (6.5) or (6.4). The station which would result in the maximum minimum SINR_l, which we will call SINR_m, among the stations in the current time slot is added, provided that SINR_m is above a threshold SINR_{min}. If successful, the algorithm continues to search for more stations to add to the current time slot. Otherwise, the algorithm advances to the next time slot.

Uncoordinated Largest-p Each basestation sorts the signatures in order of descending power, and selects the $100p$ per cent of the stations with the highest power for DSA. The stations are sorted in descending order so that the search can be stopped when the $100p$ per cent of the stations are determined. Then these stations are scheduled for transmission using the Best Fit SDMA/TDMA algorithm described above. The advantage with this technique over the Uncoordinated Equal Split is that basestations tend to select stations that are not in a fade.

If a station is in a fade at every basestation then it is possible that it will not be scheduled in any SDMA/TDMA frame. To minimize the chance of this happening, the value of p is set so that this is very improbable.

6.3.2 Coordinated Transmission

With coordinated transmission, the basestations exchange their signatures after polling over a wired LAN, and then run near identical algorithms to schedule a TDMA/SDMA frame. The forward and reverse links are still TDD, but transmissions involving multiple basestations can coincide. This technique will work when the wired LAN delay is small compared to the channel coherence time, and the computational performance at each basestation is ample. The entire process of signature collection, DSA, and transmission needs to take place within the coherence time of the channel. The wired LAN delay needs to be small since the user signatures need to be exchanged among the basestations before the DSA can be done. The coordinated transmission DSA algorithms are more complex, so it is also important to have fast processing at the switch and basestations. Since the network wide slot assignment is known at each of the basestations, multiple basestations can be active in each data time slot. Three types of coordinated transmission are described next.

Coordinated Pre-designated Each portable station is designated a basestation with which it will communicate. The designated basestation is the one which has the strongest link, i.e., signature power, between itself and the portable station. Then the allocation is done using the Best-Fit algorithm given earlier.

Coordinated Un-designated Here each portable station is tested for allocation in all basestations. Therefore, the algorithm proceeds the same as the Best-Fit algorithm given earlier with the exception that A tests are made for each unallocated candidate station in each time slot. Each candidate station is tested for allocation to each of the A basestations. The portable station which is added, and the basestation to which it is allocated, are the pair which give the maximum minimum SINR among all possible portable station-basestation combinations. The minimum SINR here is taken across all portable stations which are allocated among all basestations in the current time slot.

Macroarray Best-Fit With this algorithm the A basestation smart antennas are combined to logically create a single smart antenna with $A \cdot N$ antennas. The

advantage of this over having $A{\cdot}N$ antennas on the same basestation is that with the latter there is no macroscopic diversity. With macroscopic diversity it is possible to minimize the tendency of lognormal shadowing and exponential power path loss to increase the variance of the received signal strength. The allocation is done using the Best-Fit algorithm. In Equations (6.3), (6.4), and (6.5), $b(l)$ is always 1 since there is only one logical basestation with $A{\cdot}N$ antennas.

6.3.3 Enhancements for Variable Packet Size

Many of the existing packet switched protocols permit variable sized packets, and this needs to be taken into account for efficient DSA. We will assume that the weights being used to receive a packet cannot be changed in the middle of a packet. Therefore in order to guarantee the minimum SINR, transmissions of packets need to start simultaneously, but they can end at different times. This way, in a static channel, the lowest SINR is always at the start of the time slot. This implies that each time slot has to be the length of the longest packet in that slot. Therefore, in general all but one of the packets in a time slot will finish before the end of the slot, leading to idle time in which the beamforming modules are not being used. Idle time is undesirable as it increases the length of the frame, and hence reduces the frame capacity. As an example, Figure 6.2 shows a diagram of the packets in three consecutive time slots of a SDMA/TDMA frame in such a system. The packets are given with different heights only for illustrative purposes. In this example all time slots contain 4 packets. However, in time slot $i+1$, two of the beamformers remain idle for more than half of the time slot, which leads to a reduction in overall frame capacity. This suggests that the optimization criteria for DSA with variable sized packets should also attempt to minimize the idle time. What follows are two modifications made to the Best Fit algorithm to attempt to minimize the amount of idle time.

SINR/W In its original form, the Best Fit algorithm attempts to maximize SINR_m. Recall that that SINR_m is the maximum minimum SINR among the stations in the current time slot. In the SINR/W multicell DSA heuristic the Best Fit

algorithm is modified to maximize $\frac{\text{SINR}_m}{W}$, where W is the length of the time slot if the candidate user is added. That is, W is equal to the length of the longest packet in the time slot. In this way a penalty is incurred for both a low SINR_m and a large packet. This tends to place packets of similar size in the slot. The smaller packets are more likely to be situated near the start of the frame.

Busy Time Here the Best Fit algorithm is modified to maximize the busy time, which is equal to

$$\text{busy time} = \frac{\sum_{i=1}^{M} W_i}{M \cdot W}, \tag{6.6}$$

where M is the number of users in the time slot, W_i is the length of the packet from user i, and W is the same as before. The busy time is therefore the percentage of time during which the beamformers involved in the current time slot are actively communicating with portable stations. It is equal to 1.0 if each packet is of the same length.

For both of the above modifications, the requirement that SINR_m be above SINR_{min} still remains.

Figure 6.2: SDMA/TDMA frame structure with variable packet size.

6.4 Capacity Results

As in the single cell case, we focus exclusively on the efficiency of the SDMA/TDMA frame generation process. The frame capacity Equation (4.2) is repeated here for convenience.

$$C_f = \frac{T}{E[L]},$$

where T is the batch size and $E[L]$ is the expected length of the frame. Note that the capacity is not being normalized by the number of basestations A. For the variable sized packets, the expected length of each packet is equal to 1, so the expected length of the frame using an omni-directional basestation antenna is equal to T. Because the outage probability on the reverse and forward links is the same, C_f is the same for the reverse and forward link. In the discussions which follow, concentration will be on the frame capacity with a large number of users as this is when the frame generation process is most efficient. Unless otherwise stated, there are $A = 2$ basestations, $N = 8$ antennas per basestation, the SNR is 6 dB, SINR_{min} is 10 dB, and n_{bfm}=8 beamforming modules are employed.

Figure 6.3 is the frame capacity of the Uncoordinated Equal Split protocol for different values for D_{12} and σ_l. It can be seen that with a large number of users capacity with $D_{12} = 2.0$ is only about 60 per cent of that with $D_{12} = 0.5$. This is because one half of the users are very distant from their designated basestation, so the received signal strength is low and the signature strength variation is high. C_f is seen to decrease as σ_l increases because this further increases signature strength variation.

With $D_{12} = 2.0$, the capacity is only slightly better than having just one transmission per slot. Such a low capacity suggests that in a low SNR environment with large variation in signal strength, it may be possible to reduce the number of beamforming modules at the basestations without significantly sacrificing performance. Figure 6.4 is the capacity with various number of beamforming modules. With just two beamforming modules, the capacity is more than 90 per cent of the capacity with eight beamforming modules.

Figure 6.5 is a graph of the frame capacity with various protocols for a high signal strength variance situation. The value of p in the Uncoordinated Largest-p protocol is set so that the chance of a portable station not being selected by either basestation is less than one per cent. The Uncoordinated Largest-p protocol is about 27 per cent better than Uncoordinated Equal Split, because with the former the basestations ignore the 100(1-p) per cent of the portable stations with a weak signal in the hope that they have a better link with the other basestation. Both Coordinated

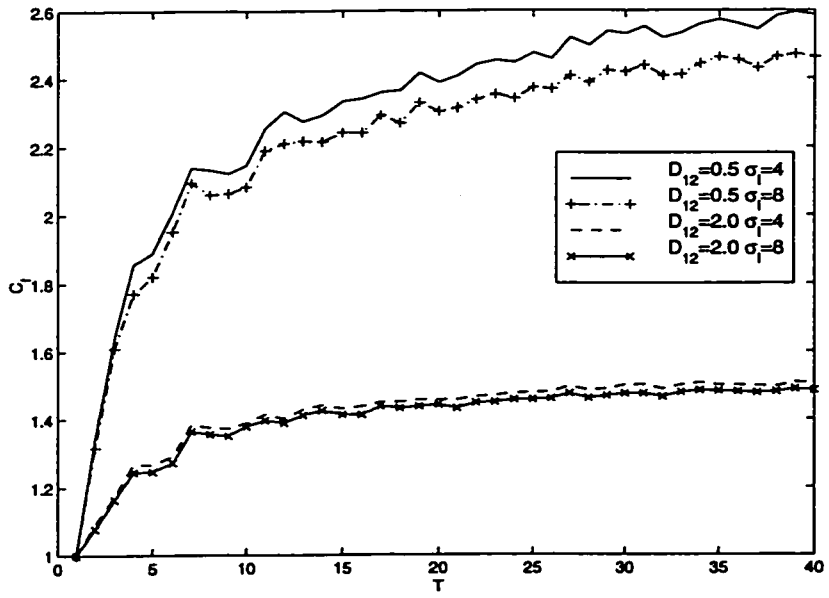

Figure 6.3: Frame capacity for Uncoordinated Equal Split, α=6.0.

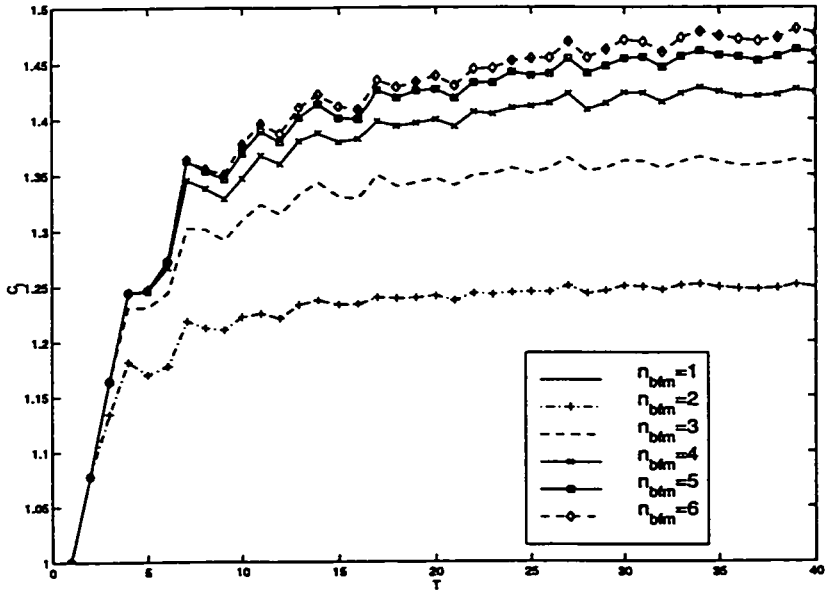

Figure 6.4: Frame capacity for Uncoordinated Equal Split, D_{12}=2.0,σ_l=8.0,α=6.0.

Predesignated and Coordinated Undesignated have slightly over twice the capacity as Uncoordinated Equal Split. The reason is that for Coordinated Predesignated, each portable is always assigned to the basestation with the higher received signal strength. Uncoordinated Largest-p does not work as well since in order to keep the outage probability below 1 per cent, some portable stations need to be assigned to both basestations. For these portable stations the packet is successfully received twice, and the duplicate packet is discarded at the receiver. Coordinated Undesignated does not perform any better than Coordinated Predesignated in this graph because with a large variance in received signal strength, the signal strength is a very good indicator of the best basestation.

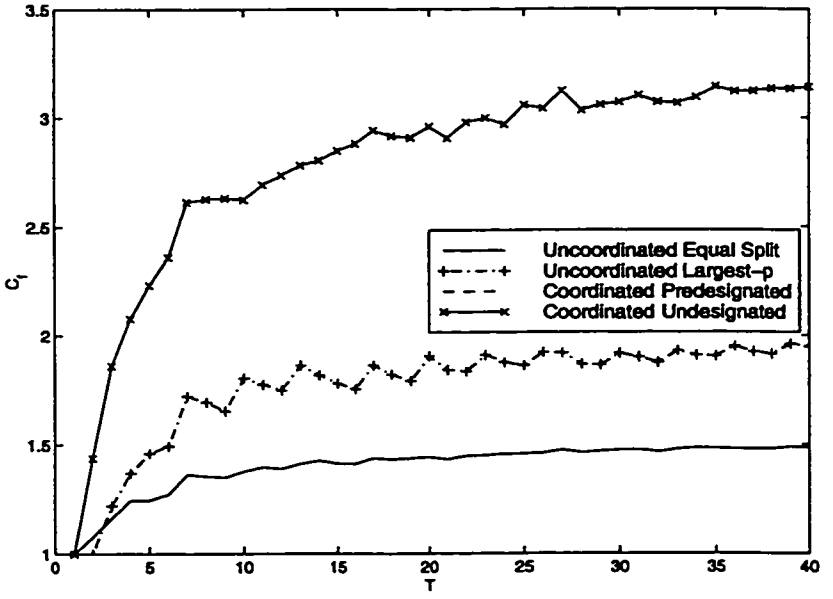

Figure 6.5: Frame capacity D_{12}=2.0,σ_l=8.0, α=6.0. Note that the two coordinated schemes perform the same.

Figure 6.6 is a graph of the frame capacity for various protocols with a very small variation in received signal strength. Such a situation may occur if there is an U-LOS path between the smart antenna basestations and portable stations, and the size of the floor in which the basestations and portables are located is small. In this case, the capacity of all the protocols is much higher than before because with lesser variance in signal strength, the likelihood of one station capturing the

others is greatly reduced. The two uncoordinated algorithms work almost as well as the coordinated ones because the channel is often almost equally good at either basestation. Unlike the previous graph, Coordinated Undesignated works slightly better than Coordinated Predesignated because it is harder to tell which is the best basestation just by looking at the received signal strength.

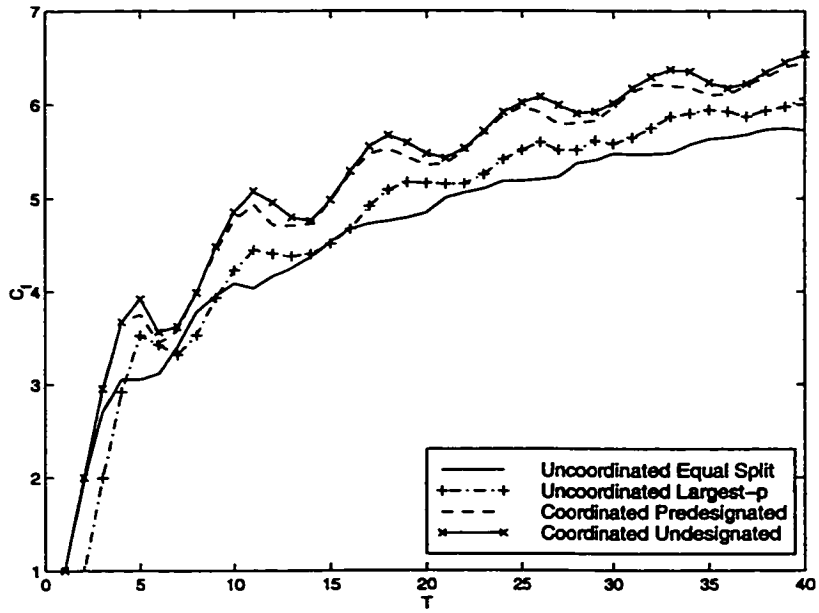

Figure 6.6: Frame capacity with neither lognormal fading ($\sigma_l = 0$) nor exponential path loss ($\alpha = 0$).

Figure 6.7 is a graph of the frame capacity using a single 16 element array and a 2×8 element macroarray. With many users, the capacity of the latter is over twice the former. The reason is that although the mean received signal strength is identical in both cases, with the macroarray it is less likely that all smart antenna outputs are in a lognormal fade. Also, a portable station cannot be very distant from all 16 antennas. These two results combine to reduce the variance of the signal power of the 16 element signature vector of the macroarray, thereby improving the processing gain against noise, and increasing the compatibility with other others in the same time slot.

The forward channel of the macroarray is relatively easy to implement by running

the same algorithm at both basestations. Each basestation just applies the weights for the antennas it controls. The reverse channel is a little more complicated since only one half of the received signal is at each basestation. Therefore, both basestations send an $N \times 1$ dimensional complex baseband vector up to the switch where the two vectors are concatenated and an inner product is taken with the $2N \times 1$ weight vector for a scalar output. The computational requirements for implementation of the macroarray are significant. To solve Equation (6.3), the macroarray needs to invert a matrix twice as tall and wide.

The primary difficulty with implementation of the macroarray is that two independent clock generators cannot produce identical frequencies. The beamforming requires that the inter-element phase information remain the same from the time the signatures are sampled to when the corresponding packets are sent. The use of two different clock generators will not work because there will be an unacceptable frequency difference between the two. A straightforward solution to this is to use one clock to feed both basestations. This clock can be located anywhere in the network as long as the electrical length of the wires feeding the basestations remain fairly steady for the duration of a frame.

Figure 6.8 is the frame capacity C_f with variable packet size using the original and modified Best Fit algorithms with the Uncoordinated Equal Split protocol. The Erlang-r, exponential, and two-stage hyper-exponential distributions [LG94] have been used to model the packet size distribution for a packet size with a coefficient of variation (C_v) of less than 1.0, equal to 1.0, and greater than 1.0, respectively [MTH90]. For the two-stage hyper-exponential distribution, the small job probability is 90 per cent. The three lines indicate C_f using the Uncoordinated Equal Split protocol where the objective in the Best Fit DSA is to maximize the SINR_m, SINR_m/W, or busy time. With a C_v of 0.0, meaning the packet size is fixed, the capacity is highest because there is no loss due to idle periods in the time slots. As C_v increases, the capacity of all protocols reduces dramatically. For small values of C_v, maximizing SINR_m or SINR_m/W works better than maximizing the busy time because it is more important to concentrate on getting the best signature compatibility when packets are nearly the same size. For large values of C_v, the graph indicates that it is best to

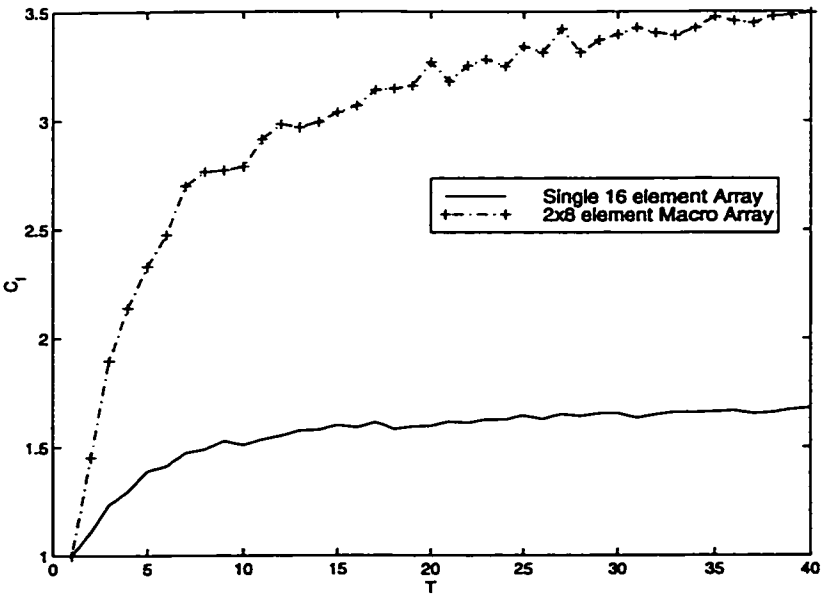

Figure 6.7: Frame capacity with single 16 element array and a 2×8 element macroarray, σ_l=8.0, α=6.0, D_{12}=2.0, $n_{bfm} = 16$.

maximize busy time, followed by SINR_m/W and then SINR_m. For a system where C_v is not known in advance, it seems that it may be best to maximize SINR_m/W as it works fairly well for a broad range of values.

6.5 Conclusions

In this chapter the static SDMA/TDMA frame capacity of an indoor multicell system was considered. The portable stations communicate with multiple basestations which use a smart antenna operating in SDMA/TDMA mode. An indoor multipath model that permits various degrees of variation in received signal strength was used. The Best Fit DSA algorithm from Chapter 4 was adapted for operation in a multicell environment.

It was found that basestation separation had a bigger impact on frame capacity than lognormal shadowing. This was particularly true with the uncoordinated DSA

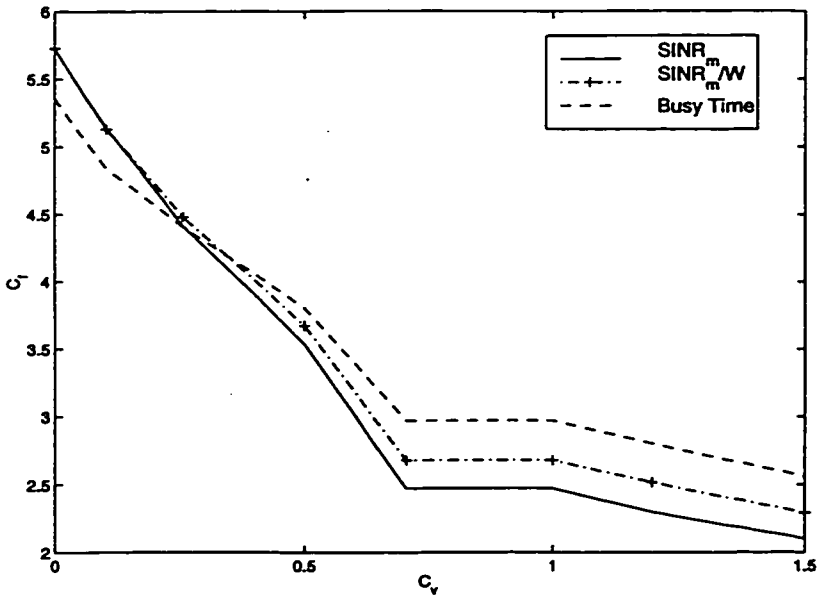

Figure 6.8: Variable packet size frame capacity with with no lognormal fading ($\sigma_l = 0$) nor exponential path loss ($\alpha = 0$).

protocols as they did not perform as well at assigning portable stations to the electrically closer basestation. With the coordinated DSA protocols, it was discovered that using the signature strength to select the basestation was an excellent method for selecting the best basestation, and it gave comparable performance to using SINR_m directly.

It was also discovered that significant capacity advantage is achievable by combining the signatures from two distant antennas to create a macroarray. Exploiting the macroscopic diversity of distant antennas to create a 16 element macro array in fact gave over double the capacity of a single 16 element basestation. Finally, modifications to the DSA optimization criteria were explored for situations when the packets vary in size. If was found that maximizing the ratio of SINR_m to the length of the time slot W gave good performance for a broad range of values for packet size coefficient of variation C_v.

Chapter 7

Conclusions

The topic of this thesis was SDMA/TDMA dynamic slot assignment using a smart antenna at the basestation, and omnidirectional antennas at the portable stations. It was discovered that by applying the SDMA concept to a TDMA frame, the system capacity could be dramatically improved. More sophisticated slot allocation schemes were found to significantly improve capacity at the cost of increased computational complexity. However, even the most complex DSA algorithms explored in this thesis could be implemented using current DSP technology. Using a smart antenna testbed developed at the Communications Research Laboratory at McMaster University, the capacity gains that can be realized in a practical system were confirmed. It was found with a stationary transmitter and receiver, channel coherence times in the low 10's of msec were possible.

The DSA algorithms were applied to various S-ALOHA type protocols using a reservation channel. It was found that for low SNRs and data slot sizes of 1 kbit or greater, it is possible to achieve a higher capacity using a S-ALOHA reservation protocol with a single-beam reservation channel as compared to transmitting the data packet in an SDMA contention channel directly. This result is an important one because the single-beam reservation channel permits significant reduction in hardware complexity. DSA was also considered for multicell scenarios with various degrees of real-time synchronization between the basestations. It was discovered that basestation synchronization dramatically improves system capacity because portable stations

can be assigned to the most compatible basestation for data transfer.

Future work in smart antenna research is likely to involve space-time signal processing techniques as the data rates get to levels where there is a significant level of intersymbol interference present. For these systems protocols need to be developed that exploit the two-dimensional space-time signature profile of the mobile stations. Next generation cellular systems will employ multiple carriers which may not be allocated in contiguous frequency bands. Further, many of these systems will be frequency division duplexed (FDD). Signature acquisition techniques and DSA algorithms need to be developed to accommodate these broadband systems.

As the smart antenna technology is employed in higher frequency bands, the shorter wavelengths may make it possible to have smart antenna operation at the mobile station as well. Protocol innovations need to take place where a smart antenna at the mobile station permits multiple electronically selectable spatial signatures for the mobile station. Efficient DSA algorithms need to be developed for these systems.

Appendix A

Smart Antenna Testbed

The Talaris vector channel sounding testbed constructed at the Communications Research Lab (CRL) was used for the experimental data collection. This testbed was configured for transmission in the reverse link direction. Photographs of the testbed are given in Figures A.1 through A.3. A photograph of the omni-directional transmitter is given in Figure A.1. A photograph of the 8-element circular array smart antenna is given in Figure A.2. A photograph of a closeup of the same 8-element circular array smart antenna is given in Figure A.3.

The receive section of the smart antenna testbed is shown in Figure A.4. The antenna outputs for each element are down-converted and coherently demodulated. These outputs are then input to a data acquisition system. The array receivers have a noise figure of 5 dB. For the measurements used in this thesis, the system was configured to have an effective bandwidth of 10 kHz.

The measurements were taken with two antenna array diameters. The first set were taken with an antenna diameter of 0.51 m, while the second set were taken with an antenna diameter of 0.20 m. Figure A.5 shows the diagram of the transmitter and the receiver for a single element of the 8 element array. All antennas are 2 dBi vertical dipoles. The transmit power is variable between -30 dBm and 0 dBm by switches located on the transmitter. The data collected with the 0.51 m antenna array diameter was taken with a continuous wave (CW) transmitting at the source, meaning $p(t) = 1.0$ for all t. With the 0.20 diameter array, the data was collected in

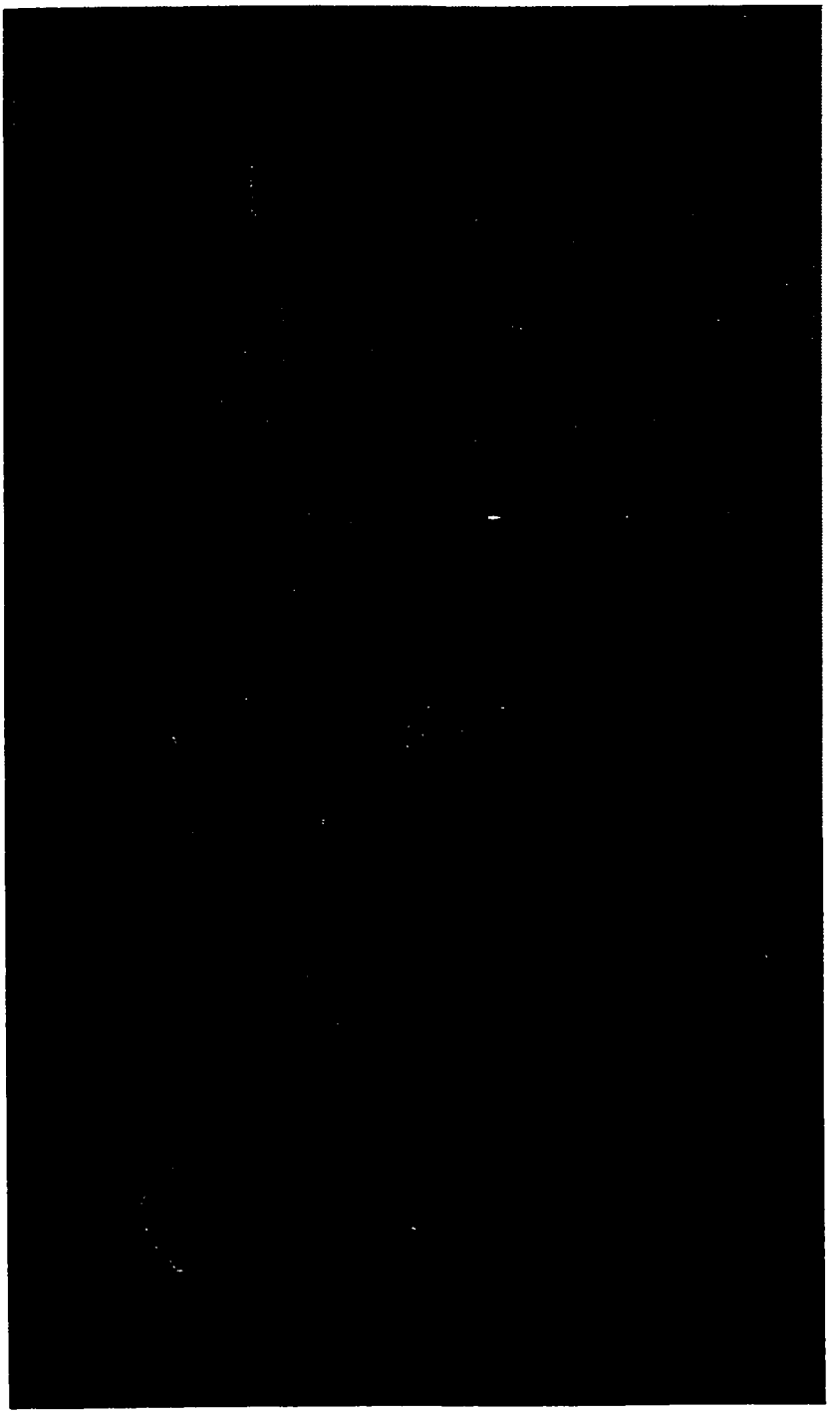

Figure A.1: Photograph of the omni-directional transmitter. A 3.5" high coffee mug is placed on top of the cart for reference.

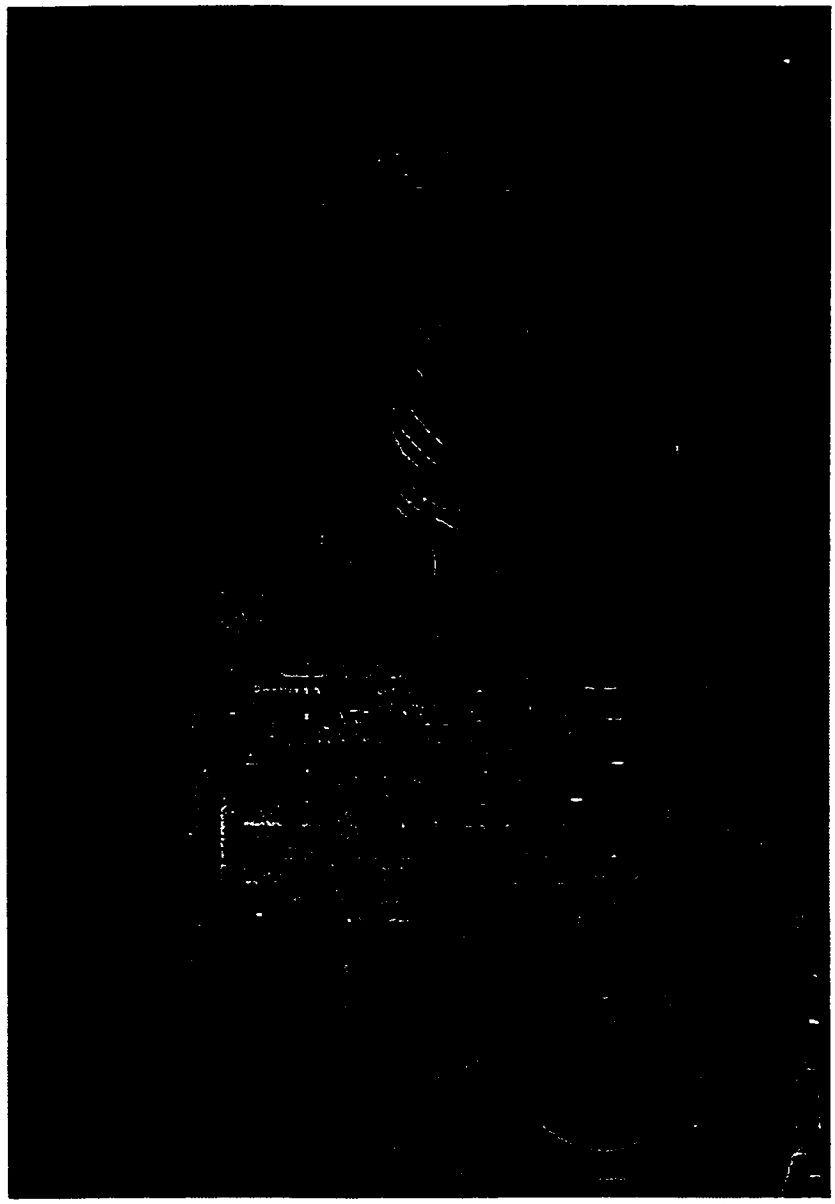

Figure A.2: Photograph of the 8-element circular array smart antenna with 0.20 m diameter.

Figure A.3: Photograph of a closeup of the 8-element circular array smart antenna with 0.20 m diameter.

wideband for the purpose of combating narrowband interferers and also for angle of arrival and delay spread estimation. The next section details the procedure by which this is done.

Both the narrowband and wideband measurements were taken at a center frequency of 1.86 Ghz. For the experimental DSA capacity measurements considered in this thesis, the transmitter was carried by a person in a random fashion around the room of interest. With the array stationary, the transmitter was carried at approximately 2 ft/s. A vector channel sounding was done 6.25 times per second, which corresponds to spacing of about 10 cm between samples. Between four and eight hundred samples were collected for each room.

A.1 Vector Channel Sounding in Wideband

Some of the data was collected with the smart antenna configured for wideband reception. The wideband data needed to be converted to its narrowband equivalent. This was done by adding up the primary multipath components as complex numbers. What follows is a description of how the main multipath components are identified and combined to construct the narrowband complex envelope. Figure A.5 is a block

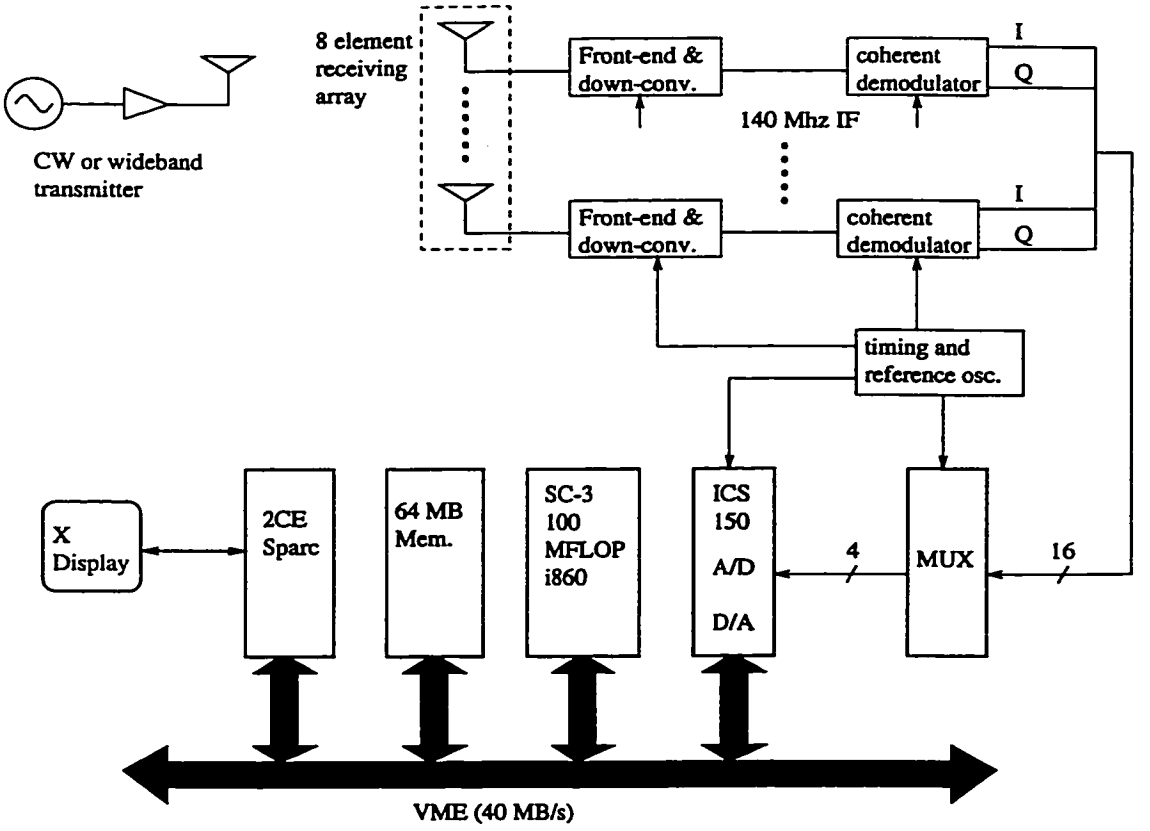

Figure A.4: Smart Antenna Testbed in Receive Configuration.

diagram of the transmitter and a single element of the receiver. A sinusoid at angular frequency w_o is modulated by a 5 Mhz real valued pseudo-noise (PN) sequence $p'(t)$ of length $\frac{N_s}{2}$. N_s was equal to 510 for the smart antenna testbed. The autocorrelation function of the pseudo-noise sequence $p(t)$, which is $p'(t)$ oversampled by a factor of 2, is

$$\begin{aligned} R_p(k) &= E[p(t+k)p(t)] \\ &= \begin{cases} N_s & , \text{if } k = 0 \\ \frac{N_s}{2} - 1 & , \text{if } k = \pm 1 \\ -2 & , \text{otherwise.} \end{cases} \end{aligned}$$

In the presence of multipath, the received broadband signal can be written as

$$r(t) = 2A_1\cos(\omega_o t - \phi_1)p(t-\tau_1) + 2A_2\cos(\omega_o t - \phi_2)p(t-\tau_2) + \ldots, \qquad \text{(A.1)}$$

where ϕ_i and τ_i are the phase delay of the carrier and the time delay of the PN sequence of the i^{th} multipath, respectively. After down conversion the in-phase and quadrature phase components of the baseband signal are

$$r_{Ib}(t) = n_{Ib}(t) + I_{DC} + A_1\cos(\phi_1)p(t-\tau_1) + A_2\cos(\phi_2)p(t-\tau_2) + \ldots, \quad \text{(A.2)}$$

and

$$r_{Qb}(t) = n_{Qb}(t) + Q_{DC} + A_1\sin(\phi_1)p(t-\tau_1) + A_2\sin(\phi_2)p(t-\tau_2) + \ldots. \quad \text{(A.3)}$$

I_{DC} and Q_{DC} are the undesirable in phase and quadrature phase offsets introduced by the smart antenna testbed which need to be removed. $n_{Ib}(t)$ and $n_{Qb}(t)$ are the in phase and quadrature phase noise components. $r_{Ib}(t)$ and $r_{Qb}(t)$ can be written in complex notation as

$$r_b(t) = A_{nb}(t)e^{j\phi_{nb}(t)} + A_{DC}e^{j\phi_{DC}} + A_1e^{-j\phi_1}p(t-\tau_1) + A_2e^{-j\phi_2}p(t-\tau_2) + \ldots, \quad \text{(A.4)}$$

where $A_{nb}(t)e^{j\phi_{nb}(t)}$ is noise, and $A_{DC}e^{j\phi_{DC}}$ is the DC offset.

The baseband signal is oversampled by a rate of two, i.e., twice the frequency of $p'(t)$, in order to ensure that the sampling is done at most one-fourth the symbol period away from the peak value of the received symbol. N_s samples of the signal are taken $0.1\mu s$ apart. With the Talaris testbed, $N_s + 3 = 513$ samples are taken for each antenna output. Since there are 8 antennas, a vector channel sounding can be done as often as every 0.1x513x8 μs=410 μs.

The receiver used for sampling was linear in the -.85 to +.85 volt range. The percentage clipping is therefore

$$\%\ \text{Clipping} = \frac{P(|r_{Ib}(t)| > 0.85) + P(|r_{Qb}(t)| > 0.85)}{2}. \quad \text{(A.5)}$$

The mean of the received signal is

$$\begin{aligned} E[r_b(t)] &= \frac{1}{N_s}\sum_{t=1}^{N_s}\Big(A_{nb}(t)e^{j\phi_{nb}(t)} + A_{DC}e^{j\phi_{DC}} + \ldots \\ &\qquad A_1e^{-j\phi_1}p(t-\tau_1) + A_2e^{-j\phi_2}p(t-\tau_2) + \ldots\Big) \\ &= A_{DC}e^{j\phi_{DC}} + \frac{1}{N_s}\textstyle\sum_{t=1}^{N_s}A_{nb}(t)e^{j\phi_{nb}(t)} + \ldots \end{aligned}$$

$$\begin{aligned} & \frac{-2}{N_s}(A_1 e^{-j\phi_1} + A_2 e^{-j\phi_2} + \ldots) \\ \approx\ & A_{DC} e^{j\phi_{DC}}, \end{aligned} \tag{A.6}$$

because $\sum_{t=1}^{N_s} p(t-\tau_i) = -2$. The DC offset is removed from the signal by subtracting the mean. This signal with the DC offset removed is equal to

$$r_b'(t) = r_b(t) - E[r_b(t)]. \tag{A.7}$$

The cross-correlation between $r_b'(t)$ and $p(t)$ is

$$\begin{aligned} R_b(k) &= E[r_b'(t)p(t+k)] \\ &= \frac{1}{N_s}\sum_{t=1}^{N_s} r_b'(t)p(t+k) \end{aligned} \tag{A.8}$$

Taking the power of Equation (A.8) and averaging across the N antennas to mitigate multipath,

$$\begin{aligned} \hat{R}_b(k) &= \overline{|R_b(k)|^2} \\ &= E[|R_b(n,k)|^2] \\ &= \frac{1}{N}\sum_{n=1}^{N} |R_b(n,k)|^2, \end{aligned} \tag{A.9}$$

where $R_b(n,k)$ is the cross-correlation at antenna n for a lag of k. The values of k for which $\hat{R}_b(k)$ is large indicate delays at which there is a significant amount of signal impinging upon the array. Figure A.6 is a typical plot of $\hat{R}_b(k)$. In the figure there is a significant amount of signal present for $k = 3,..,7$, which means that the delay spread is about 400 ns. The time lags which have high $\hat{R}_b(k)$ are

$$K_{pk} = \{k_{pk} - \delta_{chips}, k_{pk} - \delta_{chips} + 1, \ldots, k_{pk} + \delta_{chips}\}, \tag{A.10}$$

where K_{pk} is the value of k at which cross-correlation peaks. Therefore the complex narrowband envelope v at the antenna is the sum of these signals [Has93], and it is equal to

$$v = \sum_{k \in K_{pk}} R_b(k). \tag{A.11}$$

A value of 3 was used for δ_{chips} in this thesis, implying that the delay spread was assumed to be no more than 600 ns.

The mean signal power to mean noise power ratio (SNR) of the collected data should be very large. For the experimental measurement graphs in this thesis, it is assumed to be infinity. In order to calculate the SNR of the sampled data, the noise power was obtained by sampling with the transmitter off. Therefore, the mean noise power per sample was

$$\sigma_n^2 = \frac{1}{\text{num. samples}} \sum_{\text{all samples}} |\frac{1}{N_s} \sum_{t=1}^{N_s} r_b'(t)|^2. \tag{A.12}$$

The SNR is decibels is then

$$\text{SNR} = 10 \log_{10}(\frac{|v|^2}{(2\delta_{chips}+1)\sigma_n^2}). \tag{A.13}$$

Figure A.7 is a typical plot of the SNR's for the data collected. In all files used, the percentage clipping was 0 and the SNR was typically around 40 dB's.

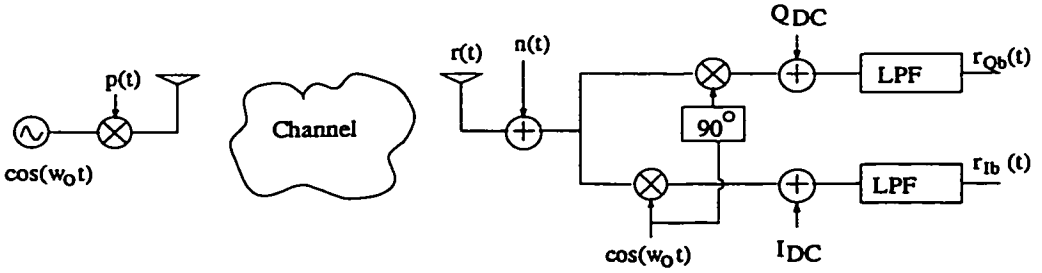

Figure A.5: Transmitter and single element of smart antenna receiver.

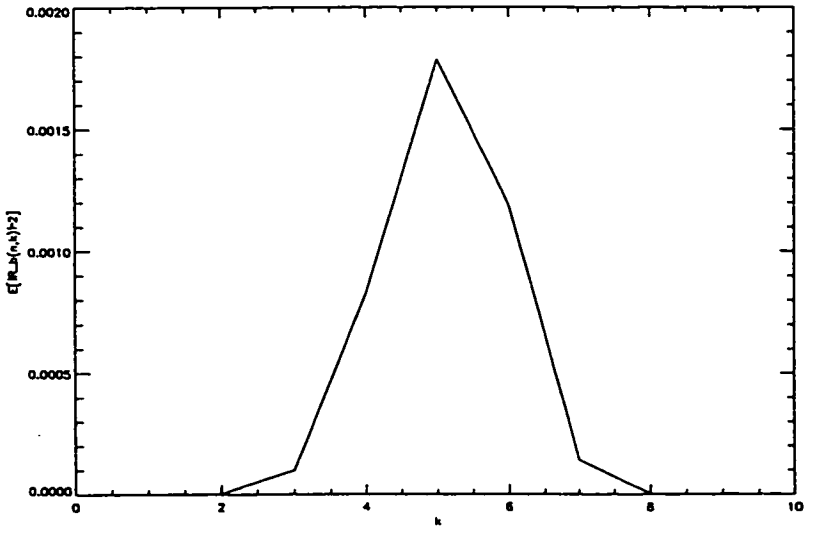

Figure A.6: Example cross-correlation from Room 103, sample 2.

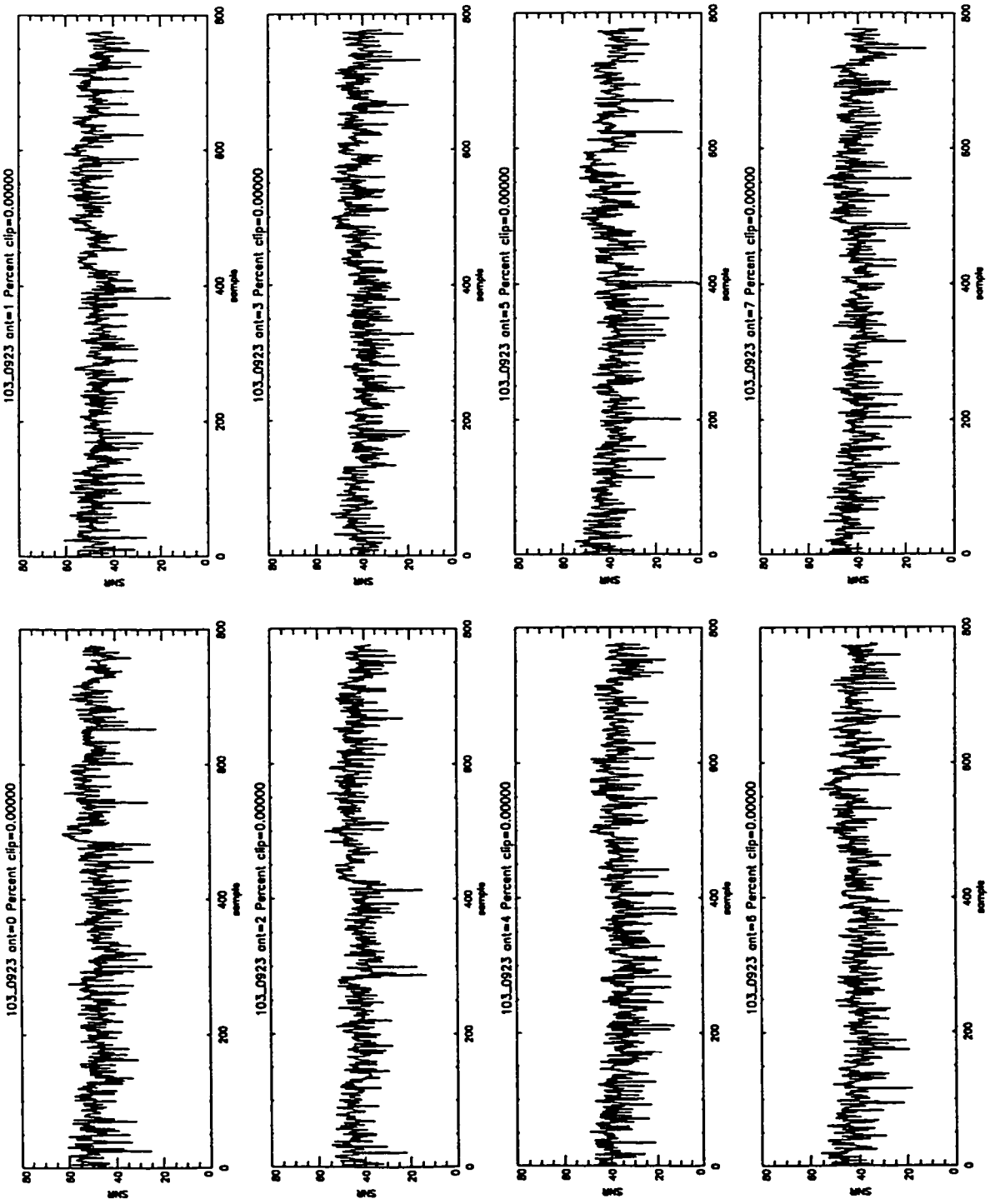

Figure A.7: Room 103 SNRs at each antenna output.

Appendix B

Optimum DSA NP-Completeness Proof

In this appendix it is proven that the optimum solution to the dynamic slot assignment (DSA) problem posed in Chapter 4 is NP-complete. The proof is accomplished by performing a reduction to the well-known "graph coloring" problem, i.e., that of finding the minimum number of colors needed to color the vertices of a graph, such that no two vertices of the same color share an edge [GJ79]. The proof gives a construction which shows that the optimal slot assignment solution can be used to solve this problem for any instance of the graph coloring problem.

We assume that the graph, G, to be colored has V vertices, V_i, for $i \in \{1, 2, \ldots, V\}$ and each vertex is associated with a portable station in the SDMA network. Here, the spatial signature of station i is assigned a real-valued vector, denoted by $\mathbf{x}_i$. Station signature vectors are generated based on the edges in G. The construction used is such that when two vertices V_i and V_j do not share an edge in G, then their assigned spatial signatures are orthogonal, that is, $\langle \mathbf{x}_i, \mathbf{x}_j \rangle = 0$. When the vertices share an edge, this product is non-zero.

The spatial signature vectors are generated from G as follows. The signature vector for station i contains three sections, namely, the Self or S-section, the Coupling or C-section, and the Normalization or N-section. The S-section is V bits long and contains a single "1" in position i. All other values are "0". The C-section introduces

non-orthogonality amongst the signature vectors as follows. This section consists of $\binom{V}{2}$ bits, where each bit corresponds to a unique selection of distinct pairs of vertices, V_i and V_j, for $i \neq j$. If these two vertices share an edge in $\mathbf{G}$, then the corresponding bit in the vector is "1", otherwise it is set to "0". The N-section is used to ensure that the norm of all the spatial signature vectors is the same. This is done by first finding the spatial signature with the maximum number of non-zero entries in the C and S sections. This corresponds to the graph vertex (or vertices) with the highest edge degree. The norms are equalized by adding enough "1" bits to each spatial signature vector so that all stations have the same number of non-zero entries. The N-section thus consists of V separate subsections, one for each vertex. The only non-zero subsection for signature i is subsection i which contains the number of "1" entries needed for the normalization.

As an example, consider a graph with $V = 3$ vertices where edges exist only between $\{V_1, V_2\}$ and $\{V_1, V_3\}$. The spatial signature constructions for this graph are as follows.

$$\begin{array}{lcccccccccc} \mathbf{x}_1^T & \rightarrow & 1 & 0 & 0 & 1 & 1 & 0 & 0 & 0 & 0 \\ \mathbf{x}_2^T & \rightarrow & 0 & 1 & 0 & 1 & 0 & 0 & 0 & 1 & 0 \\ \mathbf{x}_3^T & \rightarrow & 0 & 0 & 1 & 0 & 1 & 0 & 0 & 0 & 1 \\ & & \underbrace{}_{S} & & & \underbrace{}_{C} & & & \underbrace{}_{N} & & \end{array}$$

In this diagram, the sections introduced above are shown. When forming the "signature matrix" as shown, the S-section is always a unit matrix. In this example the columns of the C-section correspond to the unique pairwise selections of vertices, $\{V_1, V_2\}$, $\{V_1, V_3\}$ and $\{V_2, V_3\}$. The N-section adds a single "1" to both $\mathbf{x}_2$ and $\mathbf{x}_3$ so that $\|\mathbf{x}_1\| = \|\mathbf{x}_2\| = \|\mathbf{x}_3\|$. It can be seen that this construction leaves $\mathbf{x}_2$ and $\mathbf{x}_3$ orthogonal, whereas $\mathbf{x}_1$ is not orthogonal to the other two.

Using the above construction we can generate the appropriate spatial signatures for any graph coloring problem in polynomial time. We now consider the output signal to interference plus noise power, SINR, when optimal SINR beamforming is used for a given desired signal. Consider a set of stations that are assigned to the same SDMA/TDMA time slot. Without any loss in generality, we will consider a

particular antenna beam and identify the desired station signature vector as $\mathbf{x}_d$. The optimal SINR, after beamforming, can be written as

$$\text{SINR} = \max_{\mathbf{w}} \frac{\langle \mathbf{x}_d, \mathbf{w} \rangle^2}{\sum_{i=1}^{I} \langle \mathbf{x}_i, \mathbf{w} \rangle^2 + \sigma^2 \|\mathbf{w}\|^2}, \tag{B.1}$$

where we have assumed that there are I interfering stations assigned to the slot in addition to the desired station. $\|\cdot\|$ is used to denote the 2-norm, σ^2 is the noise power at each antenna output, and $\langle \mathbf{x}, \mathbf{y} \rangle$ is the absolute value of the complex inner product. We have also assumed that the interfering stations are numbered from 1 to I. In this expression, σ^2 is the Gaussian noise power at the input to the beamforming module.

In general, the I interferers will consist of I_o orthogonal interferers and I_{no} non-orthogonal interferers as discussed above, where $I = I_o + I_{no}$. We will denote the set of non-orthogonal interfering station indices as $\mathbf{I}_{no}$. It can be seen from the form of the SINR that we can choose the appropriate terms in $\mathbf{w}$ such that $\langle \mathbf{x}_i, \mathbf{w} \rangle = 0$ for all I_o orthogonal interferers. This can be done without affecting the other terms in the SINR. As a result, we can write that

$$\text{SINR} \leq \max_{\mathbf{w}} \frac{\langle \mathbf{x}_d, \mathbf{w} \rangle^2}{\sum_{i \in \mathbf{I}_{no}} \langle \mathbf{x}_i, \mathbf{w} \rangle^2 + \sigma^2 \|\mathbf{w}\|^2}, \tag{B.2}$$

$$\leq \max_{\mathbf{w}} \frac{\langle \mathbf{x}_d, \mathbf{w} \rangle^2}{\langle \mathbf{x}_s, \mathbf{w} \rangle^2 + \sigma^2 \|\mathbf{w}\|^2}. \tag{B.3}$$

The second inequality follows from setting $I = 1$. When there is only a single non-orthogonal interferer, we denote it's signature vector by $\mathbf{x}_s$ as shown. It is clear that the SINR is a non-increasing function of I_{no}.

We now define an orthogonal transformation $\mathbf{Q}$, where $\mathbf{w} = \mathbf{Q}\bar{\mathbf{w}}$. In this case,

$$\text{SINR} \leq \max_{\mathbf{w}} \frac{\langle \mathbf{x}_d, \mathbf{Q}\bar{\mathbf{w}} \rangle^2}{\langle \mathbf{x}_s, \mathbf{Q}\bar{\mathbf{w}} \rangle^2 + \sigma^2 \|\bar{\mathbf{w}}\|^2}. \tag{B.4}$$

In view of the above construction we can choose the transformation such that

$$\mathbf{Q}^T \mathbf{x}_d = \begin{pmatrix} \|\mathbf{x}_d\| \\ 0 \\ 0 \\ \vdots \end{pmatrix}. \tag{B.5}$$

In this case, since $\mathbf{x}_s$ and $\mathbf{x}_d$ are not orthogonal, the transformation will result in two non-zero entries in $\mathbf{Q}^T\mathbf{x}_s$, i.e.,

$$\mathbf{Q}^T\mathbf{x}_s = \begin{pmatrix} r_1 \\ r_2 \\ 0 \\ \vdots \end{pmatrix}. \tag{B.6}$$

Without any loss in generality we have assumed that these occur in the first 2 positions and given by r_1 and r_2 as shown. We now have that

$$\text{SINR} \leq \max_{\bar{\mathbf{w}}} \frac{\bar{w}_1^2 \|\mathbf{x}_d\|^2}{r_1^2\bar{w}_1^2 + r_2^2\bar{w}_2^2 + \sigma^2\|\bar{\mathbf{w}}\|^2}. \tag{B.7}$$

This expression is clearly maximized by choosing $\bar{w}_2 = 0$, which gives

$$\begin{aligned} \text{SINR} &\leq \max_{\bar{\mathbf{w}}} \frac{\|\mathbf{x}_d\|^2}{r_1^2 + \sigma^2} \equiv \widehat{\text{SINR}}_1, \\ &< \max_{\bar{\mathbf{w}}} \frac{\|\mathbf{x}_d\|^2}{\sigma^2} \equiv \widehat{\text{SINR}}_0. \end{aligned} \tag{B.8}$$

This result shows that the optimal SINR obtained with one or more non-orthogonal interferers in a slot (i.e., $\widehat{\text{SINR}}_1$) is strictly less than the optimum SINR which can be obtained with zero non-orthogonal interferers (i.e., $\widehat{\text{SINR}}_0$). Accordingly, if we choose the required SINR for each station to satisfy

$$\widehat{\text{SINR}}_1 < \text{SINR}_{\min} < \widehat{\text{SINR}}_0, \tag{B.9}$$

then only those stations which have orthogonal spatial signatures will be permitted to be assigned to the same slot. Thus in making this selection, an optimal slot assignment algorithm can only allocate stations with orthogonal spatial signatures to the same time slot. Stations which have non-orthogonal signatures must be assigned to separate time slots.

Finally, assume that a polynomial-time algorithm exists for finding the minimum length SDMA/TDMA frame. By the above construction, only sets of stations which are mutually orthogonal can be assigned to the same time slot. But a set of mutually

orthogonal stations corresponds to a set of vertices in G which are not connected by edges and thus they can be colored using the same color. Hence the minimal-length SDMA/TDMA frame defines a valid coloring of G where each time slot defines a different color. Now assume that a coloring of G is possible with a smaller number of colors than that given by the optimum slot assignment solution. In that case we could use that coloring of G to place stations into an SDMA/TDMA frame with fewer time slots than the optimum solution, and by definition, only stations with orthogonal spatial codes would be assigned to the same slot. This contradicts the assumption that the original SDMA/TDMA slot assignment was minimal length. This shows the NP-completeness of the optimal slot assignment problem.

Appendix C

Algorithm Orders

In this appendix the number of floating point operations (FLOPS) is derived for the worst case situation of each of the DSA algorithms. Only the single cell reverse link case without weight vector normalization is considered here. The FLOPS are derived as a polynomial function of the batch size T, and the number of antennas N.

The heuristic DSA algorithms use the optimal reverse link beamforming solution for the weight vectors, which was derived in Chapter 3. It is reproduced here for convenience.

$$\mathbf{R}\mathbf{w}_o = \mathbf{p}. \tag{C.1}$$

Once $\mathbf{w}_o$ is known, the reverse link post-combining mean signal power to mean interference plus noise power ratio is calculated as

$$\text{SINR} = \frac{|\mathbf{w}_o^H \mathbf{v}_d|^2}{\mathbf{w}_o^H \mathbf{R}_u \mathbf{w}_o}, \tag{C.2}$$

where $\mathbf{v}_d$ is the signature of the desired user, and $\mathbf{R}_u$ is the correlation matrix of the undesired users plus noise.

The total number of FLOPS consumed in calculating (C.1) and subsequently (C.2) for a single desired user in the presence of $S-1$ interferers is

$$\text{FLOPS}(\text{SINR}_1(N,S)) \simeq \frac{8}{3}N^3 + (8S + \frac{43}{2})N^2. \tag{C.3}$$

Therefore, to calculate the SINR of all S stations, the number of FLOPS is

$$\text{FLOPS}(\text{SINR}_S(N,S)) \simeq \frac{8S}{3}N^3 + (8S^2 + \frac{43}{2}S)N^2. \tag{C.4}$$

The FLOPS required for each of the DSA algorithms can now be given in terms of Equation (C.4). It should be noted that the first user is always allocated without a SINR check.

With Random DSA, the worst case arises when $N-1$ stations are allocated to each slot, and the N^{th} station to be tested has insufficient SINR, so it is placed in the next time slot. Therefore, with a batch size of T stations,

$$\text{FLOPS}(\text{Random}(N,T)) = \sum_{S=2}^{N} \text{FLOPS}(\text{SINR}_S(N,S))\lfloor\frac{T-S+N-1}{N-1}\rfloor. \quad \text{(C.5)}$$

With First Fit and Best Fit DSA, similar to Random, the worst case is when $N-1$ stations are allocated to each slot, and the N^{th} station to be tested has insufficient SINR. Except for the first user to be allocated in the frame, each user which is allocated is the last unallocated user in the batch. First First Sorted and Best Fit sort the signatures in order of ascending power before starting. The FLOPS required to sort all T signatures is equal to

$$\begin{aligned} \text{FLOPS}(\text{sorting}) &= T\cdot(\text{FLOPS}(\|\mathbf{v}\|_2^2)) \\ &= T(8N-2). \end{aligned} \quad \text{(C.6)}$$

The FLOPS for First Fit are equal to

$$\text{FLOPS}(\text{First Fit}(N,T)) = \sum_{S=2}^{N} \text{FLOPS}(\text{SINR}_S(N,S))B(S), \quad \text{(C.7)}$$

where

$$B(S) = \frac{1}{2}\lfloor\frac{T-S+N-1}{N-1}\rfloor(2(T-S)+N+1+(1-N)\lfloor\frac{T-S+N-1}{N-1}\rfloor). \quad \text{(C.8)}$$

The FLOPS for First Fit Sorted and Best Fit are equal to Equations (C.7) plus (C.6).

The Equal Norm and Orthosigs DSA algorithms first form a compatibility matrix (see Chapter 4), and then work in a fashion identical to Random. The FLOPS required to form the compatibility matrices for Equal Norm and Orthosigs are

$$\text{FLOPS}(\text{Equal Norm Compatibility Matrix}) = T(11T-13+8N), \quad \text{(C.9)}$$

and

$$\text{FLOPS(Orthosigs Compatibility Matrix)} = \frac{T}{2}(8TN + 23T + 8N - 27). \quad \text{(C.10)}$$

Therefore, the total number of FLOPS for Equal Norm and Orthosigs dynamic slot assignment are Equations (C.5)+(C.9) and (C.5)+(C.10), respectively.

If $T \gg N$, the approximate worst case FLOPS of the dynamic slot assignment algorithms are summarized in Table C.1.

Algorithm	$O(N,T)$
Random	$\frac{T}{12}(48N^4 + 241N^3 + 354N^2)$
Random Sorted	$T(8N-2) + O(\text{Random})$
First Fit	$\frac{T^2}{24}(48N^4 + 241N^3 + 354N^2)$
First Fit Sorted and Best Fit	$T(8N-2) + O(\text{First Fit})$
Equal Norm	$T(11T - 13 + 8N) + O(\text{Random})$
Orthosigs	$\frac{T}{2}(8TN + 23T + 8N - 27) + O(\text{Random})$

Table C.1: Approximate worst case algorithm orders.

Bibliography

[Abr70] N. Abramson. The ALOHA system - another alternative for computer communications. *Proceedings, Fall Joint Computer Conference*, 1970.

[Aca96] A. Acampora. Wireless ATM: a perspective on issues and prospects. *IEEE Personal Communications*, pages 8–17, August 1996.

[AK89] E. Aarts and J. Korst. *Simulated annealing and boltzmann machines.* Wiley, 1989.

[Ake88] D. Akerberg. Properties of a TDMA pico cellular office communication system. *IEEE GLOBECOM'88*, pages 1343–1349, December 1988.

[App66] S. P. Applebaum. Adaptive arrays. SPL TR 66-1, 1966.

[App76] S. P. Applebaum. Adaptive arrays. *IEEE Transactions on Antennas and Propagation*, AP-24(5):585–598, September 1976.

[BG92] D. Bertsekas and R. Gallager. *Data networks.* Prentice Hall, second edition, 1992.

[Bul86] R. J. C. Bultitude. Propagation characteristics of 800/900 Mhz radio channels operating within buildings. *Proceedings of Thirteenth Biennial Symposium on Communications*, pages B1/1–4, June 1986.

[Bul87] R. J. C. Bultitude. Measurement, characterization, and modeling of indoor 800/900 MHz radio channels for digital communications. *IEEE Communications Magazine*, 25(6):5–12, 1987.

[CGK67] J. Capcon, R. J. Greenfield, and R.J. Kolker. Multidimensional maximum likelihood processing of a large aperture seismic array. *ProceedingsIEEE*, 55:192–211, February 1967.

[Com82] R. T. Compton, Jr. Effect of random steering vector errors in the Applebaum adaptive array. *IEEE Transactions on Aerospace and Electronic Systems*, 18(5):392–400, September 1982.

[Com88] R.T. Compton, Jr. *Adaptive antennas, concepts and performance.* Prentice Hall, 1988.

[CR98] A. Chockalingam and Ramesh R. Rao. MAC layer performance with steerable multibeam antenna arrays. *Ninth International Symposium on Personal, Indoor, and Mobile Radio Communications*, pages 973–977, Sept. 8-11 1998.

[CZMV98] A. Chockalingam, M. Zorzi, L.B. Milstein, and P. Venkataram. Performance of a wireless access protocol on correlated Rayleigh fading channels with capture. *IEEE Transactions on Communications*, 46(5):644–655, 1998.

[Dep96] IEEE Standards Department. *IEEE draft standard - wireless LAN.* IEEE Press, 1996.

[Dev87] D. M. J. Devasirvatham. A comparison of time delay spread and signal level measurements within two dissimilar office buildings. *IEEE Transactions on Antennas and Propagation*, AP-35(3):319–324, March 1987.

[Dou90] E. R. Dougherty. *Probability and statistics for the engineering, computing, and physical sciences.* Prentice Hall, 1990.

[Gab76] W. F. Gabriel. Adaptive Arrays - an introduction. *Proceedings of the IEEE*, 64:239–272, February 1976.

[GC89] M. W. Ganz and R.T. Compton, J.R. A data-derived reference signal technique for adaptive arrays. *IEEE Transactions on Communications*, 37(9):975–983, September 1989.

[GJ79] M.R. Garey and D.S. Johnson. *Computers and tractability: a guide to the theory of NP-completeness.* W.H. Freeman and Co., 1979.

[GP91] R. Ganesh and K. Pahlavan. Statistics of short term variations of indoor radio propagation. *Proceedings of International Conference on Communications*, June 1991.

[Has93] H. Hashemi. The indoor radio propagation channel. *Proceedings of the IEEE*, 81(7):943–968, July 1993.

[Hay78] S. Haykin. *Communication systems.* John Wiley and Sons, 1978.

[Hay96] S. Haykin. *Adaptive filter theory.* Prentice Hall, third edition, 1996.

[How65] P. Howells. Intermediate frequency sidelobe canceller. *U.S. Patent 3,202,990*, August 1965.

[HP91] S.J. Howard and K. Pahlavan. Fading results for narrowband measurements of the indoor radio channel. *Ninth International Symposium on Personal, Indoor, and Mobile Radio Communications*, pages 92–97, September 1991.

[Hud81] J.E. Hudson. *Adaptive array principles.* Number 11 in IEE electromagnetic wave series. IEE, Stevenage, U.K., 1981.

[Jak74] William C Jakes, Jr. *Microwave mobile communications.* John Wiley and Sons, 1974.

[JD93] D. H. Johnson and D. E. Dudgeon. *Array signal processing.* Prentice Hall, Englewood Cliffs, 1993.

[KGV83] S. Kirkpatrick, C. D. Jr. Gelatt, and M.P. Vecchi. Optimization by simulated annealing. *Science*, 220:671–680, 1983.

[Kuc91] A. D. Kucar. Mobile radio: An overview. *IEEE Communications Magazine*, pages 72–85, November 1991.

[Lee86] W. C. Y. Lee. Elements of cellular mobile radio systems. *IEEE Transactions on Vehicular Technology*, VT-35(2):48–56, May 1986.

[LG94] Alberto Leon-Garcia. *Probability and random processes for electrical engineers.* Addison Wesley, 1994.

[LL96] J. Litva and T.K.Y. Lo. *Digital beamforming in wireless communications.* Artech House, 1996.

[LQ95] V. O.K. Li and X. Qui. Personal communication systems (PCS). *European Journal of Operational Research*, 83(9):1210–1243, September 1995.

[LSEJW68] R. W. Lucky, J. Salz, and Jr. E. J. Weldon. *Principles of Data Communication.* McGraw-Hill, New York, 1968.

[MB76] M. Metcalfe and D.R. Boggs. Ethernet: distributed packet switching for local computer networks. *Communications of the ACM*, July 1976.

[MM80] R.A. Monzingo and T. W. Miller. *Introduction to adaptive arrays.* John Wiley and Sons, 1980.

[MM97] J.E. Miller and Scott L. Miller. DS-CDMA reverse link performance with a smart antenna array, fading and imperfect power control. *Vehicular Technology Conference*, 1997.

[MTH90] Y. Matsumoto, Y. Takahashi, and T. Hasegawa. The effects of packet size distributions on output and delay processes of CSMA/CD. *IEEE Transactions on Communications*, 38(2):199–214, February 1990.

[NP96] A.F. Nguib and A. Paulraj. Performance of wireless CDMA with M-ary orthogonal modulation and cell site antenna arrays. *IEEE Journal on Selected Areas in Communications*, 14(9):1770–1783, December 1996.

[NPK94] A.F. Nguib, A. Paulraj, and T. Kailath. Capacity improvement with base-station antenna arrays in cellular CDMA. *IEEE Transactions on Vehicular Technology*, 43(3):691–698, August 1994.

[OX96] G. Okamoto and G. Xu. Throughput multiplication of wireless LANs for multimedia services: spread spectrum with SDMA. *IEEE Vehicular Technology Conference*, April 1996.

[Pah94] K. Pahlavan. Wireless data communications. *Proceedings of the IEEE*, 82(9):1398–1430, September 1994.

[PL95] K. Pahlavan and A. H. Levesque. *Wireless information networks.* Wiley Press, 1995.

[PP97] A. J. Paulraj and C. B. Papadias. Space-time signal processing for wireless communications. *IEEE Signal Processing Magazine*, 14(6):49–83, November 1997.

[Pry93] M. De Prycker. *Asynchronous transfer mode: solution for broadband ISDN.* Ellis Horwood, second edition, 1993.

[Rap89] T.S. Rappaport. Indoor radio communications for factories of the future. *IEEE Communications Magazine*, pages 15–24, May 1989.

[Rap91] T.S. Rappaport. The MPRG research program - some recent propagation results. *Virginia Tech's First Symposium on Wireless Personal Communications*, pages 9.1–9.12, June 1991.

[Rap94] T. S. Rappaport. *Cellular radio and personal communications: A book of selected readings.* IEEE, 1994.

[Rap96] T.S. Rappaport. *Wireless communications, principles and practice.* Prentice Hall, 1996.

[RCM96] Y. Roy, Y Chouinard, and S. A. Mahmoud. Selection diversity combining with multiple antennas for MM-wave indoor wireless channels. *IEEE Journal on Selected Areas in Communications*, 14(4):674–682, May 1996.

[Rei96] J. Reilly. *Notes for matrix computations in signal processing course.* McMaster University, 1996.

[RM89] T.S. Rappaport and C.D. McGillem. UHF fading in factories. *IEEE Journal on Selected Areas in Communications*, 7(1):40–48, January 1989.

[RMB74] I.S. Reed, J. D. Mallett, and L.E. Brennan. Rapid convergence rate in adaptive arrays. *IEEE Transactions on Aerospace and Electronic Systems*, AES-10(6):853–863, November 1974.

[Rob75] L.G. Roberts. ALOHA packet system with and without slots and capture. *Computer Communications Review*, April 1975.

[SBEM90] S. C. Swales, M. A. Beach, D. J. Edwards, and J. P. McGeehan. The performance enhancement of multibeam adaptive base-station antennas for cellular land mobile radio systems. *IEEE Transactions on Vehicular Technology*, 39(1):56–67, February 1990.

[SES95] A. Sugihara, K. Enomoto, and I. Sasase. Throughput performance of a slotted nonpersistent CSMA with an adaptive array. *Ninth International Symposium on Personal, Indoor, and Mobile Radio Communications*, 2:633–637, September 1995.

[She77] N.H. Sheperd. Radio wave loss deviation and shadow loss at 900 Mhz. *IEEE Transactions on Vehicular Technology*, 26(4):309–313, November 1977.

[Sin97] R. Sinha. Smart antennas in packet switched indoor SDMA networks. Master's thesis, McMaster University, September 1997.

[Skl88] B. Sklar. *Digital communications: fundamentals and applications.* Prentice Hall, Inc., 1988.

[SM82] R. L. Scheaffer and J. M. McClave. *Statistics for engineers.* Duxbury Press, 1982.

[Smi80] W. Smith. Swift. *Symp. Very High Speed Computing Technology*, 1980.

[SP80] D. V. Sarwate and M. B. Pursley. Crosscorrelation properties of pseudo-random and related sequences. *Proceedings of the IEEE*, 68(5):593–618, May 1980.

[SP86] J.L. Dailing S.J. Patsiokas, B.K. Johnson. Propagation of radio signals inside building at 150, 450, and 850 Mhz. *Proceedings of IEEE Vehicular Technology Conference*, pages 66–71, 1986.

[ST97] C. Sakr and T. D. Todd. Carrier sense protocols for packet-switched smart antenna basestations. *International Conference on Network Protocols*, pages 45–52, October 28-31 1997.

[STKL97a] F. Shad, T. Todd, V. Kezys, and J. Litva. Indoor SDMA capacity using a smart antenna basestation. *Sixth International Conference on Universal Personal Communications*, 2:868–872, October 12-16 1997.

[STKL97b] F. Shad, T. D. Todd, V. Kezys, and J. Litva. Indoor SDMA capacity using a smart antenna basestation. *Seventh Virginia Tech/MPRG Symposium on Wireless Personal Communications*, June 11-13 1997.

[STSK98] R. Sinha, T. Todd, F. Shad, and V. Kezys. Forward link capacity in smart antenna basestations with dynamic slot allocation. *Ninth International Symposium on Personal, Indoor, and Mobile Radio Communications*, 2:942–946, September 8-11 1998.

[SV87] A. A. M. Saleh and R. A. Valenzuela. A statistical model for indoor multipath propagation. *IEEE Journal on Selected Areas in Communications*, SAC-5(2):128–137, February 1987.

[SXLK98] B. Suard, G. Xu, H. Liu, and T. Kailath. Uplink channel capacity of space-division-multiple-access schemes. *IEEE Transactions on Information Theory*, 44(4):1468–1475, July 1998.

[Tan96] A. S. Tanenbaum. *Computer networks.* Prentice Hall, Inc., third edition, 1996.

[TGM96] J. S. Thompson, Peter M. Grant, and B. Mulgrew. Smart antenna arrays for CDMA systems. *IEEE Personal Communications*, pages 16–25, October 1996.

[TK84] H. M. Taylor and S. Karlin. *An introduction to stochastic modeling.* Academic Press, Toronto, 1984.

[TM88] A. R. Tharek and J. P. McGeehan. Indoor propagation and bit error rate measurements at 60 Ghz using phase-locked oscillators. *Proceedings of IEEE Vehicular Technology Conference*, pages 127–133, June 1988.

[TT92] A.F. Toledo and A.M.D. Turkmani. Propagation into and within buildings at 900, 1800, and 2300 Mhz. *Proceedings of IEEE Vehicular Technology Conference*, pages 633–636, May 1992.

[Vit95] A. J. Viterbi. *CDMA - principles of spread spectrum communication.* Addison-Wesley, 1995.

[WC92] J. Ward and R.T. Compton, Jr. Improving the performance of slotted ALOHA packet radio network with an adaptive array. *IEEE Transactions on Communications*, 40(2):292–300, February 1992.

[WC93] J. Ward and R.T. Compton, Jr. High throughput slotted ALOHA packet radio networks with adaptive arrays. *IEEE Transactions on Communications*, 41(3):460–470, March 1993.

[Win84] J. H. Winters. Optimum combining in digital mobile radio with cochannel interference. *IEEE Journal on Selected Areas in Communications*, SAC-2(4):528–539, July 1984.

[Win87a] J. H. Winters. On the capacity of radio communication systems with diversity in a Rayleigh fading environment. *IEEE Journal on Selected Areas in Communications*, SAC-5(5):871–878, June 1987.

[Win87b] J. H. Winters. Optimum combining for indoor radio systems with multiple users. *IEEE Transactions on Communications*, COM-35(11):1222–1230, November 1987.

[Win98] J. H. Winters. Smart antennas for wireless systems. *IEEE Personal Communications*, pages 23–27, February 1998.

[WMGG67] B. Widrow, P.E. Mantey, L.J. Griffiths, and B.B. Goode. Adaptive antenna systems. *Proceedings IEEE*, 55:2143–2159, December 1967.

[WSG94] J. H. Winters, J. Salz, and R. D. Gitlin. The impact of antenna diversity on the capacity of wireless communication systems. *IEEE Transactions on Communications*, 42(2/3/4):1740–1750', February/March/April 1994.

[XL94] G. Xu and S.Q. Li. Throughput multiplication of wireless LANs for multimedia services: SDMA protocol design. *Proc. GLOBECOM'94*, August 1994.

[YL97] D. O. Reudink Y. Li, M. J. Feuerstein. Performance evaluation of a cellular base station multibeam antenna. *IEEE Transactions on Vehicular Technology*, 46(1):1–9, February 1997.